

Fall 2004

# Polymer-based wide-angle micro -optic lens system with dynamically variable focal length and field of view

Mangilal Agarwal  
*Louisiana Tech University*

Follow this and additional works at: <https://digitalcommons.latech.edu/dissertations>



Part of the [Electrical and Computer Engineering Commons](#)

---

## Recommended Citation

Agarwal, Mangilal, "" (2004). *Thesis*. 632.  
<https://digitalcommons.latech.edu/dissertations/632>

This Thesis is brought to you for free and open access by the Graduate School at Louisiana Tech Digital Commons. It has been accepted for inclusion in Doctoral Dissertations by an authorized administrator of Louisiana Tech Digital Commons. For more information, please contact [digitalcommons@latech.edu](mailto:digitalcommons@latech.edu).

**POLYMER-BASED WIDE-ANGLE MICRO-OPTIC LENS SYSTEM  
WITH DYNAMICALLY VARIABLE FOCAL LENGTH  
AND FIELD OF VIEW**

by

**Mangilal Agarwal, B.E, M.S**

A Dissertation Presented in Partial Fulfillment  
of the Requirement for the Degree of  
Doctor of Philosophy in Engineering

COLLEGE OF ENGINEERING AND SCIENCE  
LOUISIANA TECH UNIVERSITY

May 2004

UMI Number: 3126521

Copyright 2004 by  
Agarwal, Mangilal

All rights reserved.

### INFORMATION TO USERS

The quality of this reproduction is dependent upon the quality of the copy submitted. Broken or indistinct print, colored or poor quality illustrations and photographs, print bleed-through, substandard margins, and improper alignment can adversely affect reproduction.

In the unlikely event that the author did not send a complete manuscript and there are missing pages, these will be noted. Also, if unauthorized copyright material had to be removed, a note will indicate the deletion.

**UMI**<sup>®</sup>

---

UMI Microform 3126521

Copyright 2004 by ProQuest Information and Learning Company.

All rights reserved. This microform edition is protected against unauthorized copying under Title 17, United States Code.

ProQuest Information and Learning Company  
300 North Zeeb Road  
P.O. Box 1346  
Ann Arbor, MI 48106-1346

LOUISIANA TECH UNIVERSITY

THE GRADUATE SCHOOL

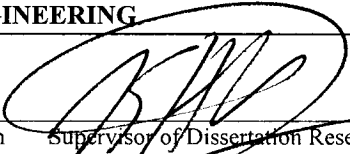
May 10, 2004

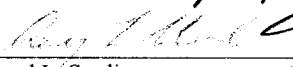
Date

We hereby recommend that the dissertation prepared under our supervision  
by MANGILAL AGARWAL

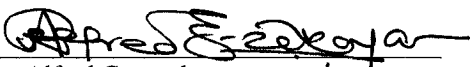
entitled POLYMER-BASED WIDE-ANGLE MICRO-OPTIC LENS SYSTEM WITH  
DYNAMICALLY VARIABLE FOCAL LENGTH AND FIELD OF VIEW

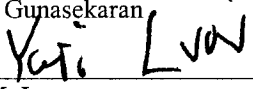
be accepted in partial fulfillment of the requirements for the Degree of  
DOCTOR OF PHILOSOPHY IN ENGINEERING

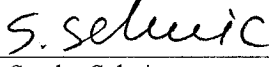
  
Dr. Kody Varahramyan Supervisor of Dissertation Research

  
Dr. Raymond L. Sterling Head of Department  
Department of Engineering  
Department

Recommendation concurred in:

  
Dr. Alfred Gunasekaran

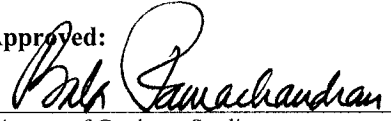
  
Dr. Yuri M. Lvov

  
Dr. Sandra Selmic


  
Dr. Cheng Luo

  
Mr. Ji Fang

Advisory Committee

Approved:   
Director of Graduate Studies

  
Dean of the College

Approved:   
Dean of the Graduate School



## ABSTRACT

A novel polymer-based integrated wide-angle dynamic micro-optical lens system that can provide variable focal length and field of view (FOV) with large numerical aperture is designed, fabricated, and tested for its optical characteristics. Optical systems often require a focal length to be variable which allows the FOV and the magnification to be altered and to focus on objects which are in motion or irregular in shape. A lens, as a conventional optical element, is devoid of variable focusing mechanism and requires many complex and expensive gears, motors, and sliders to move in order to focus on the object for observation. A non-mechanical solution is therefore required to make dynamic on-line adjustments to the optical parameters of the lens system, such as focal length, in response to the change in viewing conditions. This research demonstrates a wide-angle dynamic microlens system, whose focal length, numerical aperture, and FOV can be dynamically controlled by changing the shape of the fluidic lens without moving the lens position mechanically. This dynamic microlens system overcomes the limitations of the other types of lens systems reported to date, which either involve expensive and complex fabrication processes or suffer from limited range of tunable focal length and FOV.

Initial experiments were conducted using static glass lenses to test for configuration of lenses that could provide wide FOV. From these initial experiments, it was found that the higher FOV could be achieved with double concave (DCV) lenses compared to double convex (DCX) lenses of the same focal length. Further, it was

observed that increasing the number of DCV lenses increases FOV. Thus, an integrated dynamic polymer microlens system has been fabricated with two or three DCV lenses, which demonstrates a wide range of tunable focal length and FOV. A flexible polydimethylsiloxane (PDMS) polymer membrane is used to form the lens surface. Two such membranes with a fluidic lens chamber are actuated by fluidic pressure to form either a DCX or DCV lens. The curvature of the lens (PDMS membrane) changes because of the fluidic pressure built by a syringe pump and produces the change in the focal length and FOV without any mechanical moving parts. The relationship between the focal length and FOV of the dynamic microlens system with respect to the change in volume of the fluid pumped in or out of the lens chamber has been investigated and reported.

Experimental results show that a focal length in the range of several hundred microns to several millimeters and the smallest f-number equal to 0.76, which corresponds to a numerical aperture of 0.55, could be achieved using a single dynamic microlens system. It was observed that the FOV in the range of 0.12 to 61.08 degrees and 7 to 68.22 degrees could be achieved by actuating a single dynamic microlens system, as a DCX and DCV lens. It was also observed that the FOV could be tuned in the range of 8 to 79.65 degrees and 11.49 to 90.44 degrees, by using integrated dynamic microlenses with two or three DCV lenses, respectively. Therefore, a novel method to fabricate a wide FOV optical microlens system that is suitable for dynamic imaging of objects with minimal image distortion has been defined and demonstrated in this research. This dynamic microlens system can be applied in future generations of products such as surveillance systems in military and surgical instruments in the medical field.

## APPROVAL FOR SCHOLARLY DISSEMINATION

The author grants to the Prescott Memorial Library of Louisiana Tech University the right to reproduce, by appropriate methods, upon request, any or all portions of this Dissertation. It is understood that "proper request" consists of the agreement, on the part of the requesting party, that said reproduction is for his personal use and that subsequent reproduction will not occur without written approval of the author of this Dissertation. Further, any portions of the Dissertation used in books, papers, and other works must be appropriately referenced to this Dissertation.

Finally, the author of this Dissertation reserves the right to publish freely, in the literature, at any time, any or all portions of this Dissertation.

Author Mangilal Agarwal 

Date May 10, 2004

*This dissertation is dedicated to my parents,  
Jagdish Prasad Agarwal and  
Chawali Devi Agarwal*

## TABLE OF CONTENTS

	<b>Page</b>
LIST OF TABELS .....	ix
LIST OF FIGURES .....	x
ACKNOWLEDGMENTS .....	xviii
CHAPTER 1: INTRODUCTION AND OBJECTIVES.....	1
1.1 Introduction.....	1
1.2 Objectives.....	5
1.3 Dissertation Overview .....	6
CHAPTER 2: LITERATURE REVIEW .....	8
2.1 Fundamentals of Light and Optics.....	8
2.2 Focal Length Calculations .....	15
2.3 Lens Aberrations.....	18
2.4 Glass vs. Plastic Lenses .....	22
2.5 Soft and Flexible Polymer Materials for Optical Applications .....	23
2.6 Fish-Eye and Wide Field of View Lenses .....	25
2.7 Micro-Optics.....	28
2.8 Variable Focal Length Lenses .....	36
2.8.1 Limitations of Variable Focal Length Lenses Reported to Date .....	47
CHAPTER 3: INITIAL TESTING FOR WIDE FIELD OF VIEW DESIGN USING GLASS LENSES .....	50
3.1 Experimental Setup.....	50
3.2 Different Configuration of Double Concave (DCV) and Double Convex (DCX) Glass Lenses to Test for Wide Field of View.....	51
3.3 Results and Discussion .....	54

CHAPTER 4: MACRO-SCALE PLOYMER WIDE-ANGLE VARIABLE FOCAL LENGTH LENS SYSTEM .....	61
4.1 Overview .....	61
4.2 Initial Experiments.....	62
4.3 Macro-Scale Polymer Wide-Angle Variable Focal Length Lens System.....	68
CHAPTER 5: POLYMER-BASED WIDE-ANGLE DYNAMIC MICRO-OPTIC LENS SYSTEM.....	84
5.1 Overview .....	84
5.2 Design and Fabrication of Variable Focal Length Microlens System.....	85
5.2.1 Fabrication Process Steps .....	85
5.2.2 Mask Design .....	87
5.2.3 Lithography and Silicon Micromachining .....	88
5.2.4 Integration and Packaging.....	96
5.2.5 Fabrication of Integrated Wide-Angle Dynamically Variable Focal Length Microlens System.....	99
5.3 Results and Discussion .....	104
5.3.1 PDMS Membrane Characteristics.....	104
5.3.1.1 Roughness of PDMS Membrane .....	104
5.3.1.2 Thickness of PDMS Membrane.....	107
5.3.1.3 Transmittance and Absorption Characteristics .....	109
5.3.2 Variable Focal Length DCX and DCV Microlens System.....	112
5.3.2.1 Imaging Characteristics .....	112
5.3.2.2 Transmittance Characteristics.....	118
5.3.2.3 Contact Angle Measurements .....	120
5.3.2.4 The f-number and Numerical Aperture.....	124
5.3.3 Integrated Wide-Angle Dynamically Variable Focal Length Microlens System .....	125
CHAPTER 6: CONCLUSIONS AND RECOMMENDATIONS .....	134
6.1 Conclusions.....	134
6.2 Recommendations for Future Research .....	138
BIBLIOGRAPHY .....	142

## LIST OF TABLES

	<b>Page</b>
2.1 Change in focal length of human eye vs. object distance. ....	35
2.2 Summary of different variable focal length lenses reported to date and their optical properties. ....	47
3.1 Field of view measured using single double convex lens of focal length $f = 10$ cm and the different combinations of double concave lenses of focal lengths $-f = 10, 15,$ and $20$ cm. ....	57
3.2 Field of view measured using single double convex lens of focal length $f = 20$ cm and the different combinations of double concave lenses of focal lengths $-f = 10, 15,$ and $20$ cm. ....	58
4.1 Change in focal length and field of view with volume of fluid pumped-out of different dynamic DCV lens systems. ....	83
5.1 Parameters used for ICP etching. ....	93
5.2 Average roughness value and the roughness values of the PDMS membrane measured using AFM and RST. ....	107
5.3 Average roughness value and the roughness values of the PDMS membrane measured using RST and Tencor surface profilometer. ....	109
5.4 Optical properties of single variable focal length microlens system at different volumes of fluid pumped-in. ....	125
5.5 Change in focal length and field of view with the change in volume of fluid pumped out of different dynamic DCV microlens systems. ....	132
6.1 Technical specification of micro-pump from Fraunhofer-IMS. ....	140

## LIST OF FIGURES

	<b>Page</b>
2.1 Reflection of light ray from a smooth surface. ....	9
2.2 Refraction from Huygen's principle. ....	11
2.3 Refractive optical elements. ....	12
2.4 Schematic of converging lens (double convex). ....	13
2.5 Schematic diagram of diverging lens (double concave). ....	14
2.6 Schematic of converging lens to derive lens equation. ....	15
2.7 Schematic diagram to show spherical aberration. ....	18
2.8 Schematic diagram to show coma aberration. ....	19
2.9 Schematic diagram to show astigmatism aberration. ....	19
2.10 Schematic diagram to show field curvature aberration. ....	20
2.11 Schematic diagram to show distortion aberrations. ....	20
2.12 Schematic diagram to show field chromatic aberration. ....	21
2.13 Fish-eye view from the water-filled camera. ....	26
2.14 Schematic of fish-eye glass lens by Coastal Optical Systems. ....	27
2.15 (a) ORIFL 190-3 fish-eye lens, (b) Image captured using an ORIFL 190-3 fish-eye lens. ....	28
2.16 Schematic of compound eye found in nature (a) apposition compound eye, (b) superposition compound eye. ....	29
2.17 Schematic of artificial counterpart for compound eye found in nature (a) apposition compound eye, (b) superposition compound eye. ....	30



2.18	(a) Resist reflow process to fabricate microlenses, (b) SEM micrograph of the microlens array fabricated using resist reflow method. ....	31
2.19	(a) Microlens array mold, (b) Microlens array after replication. ....	32
2.20	(a) Schematic of drop-on demand ink-jet printing equipment, (b) Microlens array fabricated using micro-drop printer. ....	33
2.21	Projection lithography setup using microlens arrays. ....	33
2.22	(a) Schematic diagram of the human eye, (b) Diagram showing the accommodation of human eye lens for near and far objects. ....	35
2.23	Structure of liquid crystal lens-cell (a) plano-convex, (b) plano-concave. ....	37
2.24	Liquid crystal lens-cell with hole patterned electrode. ....	38
2.25	(a) Geometry of the LC cylindrical lens, (b) Simplified equivalent circuit, illustrating the distributed nature of the reactive impedance of the LC layer sandwiched between high and low resistance electrodes. ....	39
2.26	(a) An LC immersed microlens with and without applied voltage, (b) Focal length vs. applied voltage. ....	40
2.27	The schematic diagram of a LC cell with UV curable microlenses. ....	41
2.28	(a) Switchable electrowetting with invasive electrode, (b) Non-invasive electrowetting cell, (c) Equivalent circuit model. ....	42
2.29	(a) Electrowetting cell, (b) Voltage vs. focal length. ....	43
2.30	(a) & (b) Schematic cross section of the FluidFocus lens with and without applied voltage; (c) to (e) Shapes of a 3-mm diameter lens taken at different applied voltages. ....	44
2.31	(a) Dynamic focal length lens using PZLT actuation, (b) Optical characteristics. ....	45
2.32	Variable focal length lens using fluidic actuation. ....	46
2.33	Variable focal length microlens array using fluidic actuation. ....	46
3.1	Image capturing setup. ....	51

3.2	Illustrations of optical arrangements (a) two DCX lenses, (b) first DCX lens with a second DCV lens. ....	52
3.3	Illustrations of optical arrangements (a) one DCX and two DCV lenses, (b) one DCX and three DCV lenses. ....	53
3.4	Optical image of the object captured directly from the CCD camera. ....	54
3.5	(a) Series of images captured using the setup shown in Figure 3.2a with the first DCX lens of $f = 10$ cm and second DCX lens of different focal length, (b) Focal length vs. field of view (FOV) from the second DCX lenses. ....	55
3.6	(a) Images captured using the setup shown in Figure 3.3a with first DCX lens of $f = 20$ cm and a second DCX lens of $f = 10, 15,$ and $20$ cm, (b) Images captured using the setup shown in Figure 3.3b with first DCX lens of $f = 20$ cm and a second DCV lens of $-f = 10, 15,$ and $20$ cm. ....	56
3.7	Focal length vs. field of view (FOV) from DCX and DCV lenses. ....	56
3.8	Focal length of DCV lenses vs. FOV for different combinations of DCX and DCV lenses. The focal length of DCX lens is fixed in each series of the imaging experiment. ....	59
3.9	Image of the object captured using (a) a DCX lens ( $f = 10$ cm) an a DCV lens ( $-f = 20$ cm), (b) a single DCX lens ( $f = 20$ cm) and three DCV lenses ( $-f = 10$ cm). ....	60
4.1	Schematic representation of the flexible membranes behaving as dynamic DCX and DCV lenses. ....	62
4.2	(a) PDMS membrane, (b) PDMS spacer, (c) Final lens structure with a fluidic chamber. ....	63
4.3	PDMS membrane lens with rubber spacer. ....	64
4.4	(a) Two copper rings with PDMS membrane and plastic spacer, (b) Fluid actuated lens structure. ....	64
4.5	Copper ring (a) before etching, (b) after etching. ....	65
4.6	(a) Fluid actuated lens structure fabricated using small copper rings, (b) Lens structures with fluidic connection. ....	65
4.7	Pressure vs. displacement plot for two different sized PDMS membranes. ....	66

4.8	(a) Normal fluid actuated lens structure. Fluid actuated structure as (b) DCX lens, (c) DCV lens. ....	67
4.9	(a) Variable focal length lens unit (radius - 7.9 mm, thickness - 1.5 mm), (b) Variable focal length lenses with fluidic connections. ....	68
4.10	Schematic diagram showing the deflection of the PDMS membrane above the spacer unit. ....	70
4.11	Two-dimensional schematic of spherical cap. ....	70
4.12	Focal length ( $f$ ) vs. volume of fluid pumped-in ( $v_3/2$ ). ....	73
4.13	Series of images captured at different volumes of fluid ( $v_3$ ) pumped into the lens chamber using single dynamic DCX lens system. ....	74
4.14	Variation in the FOV and focal length as a function of the volume of fluid ( $v_3$ ) pumped-in achieved by using single dynamic DCX lens system. ....	74
4.15	Focal length vs. distance between the first fixed DCX and a second single dynamic DCX lens system. ....	75
4.16	The f-number ( $f_{\#}$ ) and numerical aperture (NA) with respect to the volume of fluid ( $v_3$ ) pumped-in for the single dynamic DCX lens system. ....	76
4.17	(a) Single dynamic lens system, Integrated dynamic lens system with (b) two DCV lenses, (c) three DCV lenses. ....	77
4.18	Series of images captured using single dynamic DCV lens system. ....	78
4.19	Series of images captured using integrated dynamic lens system with (a) two DCV lenses, (b) three DCV lenses at different volumes of fluid ( $v_4$ ) pumped out of each lens chamber of the integrated system. ....	79
4.20	Image of the object captured using integrated dynamic lens system with three DCV lenses. ....	80
4.21	Variation in the focal length and the field of view (FOV) with change in volume of liquid ( $v_4$ ) pumped out of each lens chamber using dynamic lens system with (a) single DCV lens, (b) two DCV lenses, (c) three DCV lenses. ....	81
4.22	Focal length vs. distance between the fixed DCX and dynamic lens system with (a) single DCV lens, (b) two DCV lenses, (c) three DCV lenses. ....	82
5.1	Fabrication steps for variable focal length microlens systems. ....	86

5.2	Mask layout for different dimensions of lens chambers with inlet and spacer with microfluidic channels. ....	87
5.3	Spin curve for coating the HMDS adhesion promoter. ....	89
5.4	Spin curve for coating AZ 4903 resist. ....	89
5.5	Scanning Electron Microscope at IfM. ....	90
5.6	SEM micrographs of the patterned AZ 4903 resist (a) Microfluidic inlet pattern, (b) Close-up of the sidewalls of microfluidic inlet pattern. ....	91
5.7	Step profile of the AZ 4903 pattern measured using surface profilometer (Tencor). ....	92
5.8	Alcatel 601E ICP Etching system. ....	92
5.9	SEM micrographs of the patterns after ICP etching (a) Alignment mark, (b) Close-up micrograph of the ICP etched side wall. ....	94
5.10	Step profile of AZ 4903 after ICP etching process. ....	95
5.11	(a) Lens chamber with fluidic inlet after ICP etching with photoresist, (b) Lens chamber and fluidic inlet after complete ICP etching and removing photoresist. ....	95
5.12	SEM micrographs of (a) Lens chamber with fluidic inlet, (b) Spacer with microfluidic channel and lens chamber. ....	96
5.13	Spin curve to form PDMS membrane. ....	97
5.14	Micro-RIE (Series 800) Instrument from Technics. ....	97
5.15	Fabrication process steps to fabricate flexible PDMS lens membrane. ....	98
5.16	Single variable focal length microlens structures with microfluidic chamber and inlet connection. ....	99
5.17	Fabrication steps for integrated dynamic microlens system with two DCV lenses. ....	100
5.18	Optical images of integrated dynamic microlens system with two DCV lenses. ....	101
5.19	Fabrication process steps for integrated dynamic microlens system with three DCV lenses. ....	102

5.20	Optical images of the integrated dynamic microlens system with three DCV lenses, (a) & (b) Three lens system, (c) Three lens system with syringe used to deflect the lens membranes. ....	103
5.21	3D profile of the PDMS membrane measured using AFM. ....	104
5.22	2D profile of the PDMS membrane measured using AFM. ....	105
5.23	(a) 3D profile of the PDMS surface, (b) 2D profile of the PDMS surface measured using RST. ....	106
5.24	SEM micrograph of the PDMS surface. ....	107
5.25	2D step profile of the PDMS membrane measured using (a) RST, (b) Tencor surface profilometer. ....	108
5.26	UV-Vis spectrophotometer 8453 from Agilent at IfM. ....	110
5.27	Transmittance of 60 $\mu\text{m}$ thick PDMS membrane measured using UV-Vis spectrophotometer. ....	111
5.28	Absorption of 60 $\mu\text{m}$ thick PDMS membrane measured using UV-Vis spectrophotometer. ....	111
5.29	Single variable focal length microlens system with syringe pump. ....	112
5.30	Series of images taken at different volume of fluid by actuating the single variable focal length microlens system as DCX lens. ....	113
5.31	Series of images taken at different volume of fluid by actuating the single variable focal length microlens system as DCV lens. ....	114
5.32	Variation in the focal length and the field of view achieved as a function of the volume of fluid (a) Pumped-in (DCX microlens), (b) Pumped-out (DCV microlens). ....	116
5.33	Focal length vs. distance between the camera and the single variable focal length microlens system as (a) DCX lens, (b) DCV lens. ....	117
5.34	Transmittance characteristics of working fluid (DI water). ....	118
5.35	The setup used to measure transmittance of single variable focal length microlens system. ....	119

5.36	Optical power of the light (with and without variable focal length microlens system) at different wavelengths of light measured using Oriel spectrometer and photodiode. ....	119
5.37	Transmittance characteristic of single variable focal length microlens system filled with DI water without deflecting the PDMS membrane. ....	120
5.38	(a) Contact angle measurement system, (b) Images of the dynamic microlens captured at different volumes of fluid pumped-in. ....	121
5.39	Measured profile of the PDMS membrane of the single variable focal length microlens at different volumes of fluid pumped-in. ....	122
5.40	Contact angle ( $\phi$ ) and radius of curvature ( $R$ ) of the single variable focal length microlens with change in the volume of fluid pumped-in. ....	123
5.41	Comparison of theoretical and experimental values of focal length with change in the volume of fluid pumped into the lens chamber. ....	123
5.42	The f-number ( $f_{\#}$ ) and numerical aperture (NA) of the single variable focal length microlens system with change in the volume of fluid pumped-in. ....	124
5.43	Images of the object captured with integrated dynamic microlens system with two DCV lenses at different volumes of fluid pumped out of the lens chambers. ....	126
5.44	Schematic ray diagram from integrated dynamic microlens system with two DCV lenses. ....	127
5.45	Variation in the focal length and the field of view (FOV) achieved as a function of the volume of liquid ( $v_3$ ) pumped out of each lens chamber of the integrated dynamic microlens system with two DCV lenses. ....	128
5.46	Schematic diagram of the light ray coming at wider angle from the object. ....	129
5.47	Images of the object captured with an integrated dynamic microlens system with three DCV lenses at different volumes of fluid pumped out of the lens chambers. ....	130
5.48	Variation in the focal length and the field of view (FOV) achieved as a function of the volume of liquid ( $v_3$ ) pumped out of each lens chamber of the integrated dynamic microlens system with three DCV lenses. ....	131

5.49	Change in focal length and field of view with the change in volume of fluid pumped out of different integrated dynamic DCV microlens systems. ....	133
6.1	Cross-section of human eye lens. ....	138
6.2	Piezoelectrically actuated micro-pump from Fraunhofer-IMS. ....	140
6.3	3D schematic of the mold to fabricate monolithic wide-angle variable focal length lens system. ....	141
6.4	Fabrication steps for monolithic wide-angle variable focal length lens system. ....	141

## ACKNOWLEDGMENTS

I would like to express my sincere gratitude to my advisor, Dr. Kody Varahramyan for his gracious support and spirited encouragement throughout my graduate study. Dr. Varahramyan initially provided me this great opportunity to pursue my research interests at the Institute for Micromanufacturing (IfM), and it is very fortunate that one finds an advisor who is willing to spare some of his precious time to listen to the minutest problems and obstacles that unavoidably crop up during the course of performing research. His technical and editorial advice was essential for the completion of this dissertation and has taught me innumerable lessons and insights on the workings of academic research in general. It was a good experience to work at IfM, one of the most important research institutes at Louisiana Tech University, over a time period that allowed me to collaborate and learn from many brilliant researchers.

This dissertation could not have been succeeded without my supervisor Dr. Alfred Gunasekaran, who has motivated and supported me throughout my course of research at IfM. Dr. Gunasekaran has played a very significant role in my research and patiently guided me throughout the dissertation process. His creativity and diligence inspired me to give my best efforts to this research. I also thank the other members of my committee namely Dr. Sandra Selmic, Dr. Cheng Luo, Dr. Yuri Lvov, and Mr. Ji Fang for providing many valuable comments and suggestions that improved the presentation and contents of this dissertation.



I would like to thank Mr. Philip Coane for his interest and valuable suggestions throughout my research at IfM. I would also like to thank the other staff members, Jeanette Futrell, Sandy Wilson, Marry Bennett, Scott Williams, Dee Tatum, Karen Xu, John McDonald, Deborah Wood, and Will Chandler at IfM for providing a good working and friendly atmosphere. Experience of working with both faculty and staff members at IfM not only enhanced my intellectual knowledge but will also help me to pursue towards my professional career.

I want to thank my optics research group Partha Dubasi, Jackie Chen, Weisong Wang, Shashi Yaralagadda, and other colleagues and friends at IfM for exchanging views and opinions on various issues throughout this project. The team work helped me to develop my problem solving intellectual by many interesting and good-spirited discussions not only related to this research but also other research projects.

There are several other people whom I would like to thank for their support and encouragement. My roommates Raju Gottumukkala and Vinay Mannava provided me much-needed support during a variety of deadline crunches. My friends Olga Nikonova, Aravind Chamarti, Rajendra Aithal, Rajneek Khillan, Jeevan Vemagiri, Jayaram Sermadevi, Mallikarjuna Kamavaram, Rohit Srivastava, Mukesh Sharma, Atul Sharma, Jitender Pal Bhaudal, Gurjeet Singh, Vishal Bhasin, Shruti Gangadhar, Christy Pitre, Holly Pitre, Kara Hare, Defi Qi, Ritu Tuladhar, and Pragati Kansakar supported and encouraged me throughout my studies here at Louisiana Tech University. I would also want to give my special thanks to Preetam Thoshniwal, Rahul Agarwal, Dinesh Sharma, Surender Sharma, Mahesh Kulkarni, Sharath Duvva, Mallika Reddy and Suparna Varma for their cheering support.

I would also like to thank Rajeev Agarwal, Amrit Pal Singh, G. D. Agarwal, and Shyamlal Gupta for their soothing support throughout my undergraduate and graduate studies.

Finally my parents, Jagdish Prasad Agarwal and Chawali Devi receive my deepest gratitude for their blessings, never ending love, encouragement and moral support right from my childhood which is the foundation of this work. I would like to give my best regards to my brother Arvind Kumar Agarwal and Vikas Agarwal for their support and wish them good luck for their upcoming future.

I would like to acknowledge the financial support provided by Defense Advanced Research Project Agency (DARPA) contract BAA 01-42 # 427 for this research.

At last but not the least, I am grateful to the God for being with me throughout the difficult times, and helping me to reach this goal.

# CHAPTER 1

## INTRODUCTION AND OBJECTIVES

### 1.1 Introduction

In research institutes and industries, miniaturization techniques have resulted in the development of higher-speed, lower-cost, higher-efficiency, and high-capacity devices. Since the 1980's, the principles and fabrication methods of micron-scale devices called MicroElectroMechanical Systems (MEMS) have been constantly developed [1-5]. These devices are miniaturized systems that consist of some dynamic system along with an integrated electronic circuitry for controlling the dynamic system [6-12]. The electronics involved in MEMS are fabricated using IC process sequences (like CMOS or BiCMOS). The micromechanical components are fabricated by simple modification of the standard IC manufacturing processes and use of compatible micromachining processes that either selectively etch away parts of the silicon wafer or add new structural layers to form the mechanical and electromechanical devices [1-6,13].

The applications of MEMS devices have reached into many fields like implantable biomedical devices, automotive applications such as airbag accelerometers and actuators for automobile brakes and suspension systems, micro-pumps, micro-thermal actuators, chemical, pressure and flow sensors, and passive liquid flow devices

such as micro-filters and micro-valves [14-23]. At present, the development of micro-optical devices using various microfabrication techniques encompasses one of the most prominent areas of extensive research.

The development of advanced micro-optical devices is essential for high performance electro-optical imaging systems [25-27]. These systems require a number of miniature mechanical and optical components, and they are useful for a number of domestic and military applications [26-28]. Optical systems often require a focal length to be variable which allows the field of view or the magnification to be altered and to focus on objects which are in motion or irregular in shape. The variable focusing mechanisms adapted for these optical systems are complicated and use many gears, motors, and sliders [29-30]. Because conventional optical elements, such as lenses and mirrors, are devoid of variable focusing mechanism, this phenomenon is achieved by moving the optical elements. In contrast, biological vision systems are much more compact as the tuning and adjustments of focal length are achieved by dynamically changing the shape the lens. Optical systems, with dynamically variable focal length lenses, can be applied to a wide range of optical imaging applications such as components for optical communication, biomedical instruments, digital cameras, camera phones, endoscopes, home security systems, optical storage drives, micro-air vehicles (MAVs), biomedical diagnostic and surgical devices, vertical scanners, optical holography devices, surveillance systems and other diverse micro-optical systems [31-33]. In the medical field, variable focal length microlens systems are ideal for advanced bioanalytical and surgical instruments and can have potential use in genomics and proteomics as well as high-throughput clinical applications [34]. The ever-increasing

demand for functional optical systems for aerial imaging and surveillance requires highly compact optical devices that can provide both wide field of view (FOV) and dynamically varying focal lengths [35,36].

An approach to looking at how nature has successfully solved similar problems, such as dynamic focusing mechanism in visionary systems found in very small creatures, could help better understand and apply these features in the present technology of optics. It has been demonstrated that many of the complex visionary features found in bio-optical systems arise from two main characteristics: the existence of a gradient of refractive indices (GRIN - symmetric variation of the refractive index within the bulk material) in the lens and the ability of the lens to change its shape dynamically [37-39]. The GRIN lenses in biological systems consist of a large number of protein layers which exhibit a variation of the index of refraction [38-40]. The large number of protein layers together with the contracting behavior of the eye lens provide exceptional degree of vision that is required to adjust for near and far focus [40]. From the fact that the eye of a fish is capable of viewing objects at 180 degrees [41], artificial wide-angle lenses were manufactured and named “fish-eye” lenses. The available fish-eye lens systems that can provide a wide FOV contain multiple lenses which are made according to tight specifications [42]. Recently, several different configurations and models for the fisheye lens systems have been reported and are being investigated for commercial applications. But, the fabrication methods of fisheye lenses still remain tedious, complicated, and expensive [43-45].

On the other hand, bio-vision systems found in nature, like the human eye, are single miniaturized lens systems, yet they display very complex and remarkable visual

acuity such as high resolution, large field of view (FOV), focusing ability, color detection, and a very large dynamic range to see both far and near objects. The human eye consists of a flexible lens for focusing, a variable pupil (iris) for fast sensitive adoption, and the retina as the image detector. The FOV view for the human eye approximates an ellipse about  $150^\circ$  high by about  $210^\circ$  wide [37-39].

Today's micro-optical design and manufacturing lack the advantages and efficiency of bio-visionary systems such as the human eye. As these design and manufacturing techniques are closely tied to ideas, concepts, and technology developed for the semiconductor industry, which includes a general restriction to flat building parts (planar lens and receptor array), matrix-oriented patterning (Cartesian coordinates), and pure bulk materials (very limited possibility of index modification) [37]. Diffractive, refractive, and graded index lenses are the three main types of microlenses which are commercially available [37]. Although graded lenses (GRIN) are well suited for imaging tasks, the difficult fabrication process severely limits the assortment of commercially available graded index lenses. GRIN lenses have been fabricated by a number of methods including printing and electrophoresis [46-49]. It should be noted that, until now, no successful research on the fabrication of GRIN lens structure that can mimic bio-optic systems is reported. On the other hand, diffractive microlenses are generally not well suited for imaging tasks as their focal length and efficiency strongly depend on the wavelength of the light and limit the lenses to monochromatic application [50]. Refractive lenses that can be used for imaging tasks are generally manufactured using resist reflow or melting resist and replication techniques [50-53]. However, these refractive lenses have limited FOV and do not have dynamic features like the human eye.

At present, efforts are being made to mimic the bio-vision systems found in living creatures and to develop artificial bio-inspired optical lens systems [38-40]. Even the development of an artificial optical system which can mimic the human eye and dynamically change its focal length is being pursued extensively. The optical lens systems that are controlled by fluid, electric, and mechanical actuation to provide variable focal length have been reported by number of groups [54-64]. The phenomenon of electrowetting is also utilized for the fabrication of dynamic lens systems that can exhibit variable focal length [54-57]. Another notable system employs birefringent nematic liquid crystal molecules to dynamically change the refractive index  $n$  and focal length values by applying electric fields [58-61]. The fluid controlled lens systems also contain a lens chamber with channels to pump optical fluids to change the radius of curvature of the thin diaphragm and in turn change the focal length of the resulting lens [63-65].

The variable focal length lenses reported to date either involve expensive and complex fabrication processes, limited range of tunable focal length, or are not capable of achieving wide FOV. The features and limitations of these lenses are discussed in detail in Chapter 2.

## **1.2 Objectives**

The main objective of this research work is to design, fabricate, and test a novel polymer-based wide-angle microlens system which can dynamically vary its focal length and field of view. The need for the proposed research is based on the necessity of having a compact optical lens system which has both dynamically variable focal length and a wide FOV. This research work focuses on fabricating a cost-effective, compact, non-mechanical dynamic microlens system. The fabrication of a dynamic microlens system,

presented in this research work, involves standard photolithography and silicon micromachining techniques which make the system more adaptable for current industrial applications. A fluid actuation mechanism is used to vary the curvature of the lens membrane which produces the change in focal plane and FOV. The advantage of using fluid actuation mechanism is discussed in Chapter 2. The final goal of this work is to design and fabricate an integrated wide-angle dynamic microlens system which can provide both wide FOV and large tunable range of focal length. Wide FOV and the tunability of focal length of the lenses are desirable for both civilian and military applications such as optical recording for surveillance and inspection.

### **1.3 Dissertation Overview**

The second chapter discusses the fundamentals of light and optics for better understanding of the optical systems. This chapter also focuses on the attempts made by different research groups to fabricate bio-inspired optical lens systems and the limitations of various approaches. The needs for wide angle optical lens systems are also explored in this chapter.

The third chapter demonstrates the initial design and experiments implemented using static glass lenses to obtain wide FOV. The results obtained from these initial experiments are also discussed in this chapter.

The fourth chapter discusses the design and fabrication of polymer-based macro-scale variable focal length lens system. The fabricated lenses are tested by implementing the design explored in third chapter.

The fifth chapter discusses the design and fabrication of polymer-based wide-angle variable focal length microlens systems. The imaging characteristics and optical



performance of the fabricated variable focal length microlens systems are also demonstrated and discussed in this chapter. The relation between the focal length of the single variable focal length microlens with respect to the FOV has been studied, and integrated dynamic microlens systems with two or three DCV lenses are fabricated and tested for their optical performance to have both wide FOV and dynamic focal length features. Finally, the sixth chapter includes a summary of the results and suggestions for future work.

## **CHAPTER 2**

### **LITERATURE REVIEW**

#### **2.1 Fundamentals of Light and Optics**

The earliest human experiences with light and optics were of the natural world: sunlight, fire, and the reflective and refractive (light bending) properties of water, crystals, and other naturally occurring substances. The origin of light has captured the imagination of many scientists since the inception of hypothetical as to what is the mechanism to explain the function and to extrapolate a theory of light. In the late 1600s, important questions were raised, asking if light is made up of particles or waves. Some scientists like Christiaan Huygen believed that light is made up of waves vibrating up and down perpendicular to the direction that the light travels. According to Huygen's theory, the light waves traveling in a vacuum or other uniform mediums are spherical and advance or spread out as they travel at the speed of light. This theory explains why light shining through a pin hole or slit will spread out rather than in a straight line. But, Sir Isaac Newton rejected the wave theory and held that light is made up of tiny particles. Newton's theory came first, but Huygen's theory described early experiments. It was only at the beginning of the 19<sup>th</sup> century that the wave nature of light was firmly proved by Thomas Young. According to studies conducted by Young, light emerging from two slits spread out according to Huygen's principle and produced interference patterns. Latter in

1815, Augustin Fresnel supported Young's experiments with mathematical calculations. Then, in 1900, Max Planck, who was working on electricity and magnetism, formulated mathematical equations and proposed the existence of a light quantum, a finite packet of energy. Following him, in 1905, Albert Einstein proved that light travels in discrete bundles of energy called photons. According to his theory, light travels at a fixed speed in vacuum without requiring any supporting medium which led to the discovery of lasers. Therefore, light can thus be regarded as a wave when it propagates and as particles when it is observed or emitted (dual nature of light) [66].

The first property of light is reflection from a surface, such as that of a mirror. This property is illustrated in Figure 2.1. Reflection of light occurs when the light encounters a boundary that does not absorb the radiation's energy, but instead bounces the light off its surface. In such cases, the incoming light ray is referred to as an incident ray, and the ray that is bounced from the surface is called the reflected ray [67,68].

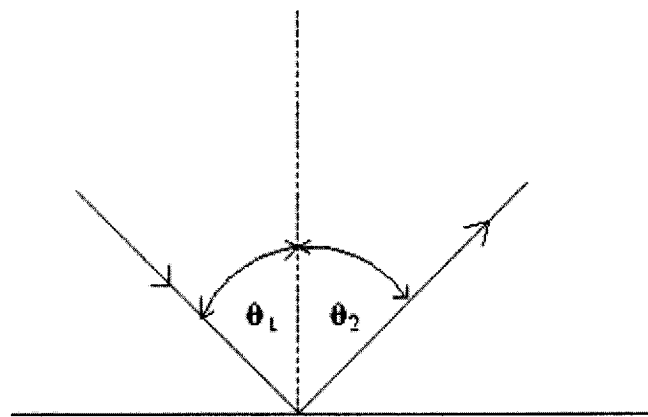


**Figure 2.1: Reflection of light ray from a smooth surface.**

The law of reflection states that, when light is reflected off any surface, the angle of incidence  $\theta_1$  is always equal to the angle of reflection  $\theta_2$ . The angles are always

measured with respect to the normal line drawn to the surface. The law of reflection is consistent with both particle and wave theories of light [67,68].

Refraction is the bending of light as it travels from one medium to another medium of different density. The change in speed and wavelength at the boundary between two mediums causes light to change direction, as shown Figure 2.2. Different optical materials are characterized by the term, index of refraction. Index of refraction ( $n$ ) of a material is the ratio of the speed of light in a vacuum ( $c$ ) to the speed of light in that material ( $v$ ) which is given by the formula in Equation 2.1 [67].

$$n = \frac{c}{v} \quad (2.1)$$

The speed of light in a particular material depends upon the density of that material such that the more dense the material, the slower the speed of light in that material. Thus, the index of refraction of any material is greater than one and increases with increasing density. The frequency of light does not change when it passes from one medium to another, but the wavelength changes according to the formula given in Equation 2.2, where  $v$  is velocity,  $\lambda$  wavelength, and  $f$  is the frequency of light [67]. This can be illustrated from Figure 2.2, where each of the lines represents a wave form corresponding to a peak of the wave. The index of refraction can therefore be written in terms of wavelengths as given in Equation 2.3 [67], where  $\lambda$  is the wavelength of light in vacuum and  $\lambda_n$  is the wavelength of light in the material.

$$v = \lambda f \quad (2.2)$$

$$n = \frac{\lambda}{\lambda_n} \quad (2.3)$$

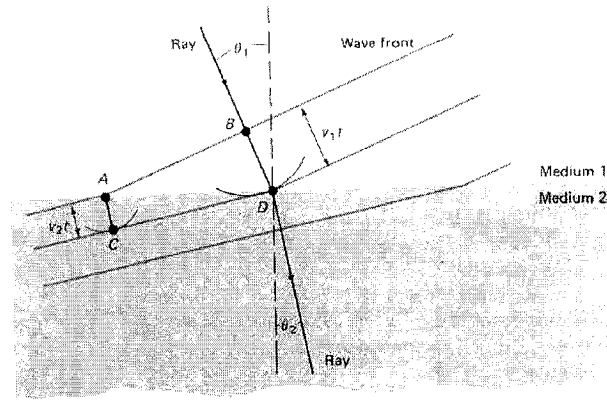


**Figure 2.2: Refraction from Huygen's principle [67].**

The angle at which refracted light travels depends upon both the angle of incidence and the composition of the medium into which it is entering. Light passing into the boundary at an angle to the normal is refracted according to Snell's Law given in Equation 2.4, where  $n_1$  and  $n_2$  are the refractive indices of medium 1 and medium 2, respectively, and  $\theta$  symbolizes the angles of light traveling through these mediums with respect to the normal [67-69].

$$\frac{n_1}{n_2} = \frac{\sin \theta_2}{\sin \theta_1} \quad (2.4)$$

There are several important points that can be drawn from Equation 1.4. When  $n_1$  is greater than  $n_2$ , the angle of refraction is always smaller than the angle of incidence. Alternatively, when  $n_2$  is greater than  $n_1$ , the angle of refraction is always greater than the angle of incidence. When the two refractive indices are equal  $n_1 = n_2$ , then the light is passed through without refraction [67-69].

In optics, one can separate the field into two different types of optical elements, refractive and diffractive elements. Diffractive optical elements (DOEs), which work on the principle of diffraction of light, change the way light propagates and can perform very complex tasks [70]. They can split an incident beam into any number of outgoing, and

possibly focused, beams (fan-out). On the other hand, refractive optical elements such as lenses or prisms, which work on the principle of refraction, focus or redirect the incoming light. The design freedom for DOEs is much higher compared with refractive optical elements, as almost any optical function can be realized with DOEs [70]. In some areas like focusing and redirecting the light, there exist equivalent refractive and diffractive elements which have the same optical function. The decision to choose refractive or diffractive elements depends on many parameters [50]. But, one can roughly say that DOEs are mostly used for monochromatic applications, such as laser lights, as DOEs have a strong wavelength dependency, which is not the case for refractive optical elements [50,71-73]. The most widely used refractive optical elements are shown in Figure 2.3 [74]. The development of optical devices using lenses dates to the 16<sup>th</sup> and 17<sup>th</sup> centuries, although the earliest record of eyeglasses dates from the late thirteenth century. Presently, the use of lenses can be found in many applications such as eyeglasses, cameras, magnifying glasses, telescope, binoculars, microscopes, and medical instruments.

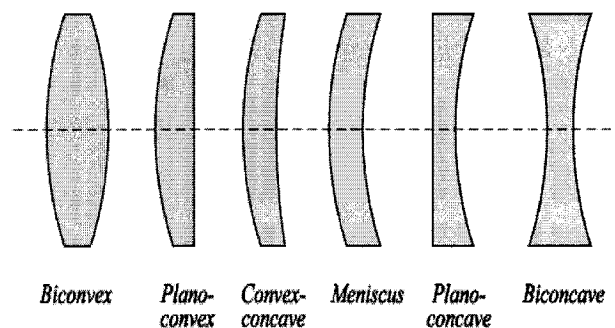


**Figure 2.3: Refractive optical elements [74].**

This research work focuses on fabrication of variable focal length lenses which can be actuated as double concave or double convex lenses, therefore, a detailed study of

these types of lenses has been demonstrated here in this section. Double convex (DCX) and double concave (DCV) lenses are the most important refractive elements used in daily life. The DCX lenses are called converging lenses as they converge and focus incoming light rays. The behavior of two incident rays approaching parallel to the principal axis of a DCX lens is shown Figure 2.4. The point at which the parallel rays converge is known as the focal point of the lens.

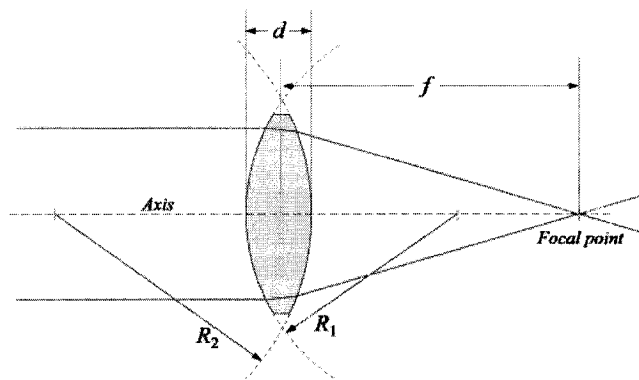


**Figure 2.4: Schematic of converging lens (double convex) [74].**

#### Refraction Rules for a Converging Lens [75]

- Incident rays traveling parallel to the principal axis of a converging lens will refract through the lens and travel through the focal point on the opposite side of the lens.
- Incident rays traveling through the focal point on the way to the lens will refract through the lens and travel parallel to the principal axis.
- Incident rays which pass through the center of the lens will in effect continue in the same direction.

The DCV lenses are called divergent lenses as they diverges incoming light rays. The behavior of two incident rays approaching parallel to the principal axis of the double concave lens is shown Figure 2.5 [74]. As in the case of a DCX lens, light bends towards

the normal when entering but bends away from the normal when exiting the lens because of the different shape of the double concave lens. For this reason, a double concave lens can never produce a real image; it produces virtual images. If the refracted rays are extended backwards behind the lens, they will intersect at a point. This point is known as the focal point. It should be noted that a diverging lens does not really focus the light rays which are parallel to the principal axis; rather, it diverges these light rays. For this reason, a diverging lens is said to have a negative focal length.

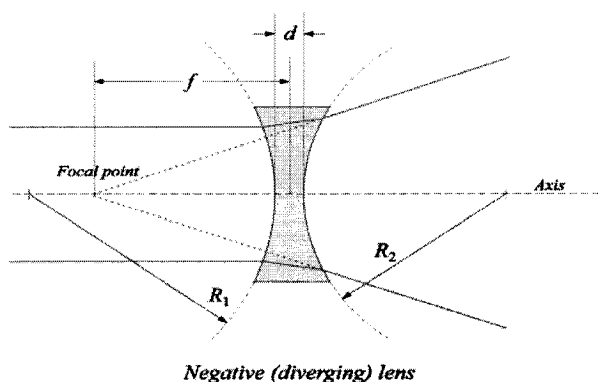


**Figure 2.5: Schematic diagram of diverging lens (double concave) [74].**

#### Refraction Rules for a Diverging Lens [75]

- Incident rays traveling parallel to the principal axis of a diverging lens will refract through the lens and travel in line with the focal point (i.e., in a direction such that its extension will pass through the focal point).
- Incident rays traveling towards the focal point on the way to the lens will refract through the lens and travel parallel to the principal axis.
- Incident rays which pass through the center of the lens will in effect continue in the same direction.



## 2.2 Focal Length Calculations

Ray diagrams, according to the refraction rules for converging and diverging lenses, provide useful information about object-image relationships, yet they fail to provide the information in a quantitative form. While a ray diagram may help to determine the approximate location and size of the image, it will not provide numerical information about image distance and object size. To obtain this type of numerical information, it is necessary to use the lens equation. The lens equation expresses the quantitative relationship between the object distance ( $d_o$ ), the image distance ( $d_i$ ), and the focal length ( $f$ ) as given in Equation 2.4 [68].

$$\frac{1}{f} = \frac{1}{d_i} + \frac{1}{d_o} \quad (2.4)$$

To derive Equation 2.4, consider the schematic of the two rays passing through the DCX lens as shown in Figure 2.6, where  $h_o$  and  $h_i$  refer to the heights of the object and image, and  $d_o$  and  $d_i$  are the distances from the lens.

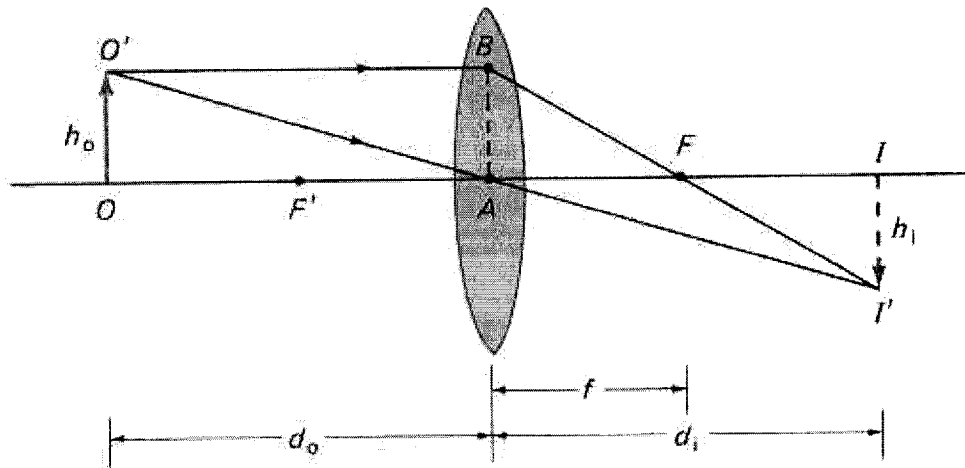


**Figure 2.6: Schematic of converging lens to derive lens equation [68].**

In Figure 2.6, it can be noted that the triangles  $F'I$  and  $FBA$  are similar and triangles  $OAO'$  and  $IAI'$  are similar; therefore

$$\frac{h_i}{h_o} = \frac{d_i - f}{f} \quad (2.5)$$

$$\frac{h_i}{h_o} = \frac{d_i}{d_o} \quad (2.6)$$

From Equations 2.5 and 2.6, the formula for focal length calculation given in Equation 2.4 using object and image distance can be computed.

The focal length from the radii of curvature of the two surfaces of the lens can be calculated using the lens-maker's equation (frequently used to calculate the focal length of the optical lenses fabricated in this research). The lens-maker's equation can be derived directly using Fermat's principle [68]. Considering the paths of light rays from object to image intersecting at the principal plane, because all these paths are equivalent, then all paths have the same optical path length. That is, the path is stationary with respect to the intersection point on the principal plane.

The optical path from the object to the sphere touching the lens and from the image to the sphere touching the lens is same for all paths. The optical path has three components: from the sphere about the object to the plane touching the centre of lens, length  $d_o$ ; from the plane touching the other side of the centre of the lens to the sphere about the image, length  $d_i$ ; the region of thickness  $t_0$  about the principal axis with refractive index  $n$  [76]. Therefore, the optical path length  $L_1$  along the axis is given by Equation 2.7, and the optical path length  $L_2$  of the hypothetical ray passing through the lens at height  $h$  is given by Equation 2.8, where  $t$  is the thickness of the lens at height  $h$  [76].

$$L_1 = d_i + d_o + t_0(n - 1) \quad (2.7)$$

$$L_2 = d_i + d_o + \left( \frac{1}{d_i} + \frac{1}{d_o} \right) \frac{h^2}{2} + t(n-1) \quad (2.8)$$

The optical path length difference  $\Delta L$  between the two rays which is equal to zero is given by Equation 2.9.

$$\Delta L = (t_o - t)(n-1) - \left( \frac{1}{d_i} + \frac{1}{d_o} \right) \frac{h^2}{2} = 0 \quad (2.9)$$

For spheres with radius  $R_1$  and  $R_2$  which form the DCX lens,  $t_o$  and  $t$  can be given as

$$t_o - t = \frac{h^2}{2} \left( \frac{1}{R_1} - \frac{1}{R_2} \right) \quad (2.10)$$

Substituting Equation 2.10 in Equation 2.9, we get

$$\left( \frac{1}{R_1} - \frac{1}{R_2} \right) \frac{h^2}{2} (n-1) - \left( \frac{1}{d_i} + \frac{1}{d_o} \right) \frac{h^2}{2} = 0 \quad (2.11)$$

$$\Rightarrow \left( \frac{1}{d_i} + \frac{1}{d_o} \right) = (n-1) \left( \frac{1}{R_1} - \frac{1}{R_2} \right) \quad (2.12)$$

$$\Rightarrow \frac{1}{f} = (n-1) \left( \frac{1}{R_1} - \frac{1}{R_2} \right) \quad (2.13)$$

For DCX lens  $R_1 > 0$  and  $R_2 < 0$

For DCV lens  $R_1 < 0$  and  $R_2 > 0$

Equation 2.13 is known as the lens-maker's equation and the focal length can be calculated using this equation if the radii of curvature of the lens are known. For thick lenses, the formula for focal length calculation is given by Equation 2.14, where  $d$  is the thickness of the lens between the principal planes of the lens [76].

$$\frac{1}{f} = (n-1) \left( \frac{1}{R_1} - \frac{1}{R_2} \right) + \frac{d(n-1)^2}{nR_1R_2} \quad (2.15)$$

### 2.3 Lens Aberrations

In Section 2.1, it was demonstrated that all rays from each point of an object are brought to a single point as the image. This conclusion was based on approximations such as that all rays make small angles with one another and that we can use  $\sin \theta \approx \theta$ . This approximation leads to the deviation from simple theory and is referred to as lens aberrations. The aberrations which occur from monochromatic light are referred to as monochromatic aberrations. The most important monochromatic aberrations are spherical, astigmatism, coma, curvature of field, and distortions [66-68].

*Spherical Aberration:* For lenses made with spherical surfaces, rays which are parallel to the optic axis but at different distances from the optic axis fail to converge to the same point, as shown Figure 2.7. This type of aberration is called spherical aberration and cannot be eliminated for a single lens [66-68].

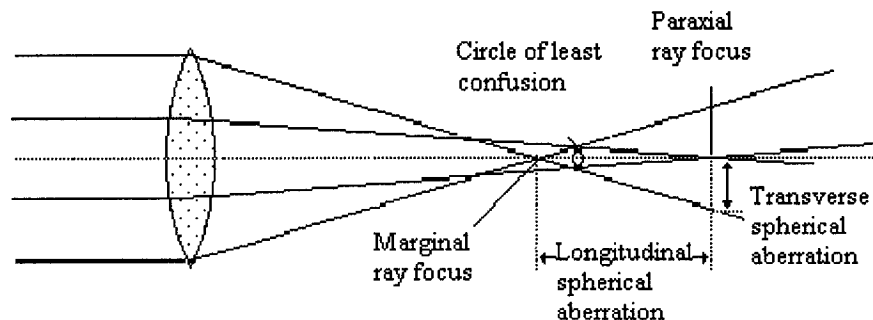


**Figure 2.7: Schematic diagram to show spherical aberration [77].**

*Coma Aberration:* Coma is an aberration which causes variation in magnification of off-axis rays, resulting in an object point blurred into a cone shape image, as shown in Figure 2.8. A lens with considerable coma may produce a sharp image in the center of the field, but become increasingly blurred toward the edges. For a single lens, coma can be

partially corrected by bending the lens. More complete correction can be achieved by using a combination of lenses symmetric about a central stop [66-68].

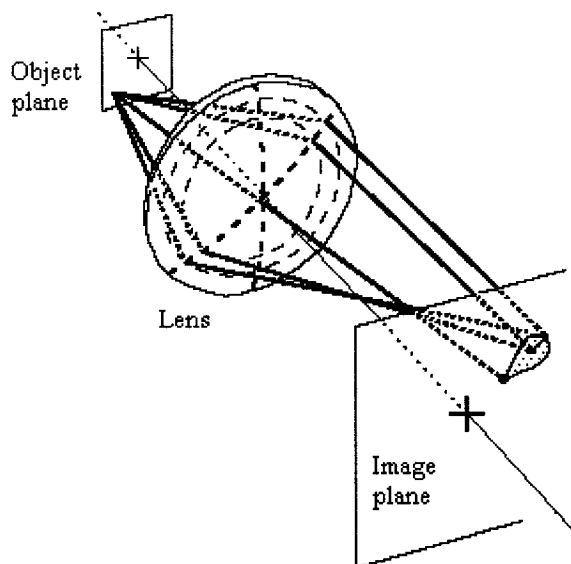


**Figure 2.8: Schematic diagram to show coma aberration [77].**

*Astigmatism Aberration:* Astigmatism arises when a cone of rays from a point off-axis strikes the lens asymmetrically, resulting in an image at two different focal planes, as shown in Figure 2.9. At the nearest point to the lens, the image of the point appears as a horizontal line; moving farther away it appears as an ellipse, then a circle, then an ellipse, and finally as a vertical line [66-68].

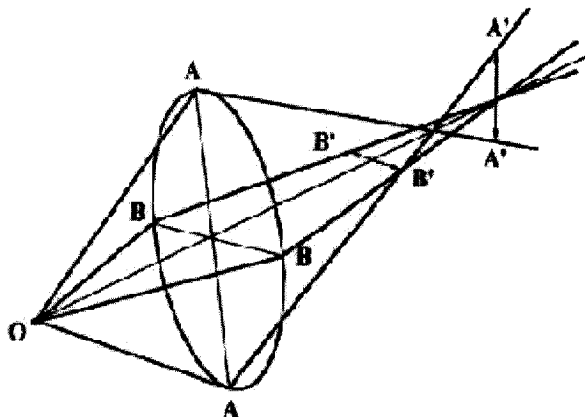


**Figure 2.9: Schematic diagram to show astigmatism aberration [78].**

*Field Curvature Aberration:* Field curvature arises when off-axis image points do not fall on a flat plane but on a curved surface, as shown in Figure 2.10. The field curvature aberration is obviously a problem in cameras and other devices where the film is placed in a flat plane [66-68].

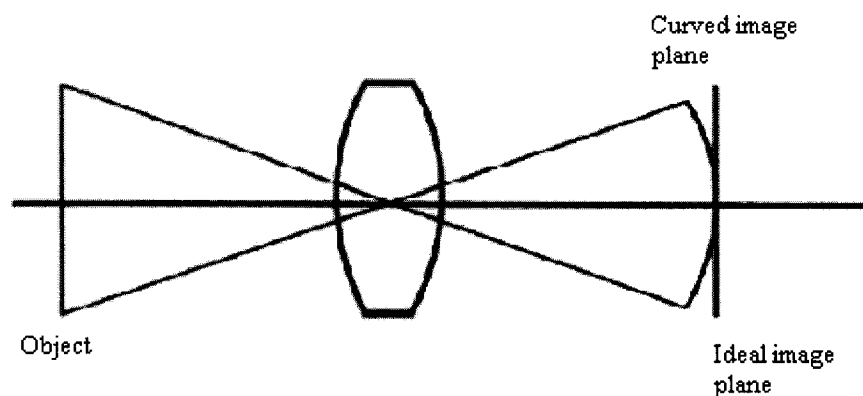


**Figure 2.10: Schematic diagram to show field curvature aberration [78].**

*Distortion Aberration:* Distortion is a result of variation of magnification at different distances from the lens axis [66-68,79]. Thus, a straight line object not passing through the axis may form a curved image. An example of distortion is shown in Figure 2.11 where a square grid of lines gets distorted to produce “pincushion distortion” or ‘barrel distortion”.

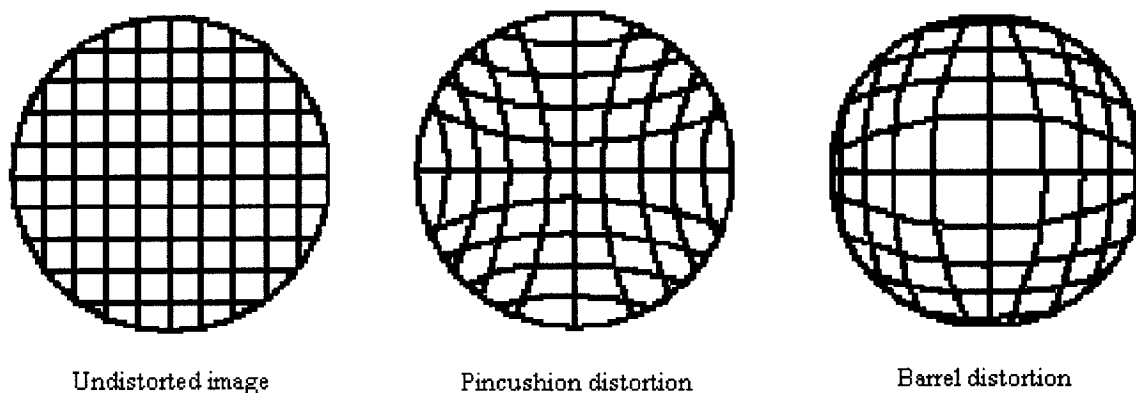


**Figure 2.11: Schematic diagram to show distortion aberrations [78].**

*Chromatic Aberration:* This type of aberration is associated with chromatic light. For example, when the white light rays are focused through the lens, they get distorted, as shown in Figure 2.12. This aberration arises because of dispersion – the variation of index of refraction with respect to wavelength [66-68].

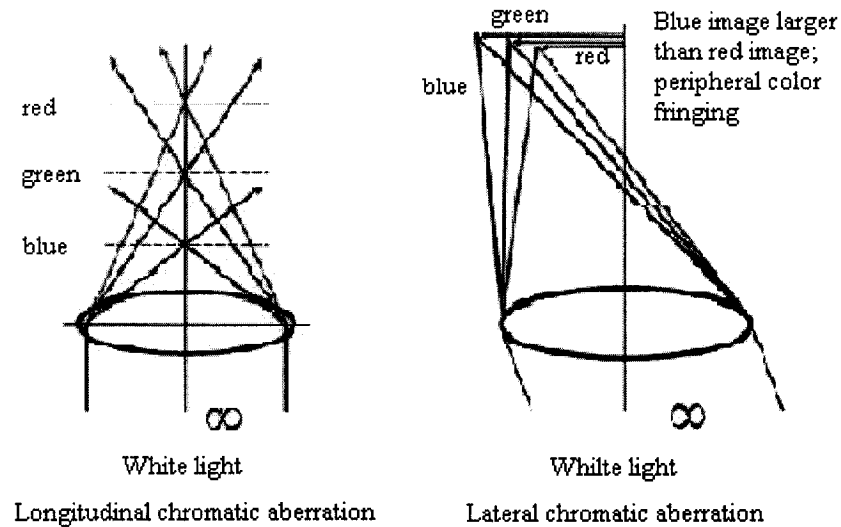


**Figure 2.12: Schematic diagram to show field chromatic aberration [78].**

The aberration can be minimized by choosing the following lens parameters [78]:

- Appropriate lens contour - e.g., spherical versus aspherical (to reduce spherical aberrations).
- Lens material - transmission, index of refraction, dispersion.
- Lens shape - ratio of curvature of two surfaces of the lens.
- Focal length – measure of refractive power of lens.
- Diameter – measure of light gathering power and thickness of the lens.
- f-number- ratio of focal length to diameter, a measure of limiting resolution and image brightness.
- Assembly of two or more single lens elements reduces the net aberration of the image.

## **2.4 Glass vs. Plastic Lenses**

Lenses made of glass or plastic have their own advantages and disadvantages as the properties of glass materials are different from plastic materials. One of the advantages of lenses made using glass is the availability of hundreds of glass material with good optical properties. The choices for plastic material with good optical properties are limited [80,81]. However, plastic lenses offer other design freedoms that are not achievable or economical with glass lenses [82,83]. Several import factors which make the use and manufacturing of plastic lenses more advantageous over glass lenses are as follows [84]:

- The injection molding process makes it feasible and economical to produce more sophisticated optical shapes such as aspherical and diffractive surfaces in plastic.
- Plastic materials are lighter in weight and are more shatter-resistant which makes the head-worn optics such as head-mounted displays more compatible and lightweight.
- Integral mounting for most of optical application can be achieved with plastic lenses. With glass lenses, it is done with separate mechanical mounting hardware.
- Plastic lenses can be made with more consistent quality as they are made from the same mold cavity.

The major drawbacks of plastic lenses are material related as:

- Plastic materials are more sensitive to environment changes such as temperature and humidity.
- Plastic lenses are the material flow pattern and shrinkage during the molding process limits their surface efficiency.



- The chemical properties of the available plastic materials limit the performance of the optical coating and use of lenses in chemical labs [82].

Currently, polymethacrylic resin (PMMA) and polycarbonate resins are mainly used for optical applications. However, these resins also have disadvantages such as high moisture absorption and high heat expansion [85]. Therefore, intensive research is being carried out to find inert polymer elastic material with good optical properties that can be used to manufacture optical elements useful in daily life and also in harsh environments [86].

### **2.5 Soft and Flexible Polymer Materials for Optical Applications**

Recent studies have focused on mechanical, optical, electrical, and chemical properties and the fabrication techniques of elastic polymers [87-95]. Elastic polymers and soft materials are extremely important in today's manufacturing environment to produce cost-effective and user-compatible optical elements [90-95]. Presently, flexible polymer materials are intensively used for the manufacturing of contact lenses [96]. These contact lenses are usually made of water (60%) and acrylic polymer (40%) such as hydrogel polymer and hydroxyethylmethacrylate (HEMA) [96]. The softness and flexibility of a soft contact lens is the result of the absorption of water which is held by the lens's polymer material. It should be noted that, when soft lenses begin to dry out (lose some of their absorbed water), they become less soft and less flexible. In other part of research, scientists at the Veterans Affairs (VA) Hospital and Washington University School of Medicine in St. Louis have developed a gel-like flexible polymer material that eventually could be used to replace diseased and aging lenses in the eye of patients with cataracts [97].

Polydimethylsiloxane (PDMS) is another commercially available soft and flexible material that has received an increasing amount of attention from researchers as it provides several major advantages that are not immediately available in traditional glasses, plastics, and other flexible polymer materials [98,99]. PDMS has been intensively used in a wide range of applications from contact lenses and medical devices to elastomers, lubricating oils and heat-resistant tiles [99,100]. The use of PDMS can also be found in other applications such as cosmetics, construction sealants, oxygen permeable membranes, biomedical implants, and drug delivery systems because of its bio-compatible nature [100-103]. PDMS is a flexible polymer with low glass transition temperature, very low surface energy, low gas permeability, good thermal stability, and biocompatibility [104,105]. Some physical and chemical attributes of PDMS compared to other polymers include, a low glass transition temperature ( $T_g \approx -125\text{ }^\circ\text{C}$  [105]), small temperature variations of the physical constants (except for thermal expansivity,  $\alpha \approx 20 \times 10^{-5}\text{ K}^{-1}$  [106]), high dielectric strength ( $\sim 14\text{ V m}^{-1}$  [106]), usability over a wide temperature range (at least from  $-100\text{ }^\circ\text{C}$  up to  $+100\text{ }^\circ\text{C}$  [107]), a unique flexibility (the shear modulus  $G$  may vary between 100 kPa and 3 MPa [105]), very low loss tangent ( $\tan\delta \ll 0.001$ ), low chemical reactivity (except at extremes of pH), and an essentially non-toxic nature. PDMS elastomers have a unique flexibility with a shear elastic modulus  $G \approx 250\text{ kPa}$  and exhibit low change in the shear elastic modulus with temperature ( $1.1\text{ kPa }^\circ\text{C}^{-1}$ ). PDMS also exhibits exceptionally low optical attenuation which is an extremely useful property apart from being flexible for the fabrication of optical elements.

PDMS materials also exhibit excellent adhesion to many surfaces (single crystal silicon, silicon dioxide, silicon nitride, glass, and other PDMS) at room temperature upon contact [107]. The surface of PDMS can be rendered hydrophilic by oxygen plasma resulting in two robust characteristics: (1) repeated cycles of bonding-debonding do not alter the adhesion energy; (2) even when particles or contaminants are present, the PDMS components can be cleaned (e.g., using acetone, alcohol, and DI water), dried, and re-used with the same surface energy.

Because PDMS exhibits cleanroom processability, low curing temperature, high flexibility, low optical attenuation, and a bio-compatible nature, it is selected for the work presented in this dissertation to fabricate a flexible membrane for the proposed optical lens system.

## **2.6 Fish-Eye and Wide Field of View Lenses**

Conventional single lenses do not have the ability to image objects at a large field of view (FOV) [50]. Present research in optical fields is focusing on designing and manufacturing wide FOV optical lens systems which can be applied in a broad range of applications such as medical instrumentation, endoscopic surgeries, microscopes, conventional all-sky imaging, and security and surveillance cameras [108-111]. Wide angle lenses are generally termed as “fish –eye” (a fish has 180 degree FOV). The term fish-eye was first originated in *Physical Optics* published in 1911 by Robert W. Wood, in the context of a discussion about the refraction of light and the refraction of rays entering the level surface of a pond [41]. In his book, Wood describes a water-filled pinhole camera (his “fish-eye” camera, dimensions - 12x12x5 cm with a hole of 3 cm in diameter) with 180 degree FOV that is capable of simulating the fish-eye view of the

world. Figure 1.13 shows one of the views captured from the water-filled camera pointing in the horizontal direction. This view corresponds to what a fish would see when looking out through the side of the aquarium.



**Figure 2.13: Fish-eye view from the water-filled camera [41].**

The first real fish-eye glass lens was manufactured in 1924 by R. Hill, and his design was found to be useful to many meteorologists for all-sky photography [42]. A fish-eye lens generally has a front lens group of a far greater negative refractive power than that of an ordinary inverted telephoto type wide-angle lens because a fairly large back focal distance, relative to the focal length of the whole lens system, is required for avoiding an increase in the size of the lens system [42-45]. The extreme power distribution of these lenses causes field curvature and astigmatism in the transmitted image. Improvement of astigmatism and field curvature has been generally attempted by providing, at the image side of the aperture stop, at least one doublet composed of a positive lens element of a low-refractive-index-low-dispersion glass and a negative lens element of a high-refractive-index-high-dispersion glass with a cemented intermediate surface of a suitable negative refractive power [42]. Fish-eye lenses for 35 mm photography are typically found in two classes [42]:

- *Full frame fish-eye lenses* capture a hemispherical image across the diagonal of the 35 mm frame. These lenses range in focal length from 14-16 mm and have a ratio of back focal distance to effective focal length of 2.2 to 2.4.
- *Circular image (hemispherical) fish-eye lenses* capture a full 180 degrees within the narrow height of the 35 mm film frame. The lenses in this class have effective focal lengths ranging from 6 to 8 mm and have a ratio of back focal distance to effective focal length of 4.55- 4.75.

The layout of a full frame fish-eye lens manufactured by Coastal Optical Systems, Florida, is shown in Figure 2.14. The total length of this lens is 16 mm with 9 optical elements forming 6 groups.

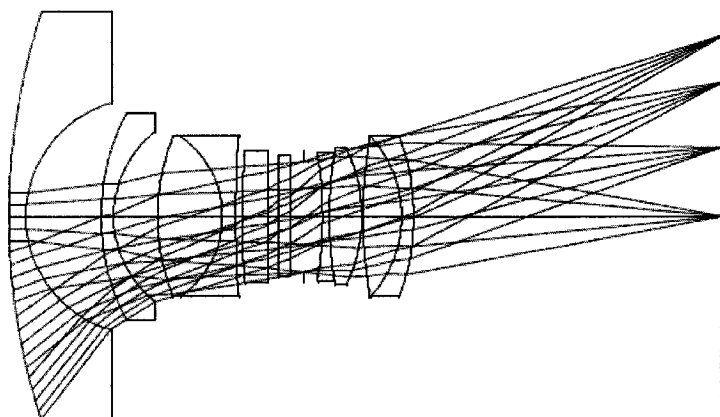


**Figure 2.14: Schematic of fish-eye glass lens by Coastal Optical Systems [42].**

The ORIFL190-3 (Figure 2.15a), manufactured by Omnitech Robotics International, is one of the commercially available high quality fish-eye lenses that provides a 190 degree FOV. Figure 1.15b shows one of the images captured by an ORIFL 190-3 fish-eye lens [1112].

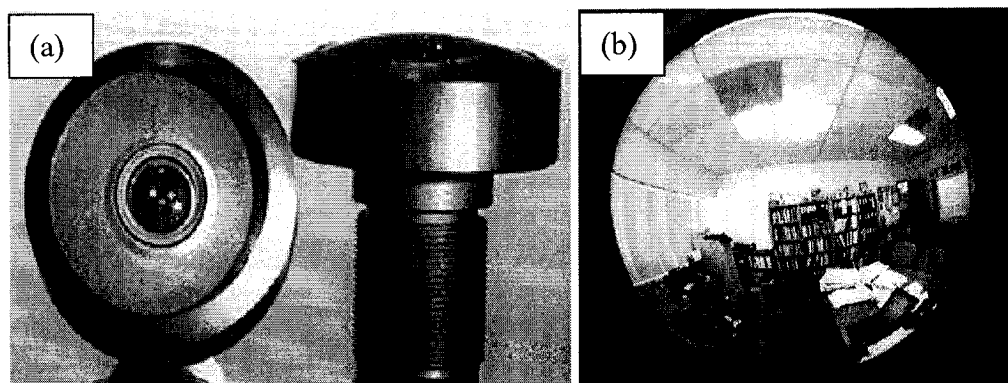


**Figure 2.15: (a) ORIFL 190-3 fish-eye lens, (b) Image captured using an ORIFL 190-3 fish-eye lens [112].**

It can be noted from Figure 2.14 that fish-eye lenses as presently manufactured consist of large number of optical elements with a complex arrangement. Also, the FOV is fixed for one particular type of fisheye optical lens system which constrains the focusing of smaller object at larger distances from the lens [113-115]. Therefore, an attempt has been made in this research to fabricate an optical lens system consisting of simple conventional lenses (DCX and DCV) to provide wide FOV which can vary dynamically. The dynamic nature is achieved using the PDMS elastic polymer material. The importance of choosing PDMS is discussed in Section 2.5.

### **2.7 Micro-Optics**

In research institutes and industries, miniaturization techniques have resulted in the development of higher-speed, lower-cost, higher-efficiency, and high-capacity devices. Following the trend of miniaturization, novel technologies have been developed to shrink the size of the optical elements which can fit in the world of micro-optics [50]. Micro-optical elements are key components for building compact optoelectronic systems and other miniaturized devices [37,50]. These systems and devices require a number of miniature mechanical and optical components, and they are useful for a number of

domestic and military applications [37,50]. Other areas where the micro-optical elements play an important role are the use of lasers in medicine, industrial machining, medical instrumentation and metrology, digital micro-cameras, etc. The key specifications of such applications are resolution, sensitivity, power consumption, manufacturing costs and packaging costs—as well as the overall size [37]. However, because of diffraction effects, miniaturization of the optical elements would drastically reduce resolution and image finesse. The influence of scale and physical dimensions on the optical properties of image forming systems has been well studied in recent years. An approach to investigate how nature has successfully solved similar problems in the case of very small creatures has helped many researchers to develop and integrate micro-optical elements with good resolution and imaging capabilities [37].

The compound eye found in insects and crustaceans are multi-aperture micro-optical sensors and are generally divided into two main classes: apposition compound eye and superposition compound eye, as shown in Figure 2.16a and 2.16b, respectively [37].

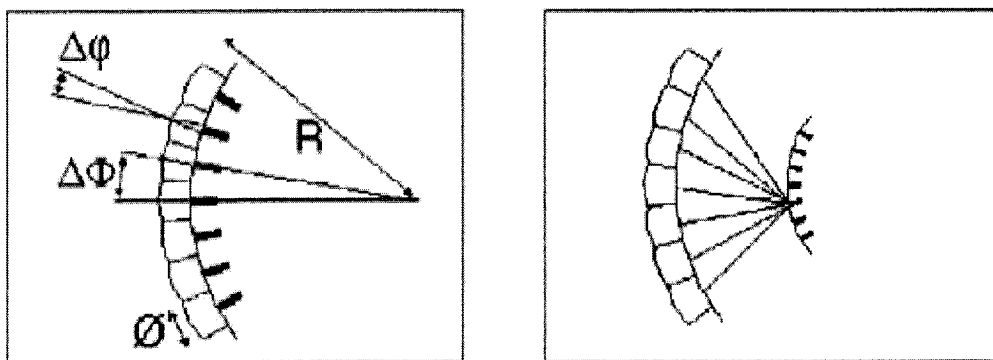


**Figure 2.16: Schematic of compound eye found in nature (a) apposition compound eye, (b) superposition compound eye [37].**

An apposition eye consists of an array of microlenses and photoreceptors. Each microlens focuses light from a small solid angle of object space onto a single

photoreceptor (ommatidia). The superposition compound eye is primarily found in nocturnal insects and deep-water crustaceans. The light from multiple facets combines on the surface of the photoreceptor layer to form a single erect image of the object, as shown in Figure 2.16 [37,39,40]. The superposition eye is much more sensitive to light than the apposition eye. Some insects use a combination of both types of compound eye.

Researchers have developed many micro-optical components based on the compound eye found in nature. Figures 2.17a and 2.17b show the schematic of the artificial counterpart of apposition and superposition compound eye, as shown in Figure 2.16 [37].

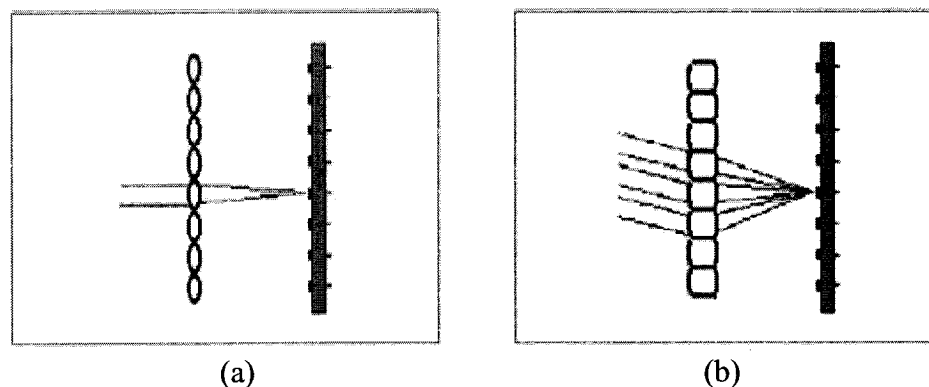


**Figure 2.17: Schematic of artificial counterpart for compound eye found in nature (a) apposition compound eye, (b) superposition compound eye [37].**

In Figure 2.17, the lenses shown to focus the light on the imaging sensor are called microlens arrays [50]. A number of new techniques were developed by using various materials and processes to fabricate microlenses and microlens arrays such as resist reflow, local melting of glass, hot-embossing, solvent assisted embossing, laser ablation, argon ion-beam etching, cup grinding wheel applying ELID grinding, photo-induced cross-linking polymer techniques, UV cured polymer technique, UV lithography using gray-tone masks, deep lithography using photons, micro-drop printing, and self-



assembly of liquid polymers on functionalized surfaces, etc. [116-134]. Microlens arrays used for imaging tasks are generally manufactured using resist reflow or melting resist techniques, as shown in Figure 2.18a [116-119]. The first stage to fabricate the array of microlenses using resist reflow technique is to coat a glass substrate with a layer (typically 1–100  $\mu\text{m}$  thickness) of positive photoresist. This layer is then exposed to a pattern of an array of circular masks and developed to form a series of cylindrical islands. These cylinders are then melted at a temperature of 150–200  $^{\circ}\text{C}$  until the resist melts and surface tension draws the melted resist into the shape of the lenses [119]. The SEM micrograph of microlens array by the resist reflow method is shown in Figure 2.18b.

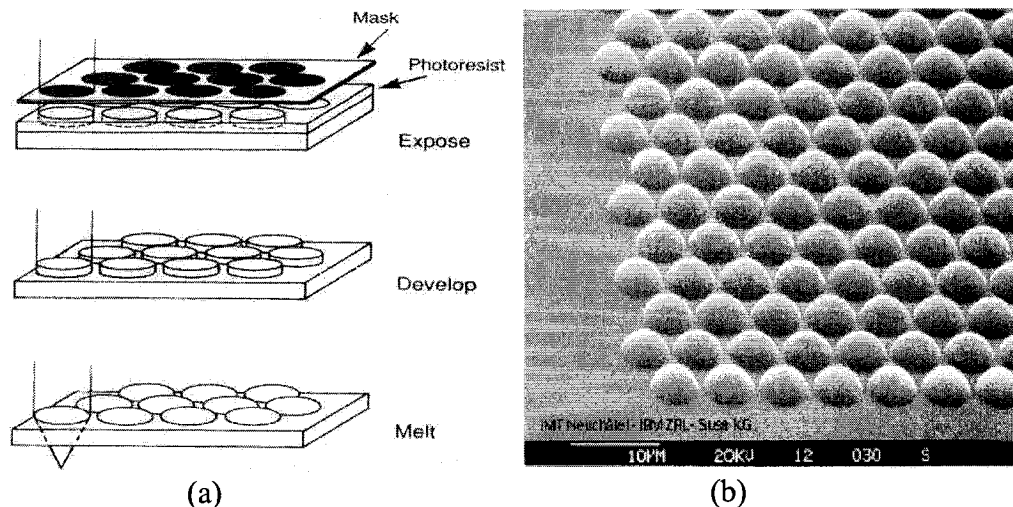


**Figure 2.18: (a) Resist reflow process to fabricate microlenses, (b) SEM micrograph of the microlens array fabricated using resist reflow method [50,119].**

Groups of other researchers focus on fabricating microlenses and microlens arrays by transferring the microlenses in fused silica by reactive ion etching (RIE) and replicated in polycarbonate and epoxy by embossing and casting techniques [120-122]. Replication in polymer or sol-gel types of material is the only commercially viable production method that can meet the demand for low-cost yet high-quality micro-optical

components produced in large volumes [121,122]. Figures 2.19a and 2.19b show the microlens mold array and replicated microlenses, respectively [123].

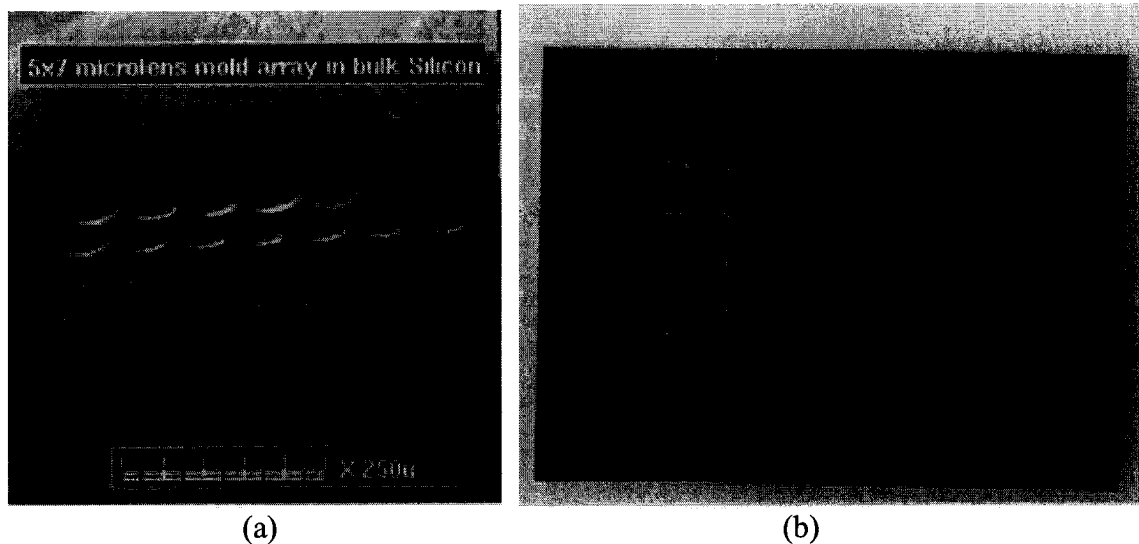


**Figure 2.19: (a) Microlens array mold, (b) Microlens array after replication [123].**

Nevertheless, it is not trivial to fabricate microlenses with good optical performance. The difference between a suitable lens profile and an unacceptable profile is only a fraction of a wavelength. Thus, careful optimization of all processing steps is necessary to obtain good quality lenses [123].

Recently, micro-drop printing techniques have been used to fabricate microlenses to overcome the disadvantage of having many processing steps such as resist reflow or replication method [124,125]. Micro-drop printing uses either a drop-on-demand or a dosing system to deposit single lenses or large arrays of high optical property refractive microlenses. The lenses are made of a silica-based inorganic-organic material which can be densified either thermally or by UV irradiation at low temperature. The schematic of micro-drop printing method and microlenses fabricated using this method is shown in Figures 2.20a and 2.20b, respectively.

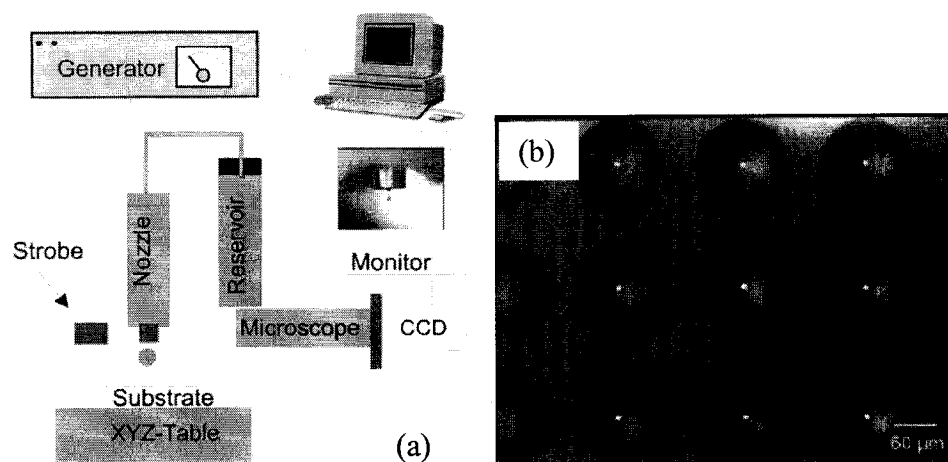


**Figure 2.20: (a) Schematic of drop-on demand ink-jet printing equipment, (b) Microlens array fabricated using micro-drop printer [125].**

The number of applications using microlens arrays has increased rapidly in many fields, for example, in optoelectronic sensors, optical communications, confocal microscopy, and miniature displays [136-139]. In optical communications, microlens arrays are used for fiber coupling in various systems [138]. Figure 2.21 shows a new contactless photolithographic technique called microlens projection lithography (MPL) which has been developed in connection with Hugel Lithography and Suss KG Munich using arrays of microlenses [139]. This new lithographic projection technique provides a resolution in the order of 3 to 5 μm, a depth of focus > 50 μm and a free working distance > 1 mm [139].

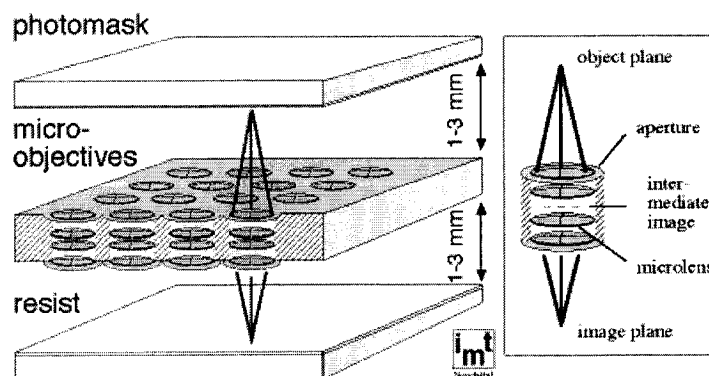


**Figure 2.21: Projection lithography setup using microlens arrays [139].**

Inspiration from the compound eye found in nature led to the development of microlens arrays which solved many of the problems which were unachievable using macro-optical lenses. But, it should be noted that the resolution of compound eye found in nature is usually poor compared to single-aperture eye [37]. In nature, this lack of resolution is often counterbalanced by additional functionality like a very large FOV, polarization, or fast movement detection [39-41,140,141]. The microlens arrays cannot achieve this counterbalance as nature does, which restricts the use of microlens arrays in many other applications such as high resolution digital cameras. Also, the FOV achieved from microlenses or microlens arrays is very low compared to the fish-eye lenses discussed in Section 2.6, and these microlenses do not have dynamic features like those found in biological vision systems.

Investigation into other bio-vision systems found in nature, such as the human eye, which has single lens systems and yet displays very complex and remarkable visual acuity [37, 142-144], could help to develop miniaturized lens systems with remarkable optical properties. The single lens systems found in nature have multi layers of protein and allow reversible contraction of the lens membrane, with a consequence of changing focal length and reducing aberration. It has been demonstrated that many of the complex visionary features in bio-vision systems arise from two main characteristics: the existence of a gradient of refractive indices (GRIN - symmetric variation of the refractive index within the bulk material) in the lens and the ability of the lens to change its shape dynamically [142-144]. Schematics of the human eye and change in lens shape for focusing on near and far objects are shown in Figure 2.22 [145].

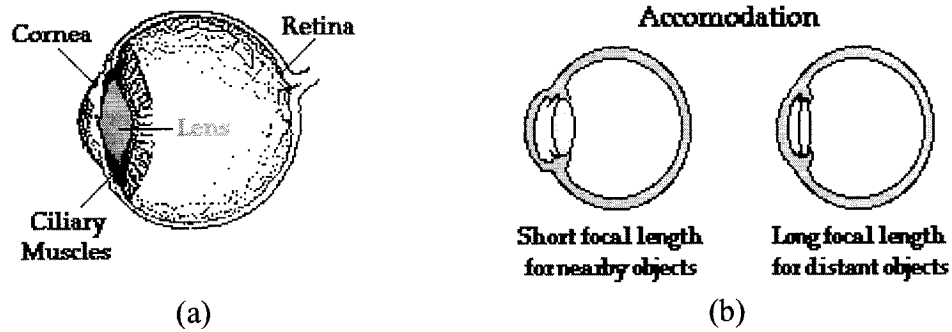


**Figure 2.22: (a) Schematic diagram of the human eye, (b) Diagram showing the accommodation of human eye lens for near and far objects [145].**

The ability of the eye to adjust its focal length is known as accommodation. As a nearby object is typically focused at a farther distance, the eye accommodates it by changing the lens shape that has a shorter focal length as shown in Figure 2.22b [143,144]. On the other hand, a distant object is typically focused at a closer distance, and the eye accommodates it by changing the lens shape that has a longer focal length as shown in Figure 2.22b. The change in focal length of the lens in the human eye to the object distance is listed in Table 2.1.

**Table 2.1: Change in focal length of human eye vs. object distance [145].**

Dependence of $f$ upon object distance (Image distance is fixed at 1.70 cm)	
Object Distance	Focal Length ( $f$ )
0.25	1.59 cm
1 m	1.67 cm
3 m	1.69 cm
100 m	1.70 cm
Infinity	1.70 cm

For some applications, like surveillance cameras, it is desirable that the micro-optics elements have a modulation that is dynamic like the human eye. Most of the lenses

developed so far have a surface or volume modulation that is permanent. Lenses and mirrors, as conventional optical elements of fixed focal length, contain no variable focusing mechanism, which should be done by controlling the separation of lenses along the optical axis [37,50]. The focusing mechanism used for these conventional optical devices is complicated and consists of many gears, motors, and sliders [30]. Therefore, a non-mechanical compact solution (absence of moving parts) is desired to avoid the need for costly maintenance. The ability of the human eye lens to accommodate near and distant objects with wide FOV focuses the interest of optical research on the development of miniaturized lenses which can have high resolution, wide FOV, and dynamic features [143,145]. The next section will focus on recent research that has attempted to mimic the human eye and fabricate dynamic focal length lenses.

## **2.8 Variable Focal Length Lenses**

For the next generation of customer products such as mobile phones, security cameras, surgical instruments in the medical field, and integrated micro-cameras, variable focal length and wide FOV lenses have become essential and challenging components [31]. The optical elements with variable focusing features are also useful for correcting the inability of the eye to adjust the focal length because of presbyopia or eye disease, where multiple pairs of glasses may be needed in order to see an object at short or long distances [34]. In medical instruments, variable focal length and wide FOV lenses are ideal for advanced bioanalytical instruments and microscopes and have the potential in high-throughput clinical applications [34]. The dynamically variable focal length lens system can also be used to make on-line adjustments to stereoscopic camera position parameters dynamically, during the execution of telemanipulation tasks, which allows

maintaining a theoretically “optimal” camera configuration, in response to changing viewing conditions. Extensive efforts were made by various researchers to realize a lens system with variable focal length and wide angle of view. A change in focal length can be achieved by electrical or other actuation mechanisms. Among the various methods developed so far, most methods rely on the use of electrically actuated nematic liquid crystals.

Originally, the idea of using nematic liquid crystal to form a liquid crystal lens was proposed and patented by Berreman [146]. The liquid crystal (LC) lens-cell with variable focal length was first investigated in Japan by S. Sato [147]. LC cells shaped like plano-convex or plano-concave lenses (Figure 2.23) were fabricated with a focal length that can be varied by applying an external electric field. The properties of liquid crystals with their electrically controllable birefringence provide a mechanism for a variable focal length lens [147].

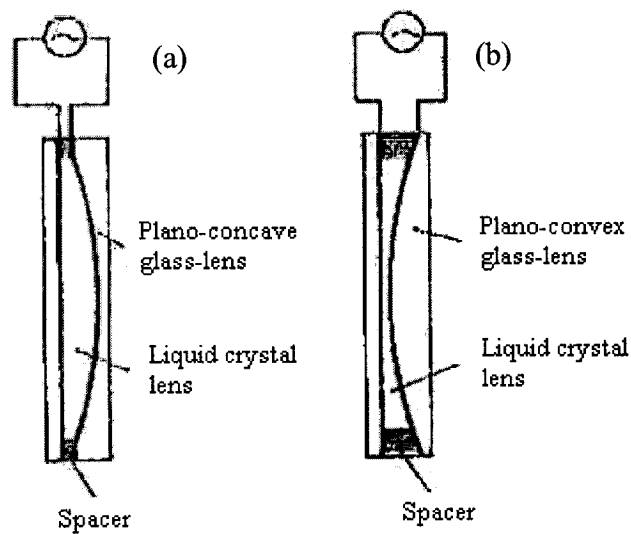


**Figure 2.23: Structure of liquid crystal lens-cell (a) plano-convex, (b) plano-concave [147].**

LC cells, when molecules align along their axes in the same direction under an applied electric field, have optical properties similar to those of uniaxial crystals. Many experiments were carried by S. Sato and his group to develop techniques to fabricate optical lens systems with variable focal length lenses using different liquid crystals. In one of the findings, a liquid crystal lens was fabricated, as shown in Figure 2.24, using a nematic LC and a hole patterned electrode structure, where a spatial distribution of refractive index is induced by an axially symmetric non-uniform electric field. It was found that, when both the surface of the electrodes were coated with polyvinylalcohol (PVA) and treated by rubbing to give homogeneous molecular orientation, LC lenses with better optical properties can be fabricated [147,148]. It was also observed that the optical properties of the liquid crystal depends significantly on  $D/t$  value ( $D$ -Diameter of the hole pattern,  $t$ -thickness of the LC cell),  $\Delta n$  (change in refractive index under applied voltage), and  $\Delta \epsilon$  (dielectric anisotropy) of the LC material [148].

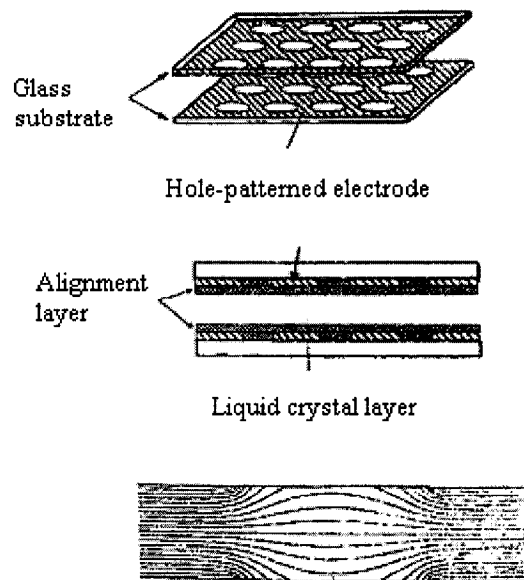


**Figure 2.24: Liquid crystal lens-cell with hole patterned electrode [148].**



F. Naumov et al. also performed extensive research on fabrication and modeling lenses using LC materials [60,61]. Figure 2.25 shows one of their proposed models, which possesses a circular aperture of 6.5 mm and the capability of focusing collimated light in the range of  $\infty$  to 0.5 m.

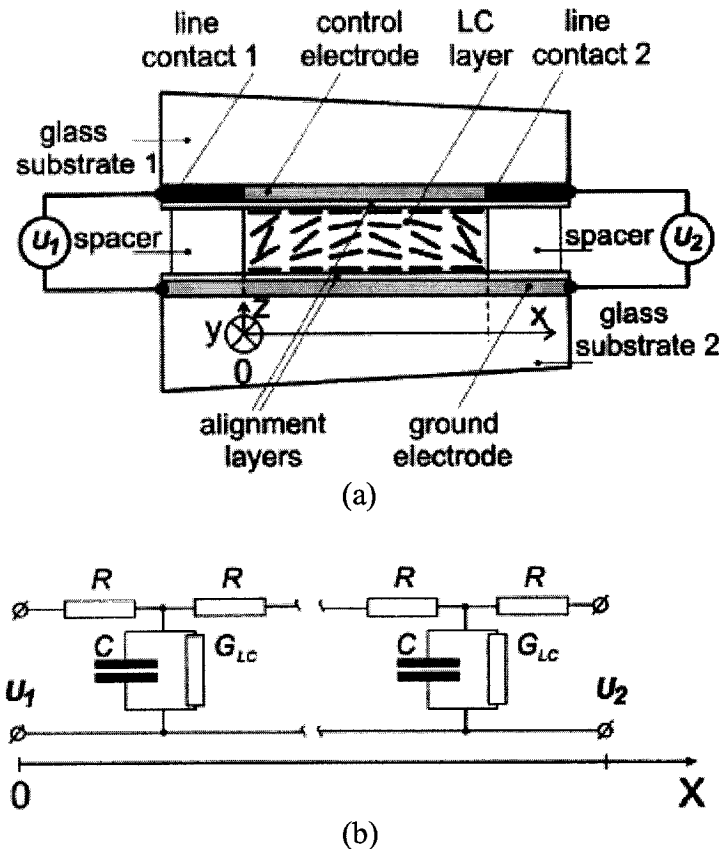


**Figure 2.25: (a) Geometry of the LC cylindrical lens, (b) Simplified equivalent circuit, illustrating the distributed nature of the reactive impedance of the LC layer sandwiched between high and low resistance electrodes [61].**

A variable focal length system with a microlens immersed in a nematic liquid crystal was developed by L.G. Commander et al. at the University College of London [58,59]. In this design, a nematic liquid crystal cell with a microlens immersed in it was fabricated, as shown in Figure 2.26a, and the focal length of this cell was controlled by applying a voltage to the nematic liquid crystal (Figure 2.26b) [59].

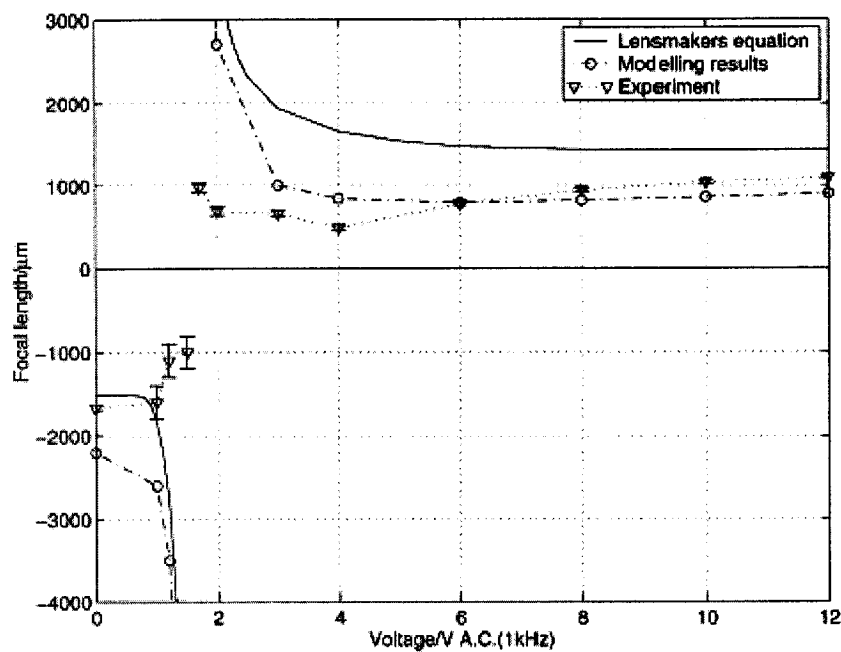
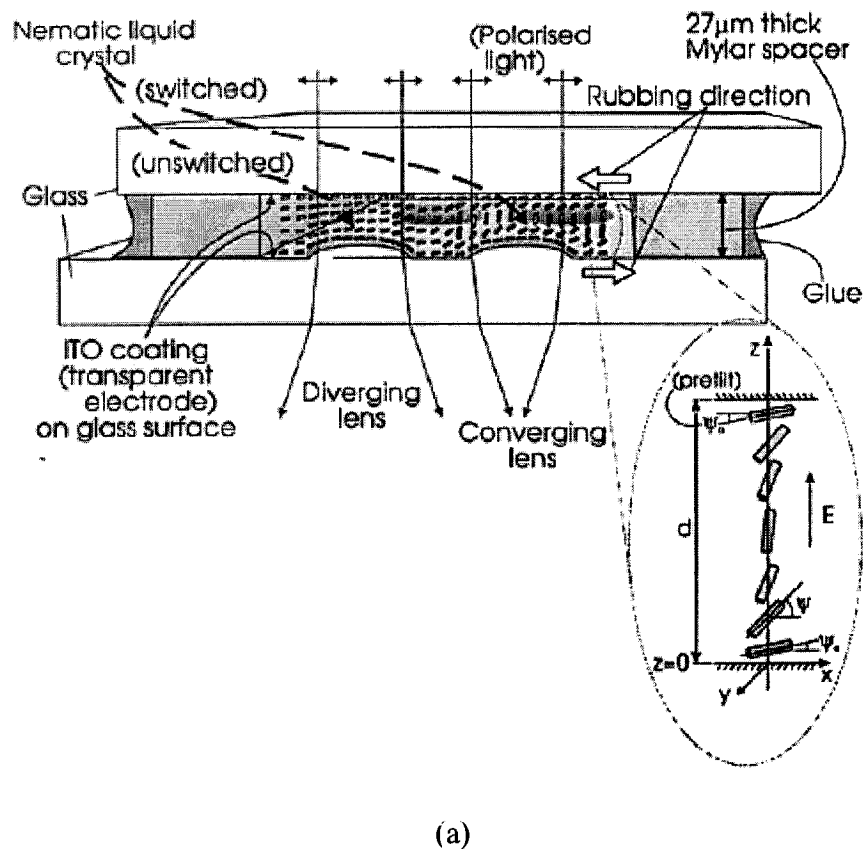
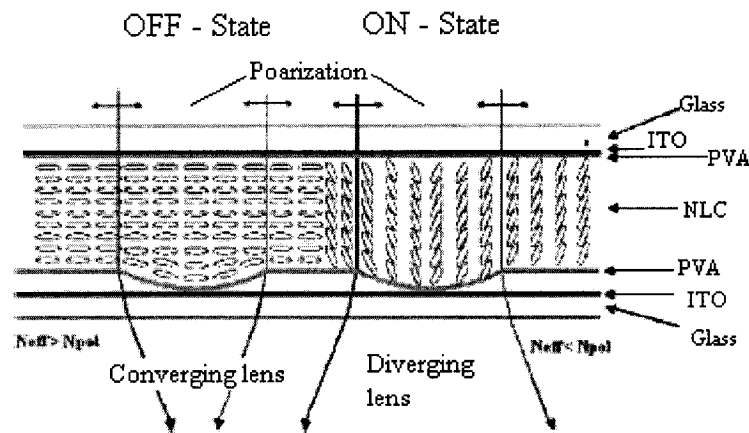


Figure 2.26: (a) An LC immersed microlens with and without applied voltage, (b) Focal length vs. applied voltage [59].

The uniaxial birefringent liquid crystal material has an extraordinary refractive index,  $n_{lc}$  crystal, between 1.74 and the ordinary refractive index of 1.52. The refractive index of the nematic liquid crystal with applied voltage is called extraordinary refractive index and without the applied voltage is the ordinary refractive index. The liquid crystal can be reoriented by an electric field so that the extraordinary refractive index is modulated between the two values. The refractive index of the photoresist microlens ( $n_p$ ) used was 1.64 such that the cell could be able to provide a positive or negative lens of focal length ( $f$ ), or just act as piece of glass when the focus changes from negative to positive. The focal length  $f$  is given by Equation 2.16, where  $C$  - curvature of the photoresist microlens [149].

$$f = [(n_{lc} - n_p)c]^{-1} \quad (2.16)$$

In the other method, an ultraviolet (UV) curable polymer microlens array was used, as shown in Figure 2.27, to fabricate the variable focal length lens system based on a nematic crystal.



**Figure 2.27: The schematic diagram of a LC cell with UV curable microlenses [149].**

Another successful attempt to fabricate variable focal length lenses involved the use of the electrowetting phenomenon for actuation [54-57]. Electrowetting is essentially

a phenomenon whereby an electric field can modify the wetting behavior of a droplet in contact with an insulated electrode [55]. Surface tension is an inherently dominant force in the small-scale. Electro-capillarity, the modification of surface tension by applying an electric field, has received renewed attention because of its potential use in microfluidics. If an electric field is applied to an electrowetting cell, then a surface energy gradient is created which can be used to manipulate a droplet sandwiched between two plates [150-153]. The electrowetting technique to vary the diameter and thereby the focal length of the liquid droplet lens is shown in Figure 2.28 [55]. The variable focal length electrowetting liquid lens structure consists of four main functional parts which includes a transparent electrode pattern, an electrolyte liquid droplet, a hydrophobic insulating layer, and protective structures. Applying an electrical field in the vicinity of the water droplet on a hydrophobic insulating layer can alter the contact angle of a droplet by virtue of an induced capacitive force.

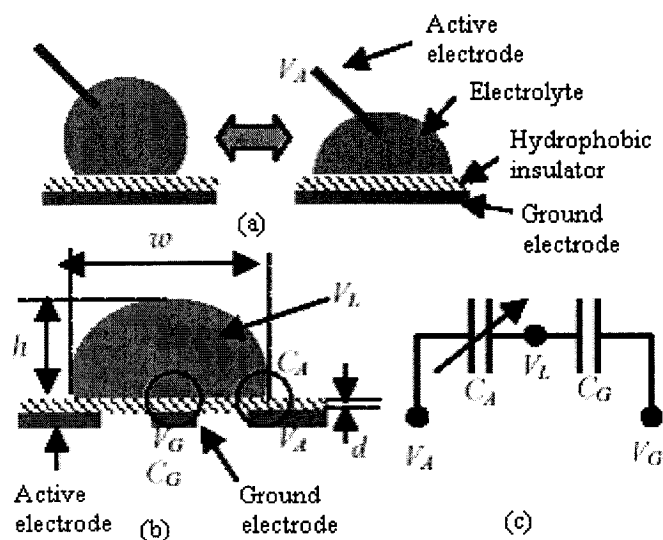


**Figure 2.28: (a) Switchable electrowetting with invasive electrode, (b) Non-invasive electrowetting cell, (c) Equivalent circuit model [55].**

In the electrowetting technique, change in droplet shape after giving the potential is directly related to the change in optical power. By measuring the width and height of the droplet, focal length can be calculated using Equation 2.17, where  $n_w$  - refractive index of water,  $n_a$  - refractive index of air,  $w$  - width of the water droplet,  $h$  - height of the water droplet [55].

$$f = \frac{r}{\Delta n} = \frac{1}{n_w - n_a} \left[ \left( \frac{w}{2} \right)^2 + h^2 \right] \quad (2.17)$$

Figure 2.29b shows the change in focal length with applied voltage using an electrowetting cell shown in Figure 2.29a [54].

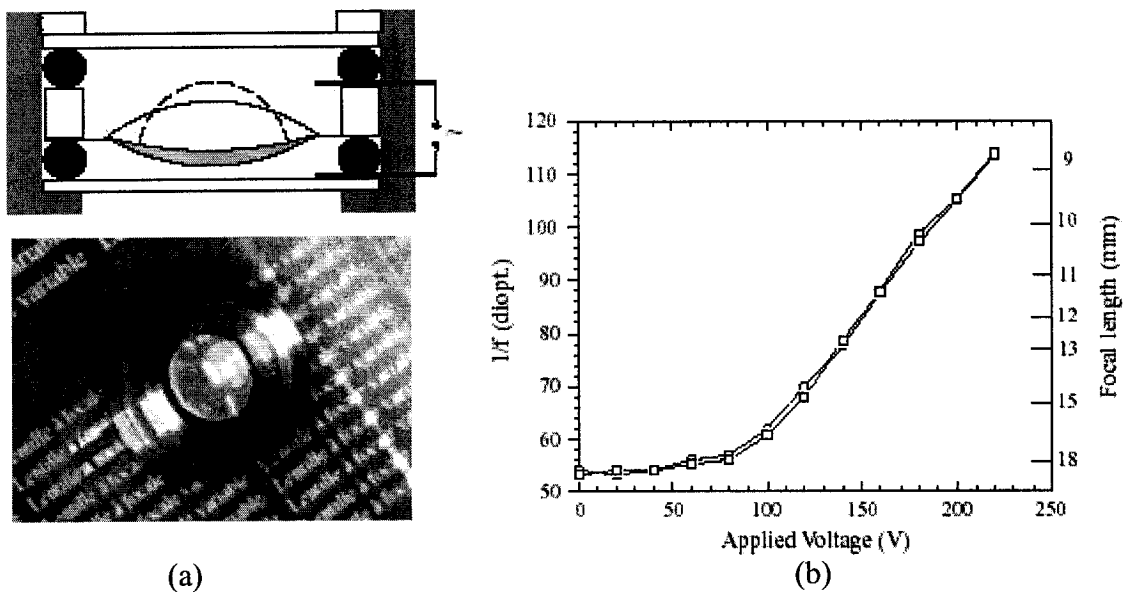


**Figure 2.29: (a) Electrowetting cell, (b) Voltage vs. focal length [54].**

Philips Research Group has also developed a unique variable focus lens system that has no mechanical moving parts which works on the principle of electrowetting [154]. The uniqueness of the Philips FluidFocus lens lies in the use of two non-mixing fluids of different refractive index, one an electrically conducting aqueous solution and the other an electrically non-conducting oil contained in a small cell. The schematic of

the variable focal length lens developed at Philips Research is shown in Figure 2.30 [154]. The internal surfaces of the cell walls and one of its end caps are coated with a hydrophobic coating that causes the aqueous solution to form itself into a hemispherical mass at the opposite end of the tube where it acts as a spherically curved lens. The shape of the lens can be adjusted by applying an electric field across the hydrophobic coating such that it becomes less hydrophobic, as shown in Figures 2.30a and 2.30b [154].

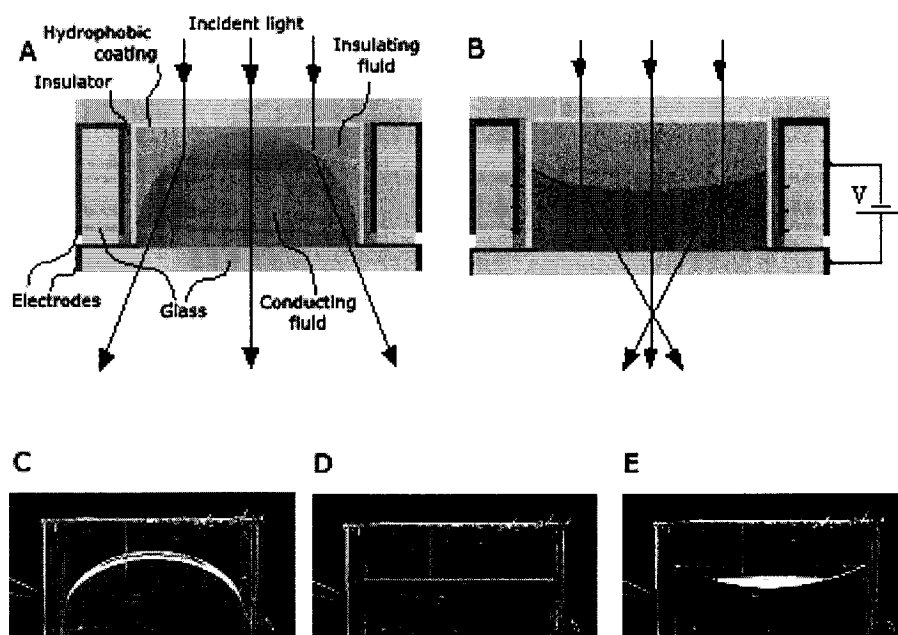


**Figure 2.30: (a) & (b) Schematic cross section of the FluidFocus lens with and without applied voltage, (c) to (e) Shapes of a 3-mm diameter lens taken at different applied voltages [154].**

Using piezoelectric material ring electrodes (Electrooptic (E-O) lead-lanthanum Zirconate-titanate (PLZT) ceramics) to actuate the transparent membrane (Figure 2.31a) is one of the other methods to fabricate a variable focal length lens using electric actuation [62,155]. This lens is comprised of two thin glass diaphragms as a refractive surface, with a transparent working fluid sealed between them, and piezoelectric actuators. The measured optical characteristics of this lens achieved by actuating the

piezoelectric with a sinusoidal voltage at a cycle of 60 Hz to shift the focal plane from -4 mm to +4 mm and by shifting the object in the direction of optical axis are shown in Figure 2.31b [62].

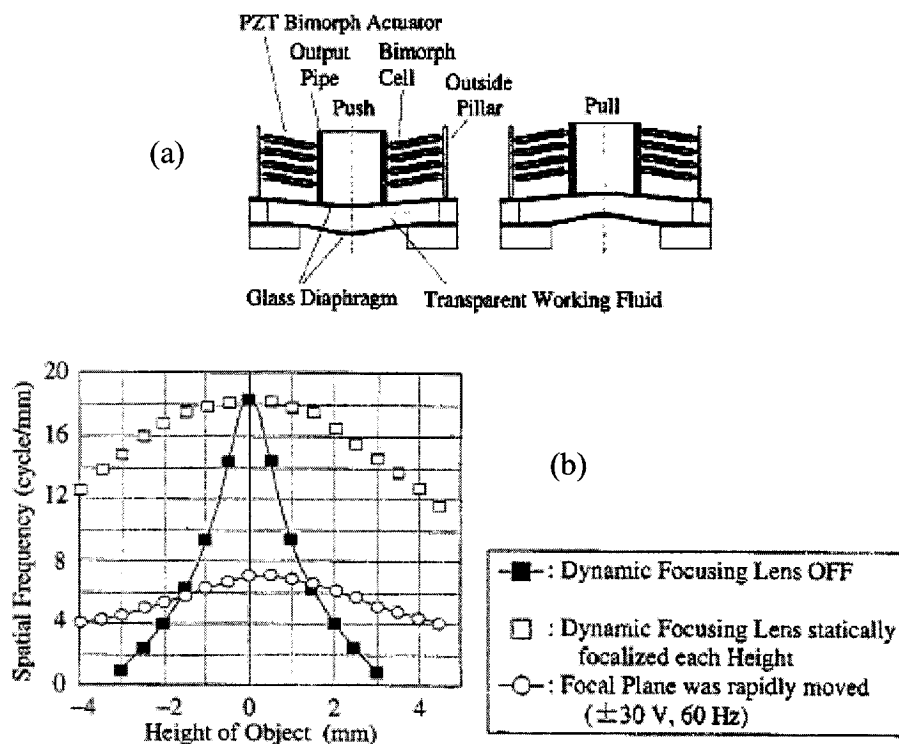


**Figure 2.31: (a) Dynamic focal length lens using PZLT actuation, (b) Optical characteristics [62].**

Other types of lenses with variable focal length features are fluidic actuated lenses, as shown in Figure 2.32 [63-65,156]. This lens consists of a square glass diaphragm (5 x 5 mm), channels, and working fluid. The chamber between a glass diaphragm and a substrate is filled with the working fluid. Refractive index matching oil such as silicone oil can be used as working fluid which is pumped into or out of the chamber through the microchannel. The curvature of the lens can change as a result of the oil pressure built by the micro-pump outside. The change of curvature of the lens

produces the focal plane shift. In addition, both a convex lens and a concave lens can be realized by pressurized working oil in this type of lens system [63-65].

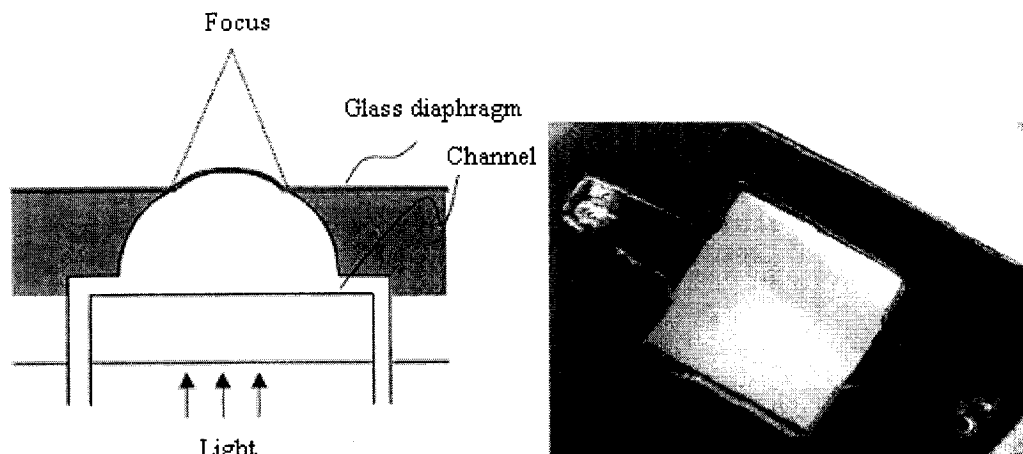


**Figure 2.32: Variable focal length lens using fluidic actuation [63].**

A fluidic actuated tunable focal length lens which has been recently developed is shown in Figure 2.33 [156]. This lens structure uses PDMS membrane and can be actuated as plano-convex lens by pumping fluid into the lens chamber as shown in Figure 2.23.

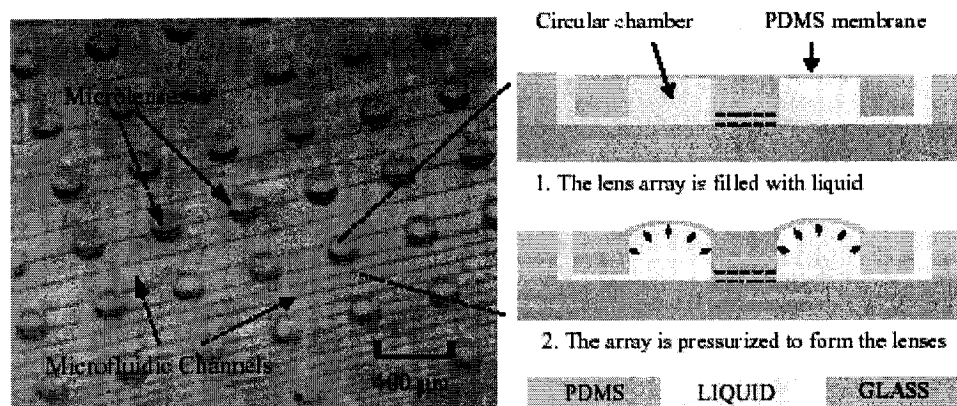


**Figure 2.33: Variable focal length microlens array using fluidic actuation [156].**



### **2.8.1 Limitations of Variable Focal Length Lenses Reported to Date**

The research done to fabricate variable focal length lenses to date is summarized in Table 2.2. Diameter of the fabricated lens, tuning range of focal length, and maximum numerical aperture (NA) from different variable focal length lenses are also summarized in Table 2.2.

**Table 2.2: Summary of different variable focal length lenses reported to date and their optical properties.**

<b>Types of variable focal length lenses reported to date</b>	<b>Dia. (mm)</b>	<b>Max. NA</b>	<b>Focal length (f) range</b>	<b>Ref.</b>
Hole patterned electrodes LC cell	0.3	0.270	1.07 m - $\infty$	148
Patterned electrodes (Cyl.) LC cell	20.0	0.001	10 m - $\infty$	157
Resistor chain patterned electrodes (Cyl.)	1.0	0.004	120 mm - $\infty$	158
Lens-shaped nematic filled cell	20.0	0.060	160 - 220 mm	146
Liquid crystal adaptive lens with modal control	4.0	0.010	500 mm - $\infty$	61
Gabor lens patterned electrode	9.8	0.010	490 mm - $\infty$	159
Fresnel zone plate patterned electrode	20.0	0.010	1 m - $\infty$	160
Fresnel zone plate patterned alignment	2.9	0.005	310 mm - $\infty$	161
Total internal reflection lens LiTaO <sub>3</sub>	0.1	0.005	10 cm - $\infty$	162
PLZT with patterned electrodes	1.0	0.005	10 cm - $\infty$	155
Deformed helix ferroelectric LC (Cyl.)	3.0	0.003	500 mm - $\infty$	163
2 Phase SLMsq2 lenses	7.3	0.037	98 - 148 mm	30
Electrowetting cell	5.0	0.100	9.5 - 19 mm	54
Liquid-filled elastic lens	27.0	0.040	37 cm - $\infty$	164
Liquid-filled elastic microlens	0.2	0.200	0.5 - 2 mm	156
Philips research group variable focus lens	3.0	0.030	5 cm - $\infty$	154

LC lenses, limited to small size and high optical distortion, have high response time with a tight range of tunable focal length [146-149]. The LC response time increases with the square of the thickness of the cell, and with thicker cells it is harder to maintain the crystal structure. As the thickness of the liquid crystal cells increases, it will take more time for the liquid crystal molecules to achieve a stable equilibrium state. On the other hand, cells with thin LC layers provide little optical path modulation ( $\Delta n \cdot d = 66 \mu\text{m}$  is achieved with a relatively thin layer:  $d = 200 \mu\text{m}$  with  $\Delta n = 0.3$ ) and, therefore, very low numerical apertures and very little change in focusing power when a voltage is applied to the LC cell [165]. The orientation of the liquid crystal molecules can be affected by a surrounding electromagnetic field or temperature which may also cause optical distortion [166].

PLZT lenses have an advantage over nematic liquid crystals of greater speed, e.g.  $2.5 \mu\text{s}$  for PLZT [155] compared to 10–100 ms for a  $5 \mu\text{m}$  nematic layer [165]. However, the low electro-optic coefficients ( $r_{33} = 30.8 \times 10^{-12} \text{ m}^2/\text{V}^2$  for  $\text{LiTaO}_3$  and  $r_{33} = 3.6 \times 10^{-16} \text{ m}^2/\text{V}^2$  for PLZT [155]) result in small optical path modulation and, hence, low numerical aperture (0.01) in PLZT lenses unless thick devices and very large voltages can be tolerated.

Variable focal length lenses using electrowetting techniques require a high electric field for the actuation mechanism [54-57,150-153]. However, this method is not practical if one wants to use the electrowetting droplets as lenses because the immersion of electrodes in the droplets causes high optical distortions.

The fluidic actuated lenses overcome most of the disadvantages of LC cells and other types of variable focal length lenses. However, the variable focal length lenses

using fluidic actuation reported to date involve complex fabrication processes, such as using glass diaphragms and etching of fluidic channels and inlet in glass. The imaging capabilities of these lenses have not yet been demonstrated. The fluidic actuated lenses reported to date also do not exhibit a wide range of tunable focal length and have low numerical aperture [63-35,156]. The field of view of the variable focal length lenses reported to date is constrained and is not demonstrated in most of the cases [54-65, 146-164].

Therefore, the work done in this dissertation, reports on an approach that has been devised to design, fabricate, and test unique variable focal length microlens structures which can provide a wide range of tunable focal length with large FOV and numerical aperture. A fluidic actuation mechanism, which has a number of advantages over other actuation mechanisms, is used to vary the curvature of the lens membrane which produces the change in focal plane and FOV. The numerical aperture can be chosen as a metric of the lenses as well as the range of focal lengths as it gives an idea of how much deflection can be introduced by the lens. The advantage of using PDMS membrane was discussed in Section 2.6. The fabrication of a dynamic microlens system, presented in this research work, involves standard photolithography and silicon micromachining techniques which make it more adaptable for current industrial applications. A wide FOV lens system achieved by integrating two or three single variable focal length lens systems has been developed to achieve large and variable FOV.

## CHAPTER 3

### INITIAL TESTING FOR WIDE FIELD OF VIEW

#### DESIGN USING GLASS LENSES

##### 3.1 Experimental Setup

Preliminary experiments were conducted using different sets of double concave (DCV) and double convex (DCX) glass lenses of different focal lengths to derive the relationship between the field of view (FOV) and focal length of the lenses, and to investigate the specific combination of lenses that can provide a wide FOV. These lenses were chosen because it is relatively easy to fabricate the system and make the polymer lens system adapt to one of these configurations. For the construction and characterization of fluid enabled optical systems, it has been realized that these simple experiments were critical to optimize the design process.

A simple optical characterization setup, which includes a CCD camera, video monitor, frame grabber system, optical rail and components, and an object with a scale attached to it, was used for imaging through the lenses. The object is a frame containing a series of letters in the form of "LOUISIANA TECH UNIVERSITY" with a scale attached at its bottom. Two such objects are placed in front of the camera, with one object placed perpendicular to the optic axis, and the other placed at an angle of  $30^\circ$  from the

optic axis. The purpose of keeping these two objects is to determine the variation of the focal length and the FOV simultaneously. All the tested lenses in this chapter are of fixed focal length and are made of glass material.

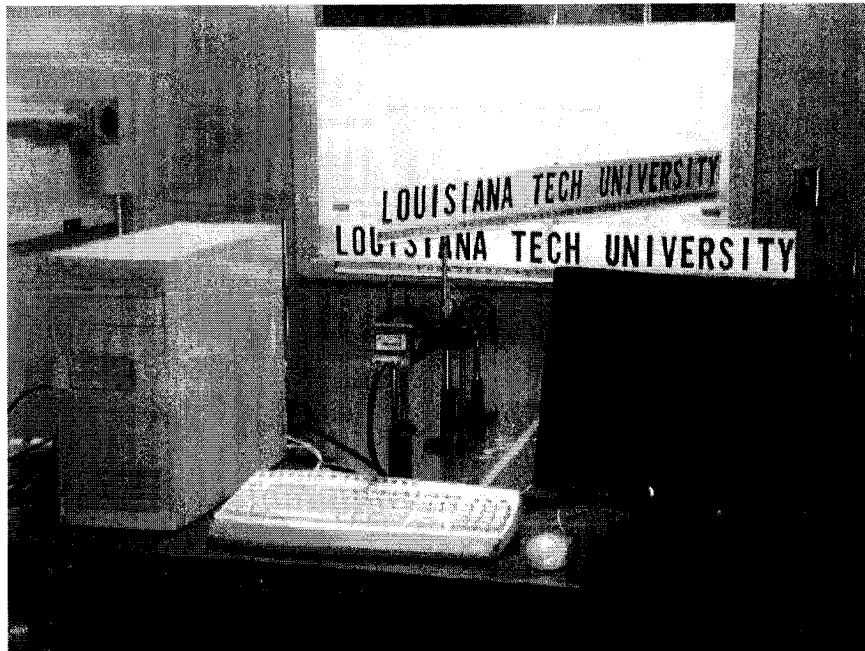


**Figure 3.1: Image capturing setup.**

### **3.2 Different Configuration of Double Concave (DCV) and Double Convex (DCX) Glass Lenses to Test for Wide Field of View**

In one set of experiments, combinations of one DCX lens of fixed focal length ( $f = 10$  cm or  $20$  cm) and a second DCX glass lens of different focal length ( $f = 5, 10, 15, 20, 30$  cm) were used to image the object and determine the variation of FOV with the focal length of the second DCX lens (Figure 3.2a). In another set of experiments, a combination of one DCX lens of fixed focal length ( $f = 20$  cm) and a second DCV glass lens of different focal length ( $-f = 10, 15, 20$  cm) was used to image the object and determine the variation of FOV with the focal length of the second DCV lens (Figure 3.2b). The first DCX lens was placed at a fixed position in front of the camera to

image the object on to the CCD chip. The position of the second DCX or DCV lens was varied to focus the object when different focal lengths of lenses were used. In all the different arrangements of lenses, four different distances were marked. As shown in Figure 3.2, 'a' is the distance between the camera and the DCX lens; 'b' is the distance between the DCX and DCV lens; 'c' is the distance between the DCV lenses and the object; and 'd' is the length of the object that is viewed by the camera. The FOV ( $\theta$ ) was calculated by using the formula given in Equation 3.1. The total FOV is twice the angle measured by taking the inverse of tangential angle ( $\tan^{-1}$ ) of the ratio of one half the length of the object viewed to the distance between the lens and the object.

$$\theta = 2 * \tan^{-1} \left[ \frac{(d/2)}{c} \right] \quad (3.1)$$

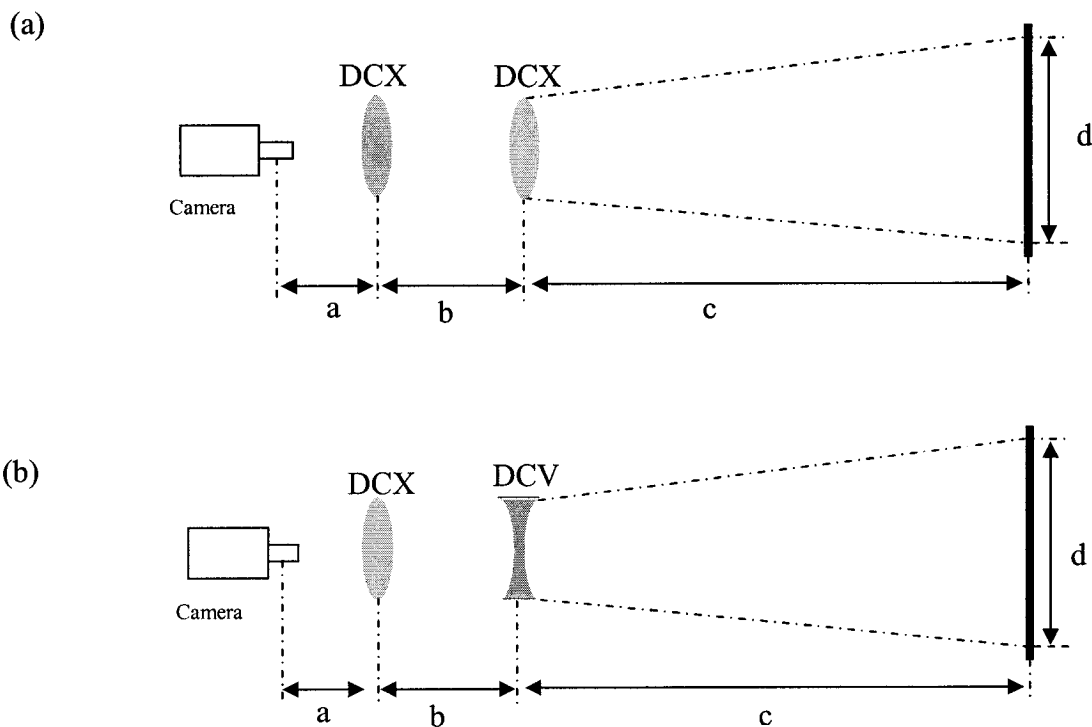


**Figure 3.2: Illustrations of optical arrangements (a) two DCX lenses, (b) first DCX lens with a second DCV lens.**

Results from the first and second set of experiments showed that DCV lenses provided wider FOV than DCX lenses of the same focal length and that wider FOV can be achieved by using DCV lenses of lower focal length. The focal length of the DCV lenses was further reduced by placing two or three identical focal length DCV lenses in contact. The effective focal length ( $f_{-}$ ) of two DCV lenses of focal length  $f_{c1-}$  and  $f_{c2-}$  in contact is given by Equation 2.

$$\frac{1}{f_{-}} = \frac{1}{f_{c1-}} + \frac{1}{f_{c2-}} \quad (3.2)$$

As it was observed that the DCV lenses give higher field of view than DCX lenses, DCV lenses were chosen for further experiments. The experiments were also performed to test the variation in the FOV with respect to the focal length of the first DCX lens along with the combination of two or three DCV lenses of different focal lengths, as shown in Figures 3.3a and 3.3b. The focal lengths of DCX lenses were 10, 20, or 30 cm, whereas the focal lengths of DCV lenses were -10, -15, or -20 cm.

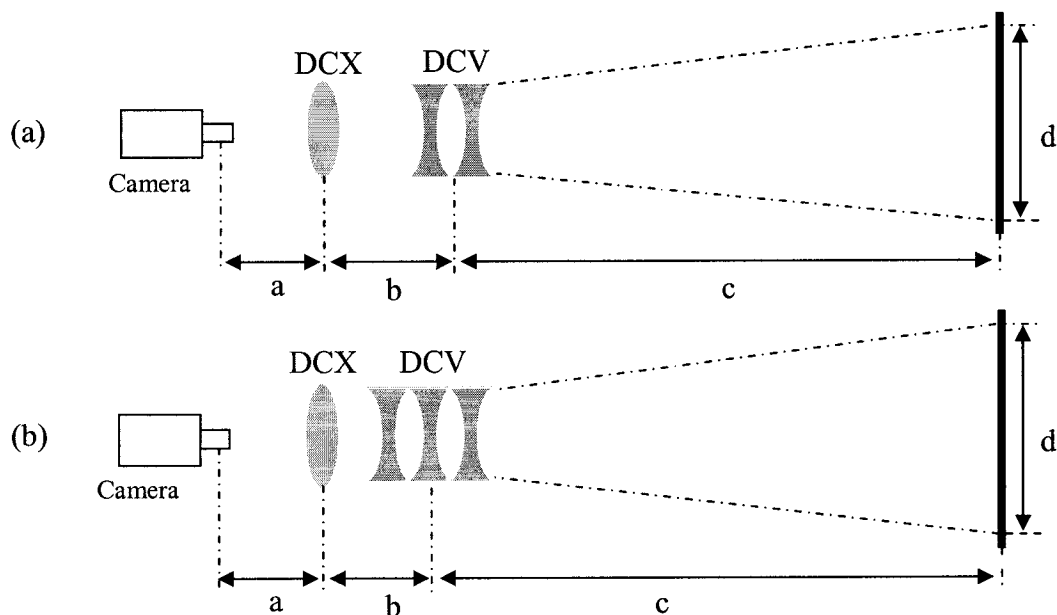


**Figure 3.3: Illustrations of optical arrangements (a) one DCX and two DCV lenses, (b) one DCX and three DCV lenses.**

### 3.3 Results and Discussion

Initially, the object was imaged by using only a CCD camera with no additional lens between the camera and the object. The partial image of the object captured by the camera using the simple setup is shown in Figure 3.4. At this imaging condition, the total FOV was measured to be  $12.2^\circ$ .

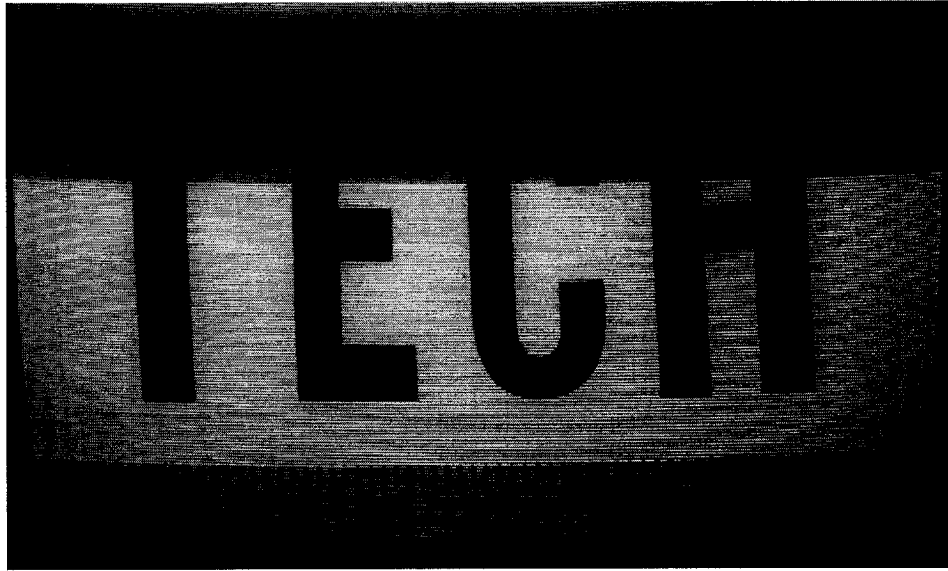


**Figure 3.4: Optical image of the object captured directly from the CCD camera.**

The series images captured using the setup shown in Figure 3.2a where the focal length ( $f$ ) of the first DCX was 10 cm and the focal length ( $f$ ) of the second DCX lens was 5, 10, 15, 20 or 30 cm are shown in Figure 3.5a. The relationship between the focal length ( $f$ ) of second DCX lens and FOV achieved is shown in Figure 3.5b. It can be observed that, as the focal length of DCX lens decreases, the FOV increases. Figures 3.6a and 3.6b show the series of images captured using the setup shown in Figures 3.2a and 3.2b, respectively, with the fixed DCX lens ( $f = 20$  cm) in front of the camera along with DCX or DCV lenses of different focal length ( $f = 10, 15, 20$ cm).



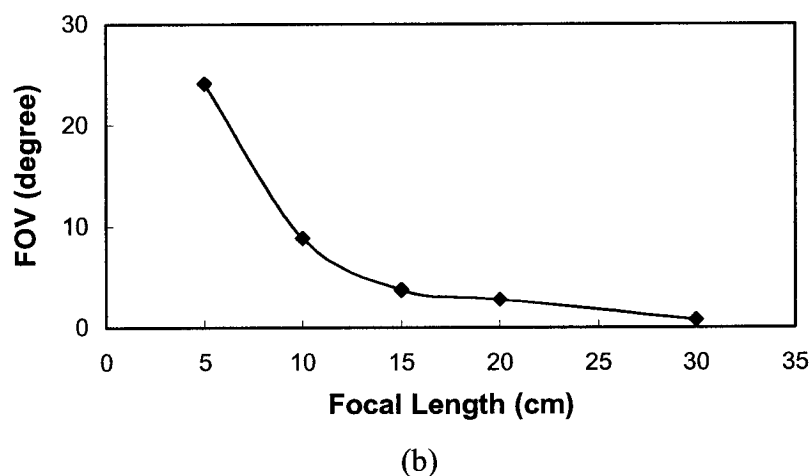
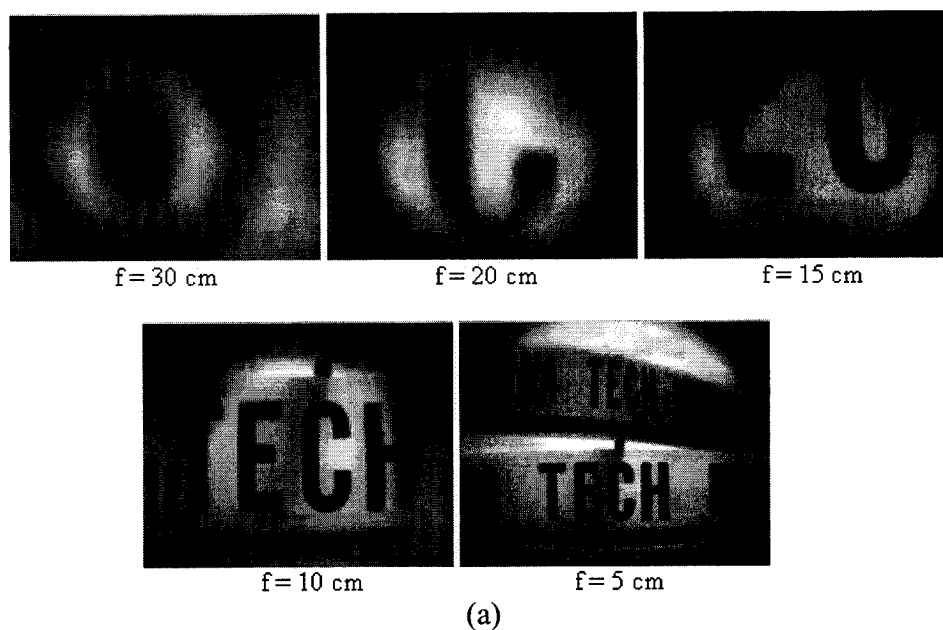


**Figure 3.5: (a) Series of images captured using the setup shown in Figure 3.2a with the first DCX lens of  $f = 10$  cm and second DCX lens of different focal length, (b) Focal length vs. field of view (FOV) from the second DCX lenses.**

Figure 3.7 shows the plot of focal length vs. FOV field of view for both DCX and DCV lenses placed as the second lens. Although the observed FOV with these lenses is significantly lower, it should be noted that, when DCV lenses are used to image the object, one can achieve higher FOV. The FOV was found to increase with the decrease of focal length of DCV lenses.

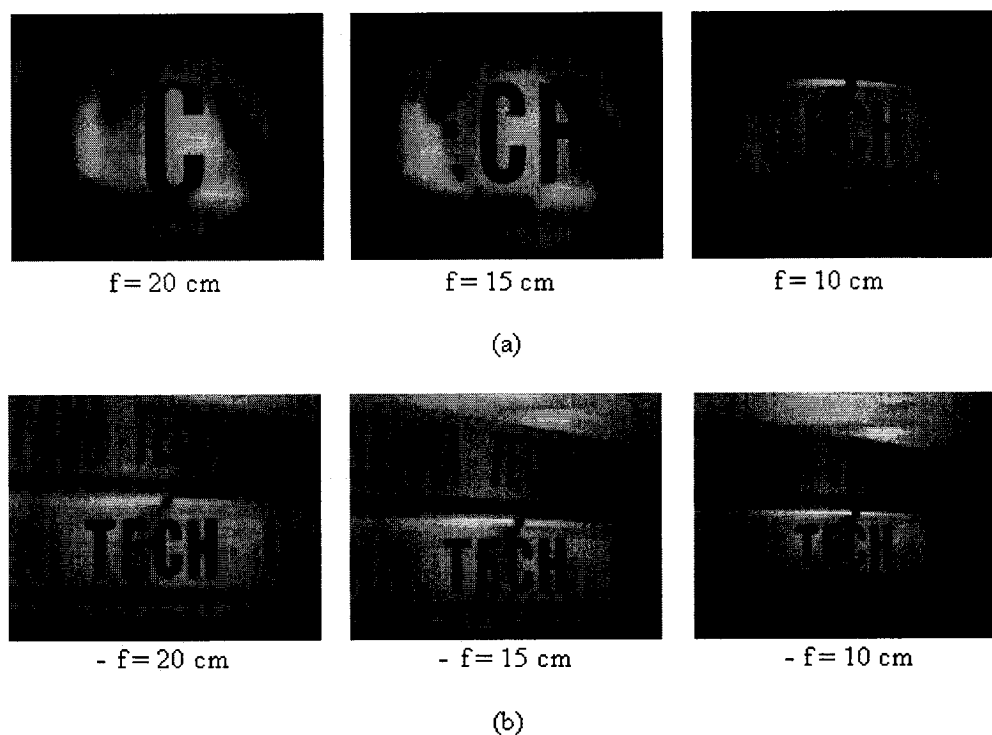


**Figure 3.6: (a) Images captured using the setup shown in Figure 3.3a with first DCX lens of  $f = 20$  cm and a second DCX lens of  $f = 10, 15,$  and  $20$  cm, (b) Images captured using the setup shown in Figure 3.3b with first DCX lens of  $f = 20$  cm and a second DCV lens of  $-f = 10, 15,$  and  $20$  cm.**

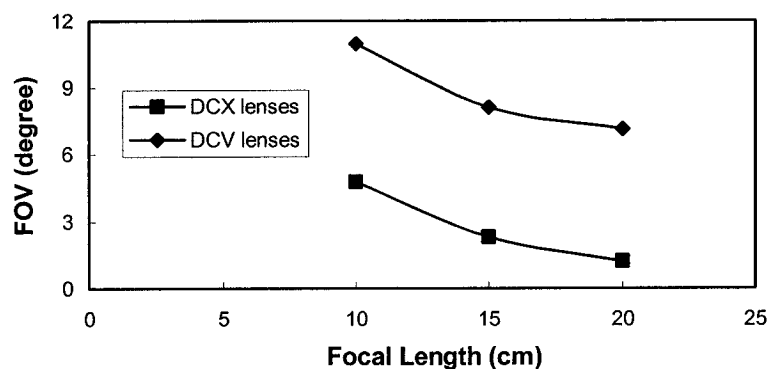


**Figure 3.7: Focal length vs. field of view (FOV) from DCX and DCV lenses.**

Table 3.1 and Table 3.2 show the measured FOV when the object was imaged using different configurations and combinations of DCX and DCV lenses of different focal lengths ( $f$ ) as shown in Figures 3.2b and 3.3.

**Table 3.1: Field of view measured using single double convex lens of focal length  $f = 10$  cm and the different combinations of double concave lenses of focal lengths  $-f = 10, 15,$  and  $20$  cm.**

First DCX lens $f$ (cm)	Single DCV lens $-f$ (cm)	Two DCV lens $-f$ (cm)	Three DCV lens $-f$ (cm)	a (inches)	b (inches)	c (inches)	d (inches)	FOV (degrees) ( $\theta$ )
10	10	-	-	2	0.5	37	9.5	14.5
10	-	10	-	2	1.5	35	18	29
10	-	-	10	2	2.5	34	26	42
10	15	-	-	x	x	x	x	x
10	-	15	-	2	1.5	37	12	18
10	-	-	15	2	1.5	34	13	21.5
10	20	-	-	x	x	x	x	x
10	-	20	-	x	x	x	x	x
10	-	-	20	2	1.5	35	12	19.5

x -- no focus was observed for these combinations

**Table 3.2: Field of view measured using single double convex lens of focal length  $f = 20$  cm and the different combinations of double concave lenses of focal lengths  $-f = 10, 15,$  and  $20$  cm.**

Single DCX lens $f$ (cm)	Single DCV lens $-f$ (cm)	Two DCV lens $-f$ (cm)	Three DCV lens $-f$ (cm)	a (inches)	b (inches)	c (inches)	d (inches)	FOV (degrees) ( $\theta$ )
20	10	-	-	2	3	30	25.5	46
20	-	10	-	2	3.5	31	32	54.5
20	-	-	10	2	4.5	32	52	78
20	15	-	-	2	1	36	22	34
20	-	15	-	2	2	34	24	39
20	-	-	15	2	3.5	33	28	46
20	20	-	-	2	0.5	36	21	32.5
20	-	20	-	2	2.5	33	22	37
20	-	-	20	2	4	32	23	40

The variation of FOV as a function of focal length of one, two, and three DCV lenses in contact and the first DCX lens is shown in Figure 3.8. It can be observed that the FOV varies systematically depending on the focal length and the type of lenses used. The results indicate that the FOV increases with the decrease in the focal length of the either DCX or DCV lens used to image the object. Also, wider FOV could be achieved using DCV lens compared to that of using DCX lens of same focal length. Interestingly, the FOV also increased with the increase in the number of DCV lenses. The FOV from three DCV lenses integrated together is much larger than that from a single DCV lens or integrated two DCV lens system. The focal length of the primary DCX lens used in front of camera to image the object also plays an important role in determining the FOV. The higher the focal length of this lens, the higher the FOV will be. The optical image with a minimum and a maximum FOV achieved from the above-mentioned lens configuration is illustrated in Figure 3.9a and 3.9b, respectively.

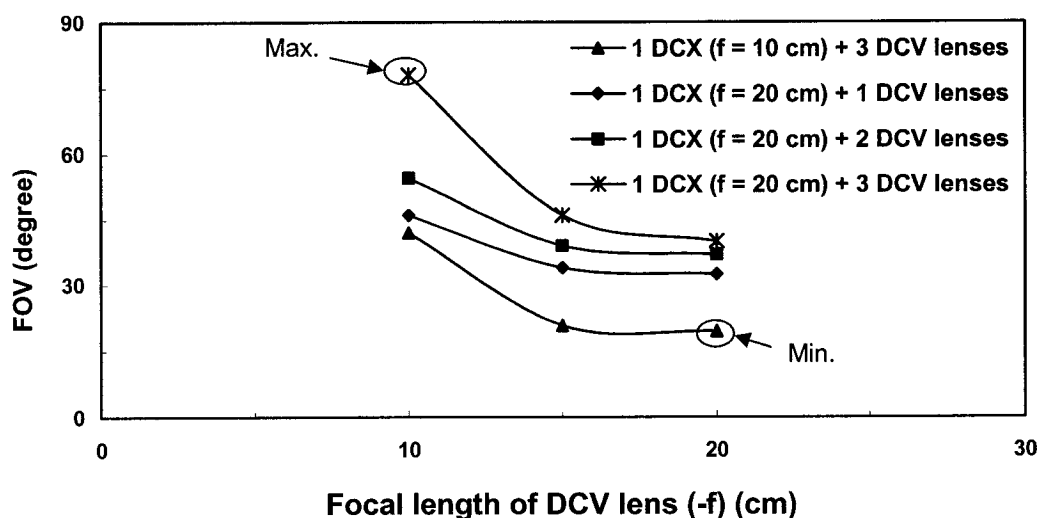


**Figure 3.8: Focal length of DCV lenses vs. FOV for different combinations of DCX and DCV lenses. The focal length of DCX lens is fixed in each series of the imaging experiment.**



(a)



(b)

**Figure 3.9: Image of the object captured using (a) a DCX lens ( $f = 10$  cm) and a DCV lens ( $-f = 20$  cm), (b) a single DCX lens ( $f = 20$  cm) and three DCV lenses ( $-f = 10$  cm).**

## **CHAPTER 4**

### **MACRO-SCALE POLYMER WIDE-ANGLE VARIABLE FOCAL LENGTH LENS SYSTEM**

#### **4.1 Overview**

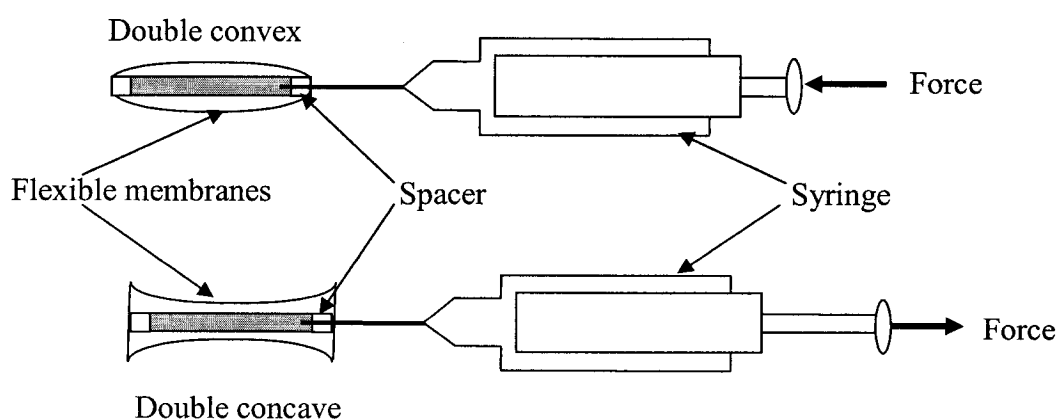
Initial experiments conducted using a set of glass lenses showed that higher field of view (FOV) could be achieved by using a double concave lens (DCV) compared to that of a double convex lens (DCX). It was also observed that the FOV increases by increasing the number of DCV lenses used to image the object. Several design concepts were conceived for fabricating the dynamic lens systems that work on different actuation mechanisms. One simple approach that is being pursued to develop a variable focus lens involves the use of microfluidic lens structures. The advantage of using a fluid actuation mechanism is discussed in Chapter 2. The change in fluid volume inside the lens chamber alters the radius of curvature of the flexible membrane and results in a change of the refractive power. The variable focal length lens structures are made in several sizes to check the viability of actuating the lenses, and also to characterize their imaging performances.

A novel small-scale fluid-controlled optical lens system that is capable of displaying dynamic variation of its focal length and FOV is designed and fabricated.

Refractive optical fluids are either pumped into or out of the lens chamber to obtain the DCX and DCV lens effects, respectively. The flexible membranes for fluid-controlled lenses were fabricated using polydimethylsiloxane (PDMS) polymer material, since PDMS is the material of choice for optical transparency, durability, flexibility, and biocompatibility films. The small-scale dynamic optical lens system designed and fabricated in this work can image the object with a wide range of focal length and FOV. The FOV and focal length could be continuously varied, and a maximum FOV of 118.34 degrees could be achieved by using the fluid-controlled integrated optical lens system demonstrated in this chapter.

#### **4.2 Initial Experiments**

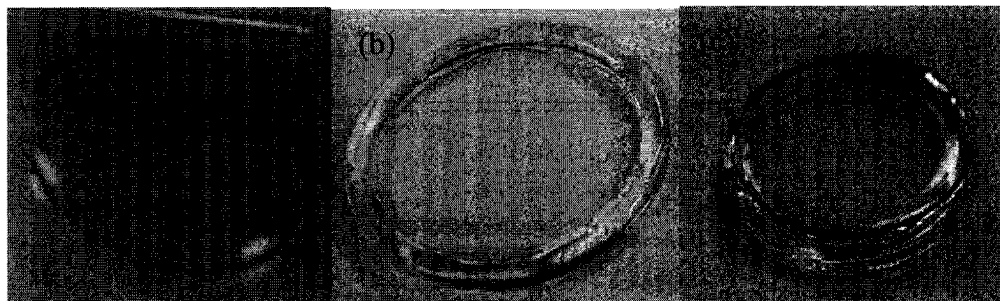
A schematic representation of the dynamic DCX and DCV lenses fabricated using flexible membranes with a spacer in between is shown in Figure 4.1. These lenses are actuated by pumping the optical fluid into the lens chamber or out of the chamber using a syringe pump, as shown in Figure 4.1.



**Figure 4.1: Schematic representation of the flexible membranes behaving as dynamic DCX and DCV lenses.**



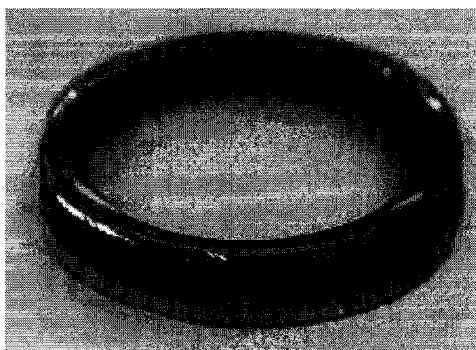
The initial work included casting PDMS in the circular molds and deriving the membranes out of it. On similar lines, the PDMS spacers were fabricated, and the three (two PDMS membrane and one PDMS spacer) were integrated using uncured PDMS elastomer. The resulting lens structure is shown in Figure 4.2c, after curing the PDMS elastomer in the joints.



**Figure 4.2: (a) PDMS membrane, (b) PDMS spacer, (c) Final lens structure with a fluidic chamber.**

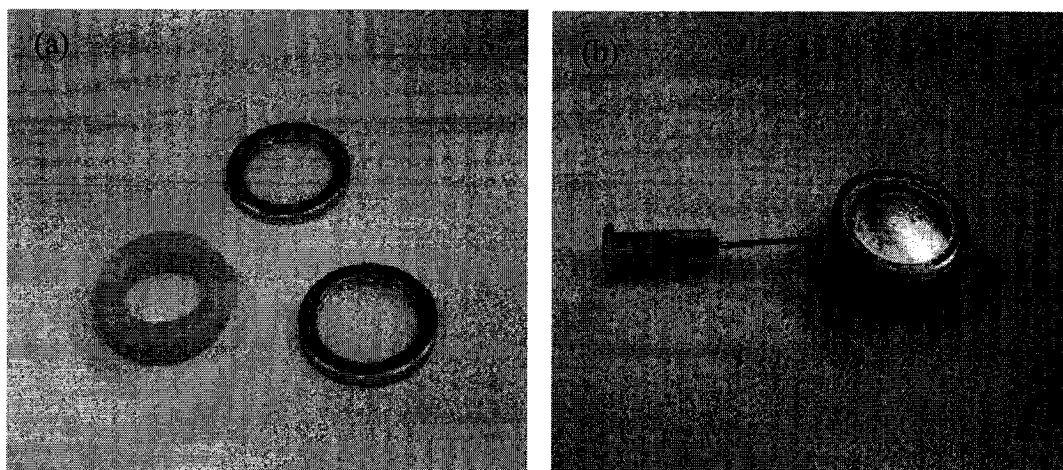
Figure 4.2 shows the first PDMS lens fabricated using PDMS membrane with 1 inch diameter. The PDMS lenses turned out to be good as far as optical clarity and functioning were concerned, but the major problem was their rigidity. PDMS, being soft material, bends easily while it is placed in the lens holder for testing.

The immediate solution for this problem was to use a rubber spacer, as shown in Figure 4.3. The problem of rigidity was solved, but the bonding of PDMS to the rubber spacer was weak and was not able to bear the pressure of the fluid pumped inside. This result was attributed to the chemical reaction between the PDMS and rubber at the interface. But it was not investigated as it was beyond the scope of work. The next solution was to use copper rings as is with the membrane and a plastic spacer in between to form the lens structure (Figure 4.4).



**Figure 4.3: PDMS membrane lens with rubber spacer.**

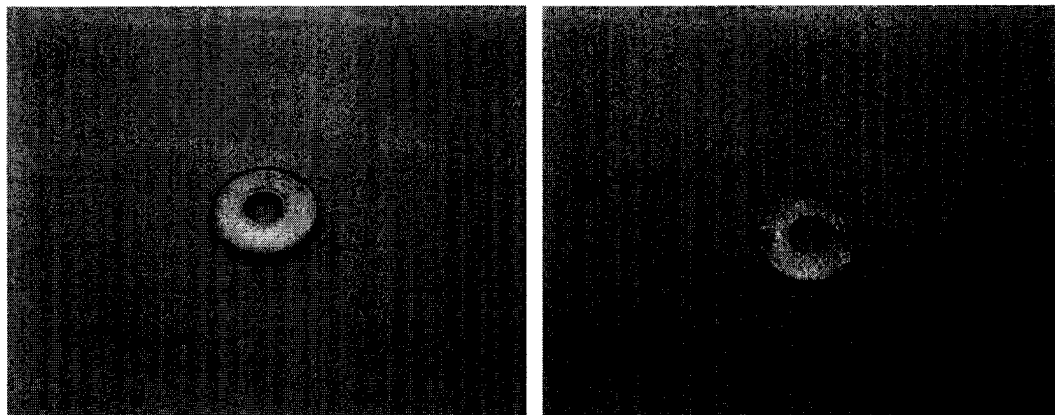
PDMS was cured in the copper ring of O.D. 2.12 cm and I.D. 1.58 cm. The thickness of the PDMS film after curing was measured to be 890  $\mu\text{m}$ . A plastic spacer was used in between these two copper rings with a PDMS membrane to form the fluid chamber, as shown in Figure 4.4. The two rings with a PDMS membrane were attached to the spacer with the fluidic connection, as shown in Figure 4.4b.



**Figure 4.4: (a) Two copper rings with PDMS membrane and plastic spacer, (b) Fluid actuated lens structure.**

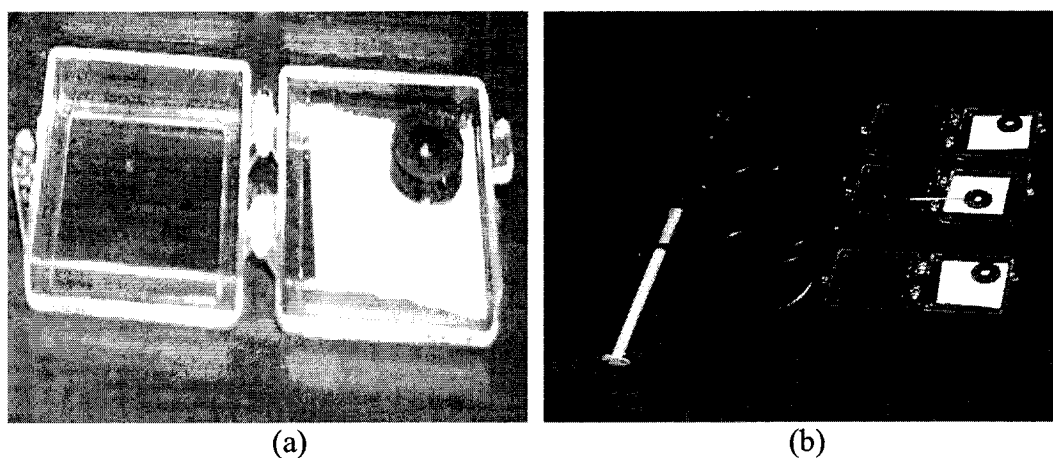
The next step was down-sizing the lens structure using a copper ring of 10 mm outer diameter and 3 mm inner diameter, as shown in Figure 4.5a. The thickness of the ring (1.5 mm) compared to the size of the ring was large which resulted in a small deflection in the PDMS film. Therefore, the ring was etched in the copper etchant to

reduce the thickness. The thickness of the ring after etching was measured to be 600  $\mu\text{m}$ . The inner diameter of the ring changed to 4.3 mm and the outer diameter to 9.5 mm. The copper ring after the etching process is shown in Figure 4.5b.



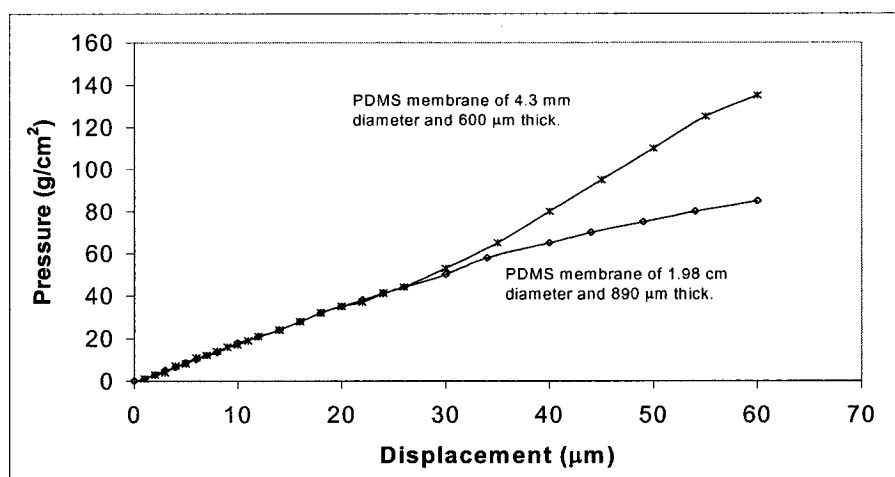
**Figure 4.5: Copper ring (a) before etching, (b) after etching.**

Figure 4.6a shows the lens structure fabricated using the above mentioned copper ring. The lens structures with the fluidic connection are shown in Figure 4.6b. A syringe pump was used to actuate these lenses.



**Figure 4.6: (a) Fluid actuated lens structure fabricated using small copper rings, (b) Lens structures with fluidic connection.**

Before pumping the fluid, the tensile strength of the PDMS membrane was tested using a force meter. The PDMS membranes formed in different sized copper rings were subjected to a slowly increasing applied pressure. The displacement of PDMS membranes as a function of applied pressure is shown in Figure 4.7. For low values of applied pressure, both membranes showed almost similar deflection. However, when the applied pressure was increased, the smaller membrane was found to deflect less than the larger membrane and tends to break.



**Figure 4.7: Pressure vs. displacement plot for two different sized PDMS membranes.**

After performing the tensile strength test, the lens structure with a larger diameter, as shown in Figure 4.4b, was tested for deflection of PDMS membrane. It was observed that this type of structure resulted in leaks when the fluid was injected into the spacer chamber. This was due to the small pores left in between the joints of the copper ring and the plastic spacer. The smaller lens structure, as shown in Figure 4.5b, was also tested for deflection of the membrane by inserting the fluid into the empty chamber using a syringe pump. It was noted that there were no leaks. It was observed that, when the fluid (DI water) is pumped-in, the structure turns into a DCX lens, and when the fluid is

pumped-out it turns into a DCV lens. The demonstration of this lens structure, when actuated as DCX or DCV lens, is shown in Figure 4.8. However, it was observed that these lens structure could not hold the fluid pressure for a long time and the fluid started leaking from the joints between the copper ring and the rubber spacer. The next solution was to use an integrated lens structure with a plastic spacer and PDMS membrane without copper rings. This structure, when tested, did not show any fluidic leaks and was able to withstand the fluidic pressure built by an external syringe pump. Therefore, in the next section of this chapter a complete fabrication and testing of this type of lens structure with PDMS membrane and plastic spacer are demonstrated.

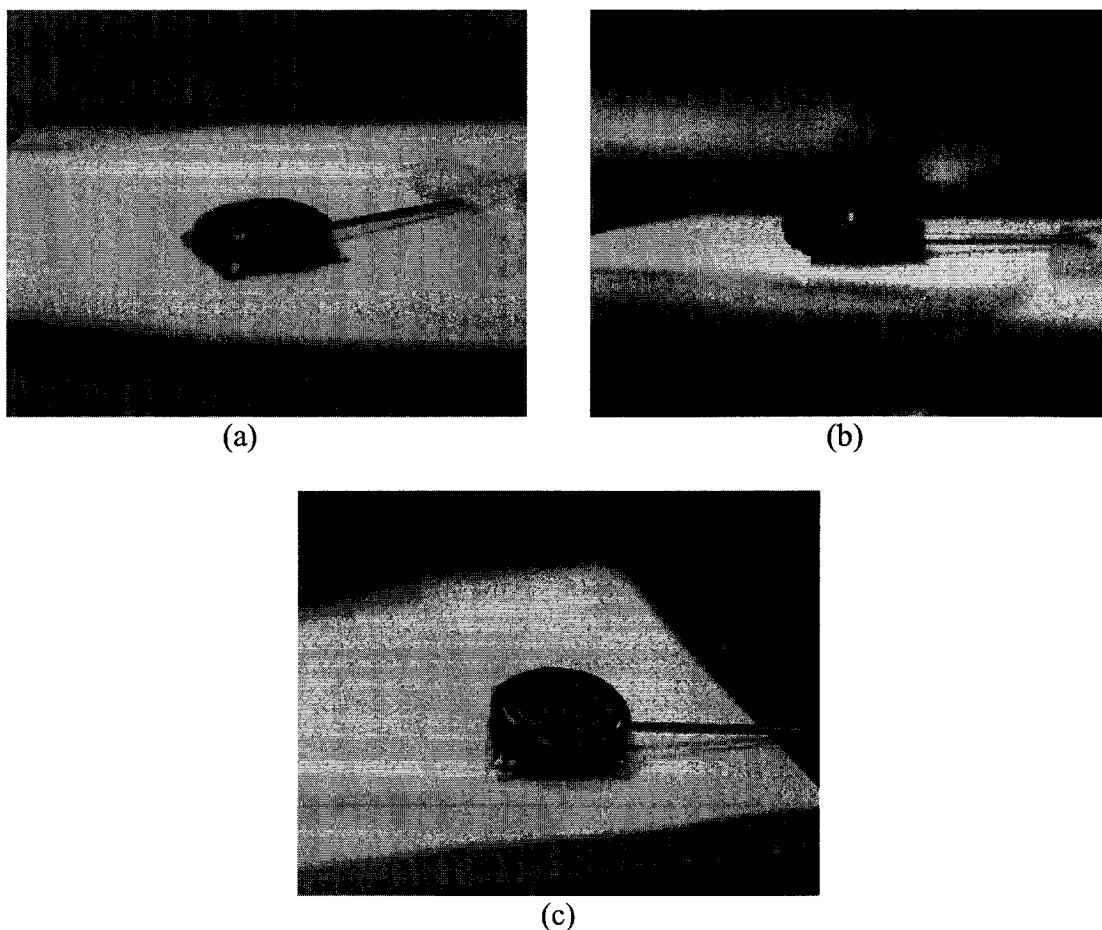


**Figure 4.8: (a) Normal fluid actuated lens structure. Fluid actuated structure as (a) DCX lens, (b) DCV lens.**

### 4.3 Macro-Scale Polymer Wide-Angle Variable Focal Length Lens System

Several polymer lenses were made by casting PDMS material in a suitable circular mold. After curing the PDMS membrane inside the circular mold, two such units were combined by placing a spacer in between, and the whole assembly was sealed and made leakproof. A small hole was made in the spacer unit to fabricate the channel through which a high refractive index fluid (in this case, DI water) could be pumped into and out of the lens chamber. Figure 4.9a shows the single unit without fluidic connection, and Figure 4.9b shows the assembled variable optical lens systems of 7.9 mm in radius with 1.5 mm thick spacer in between.

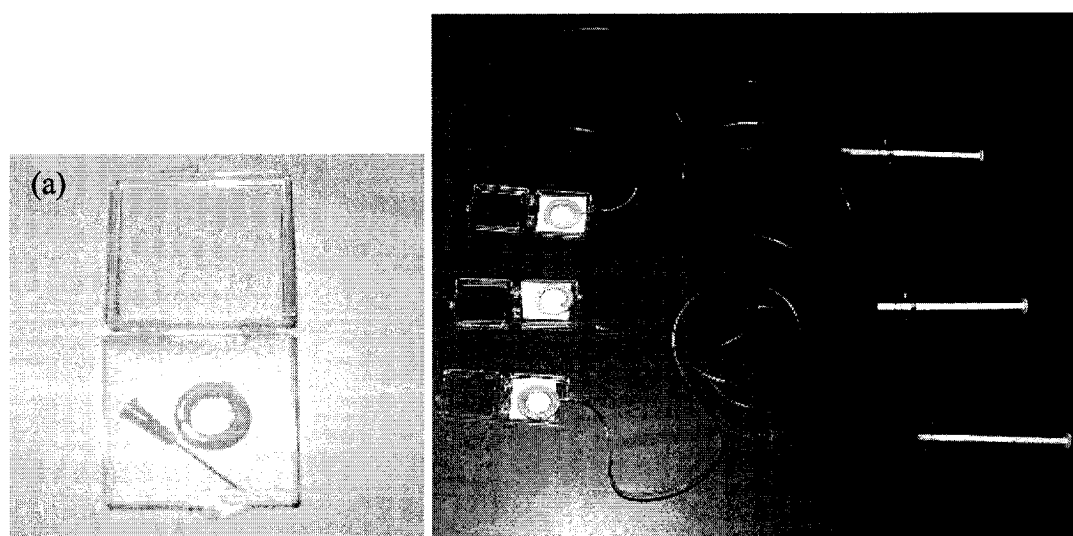


**Figure 4.9: (a) Variable focal length lens unit (radius - 7.9 mm, thickness - 1.5 mm), (b) Variable focal length lenses with fluidic connections.**

For each dynamic lens, the volume ( $v_c = 0.294$  ml) of the lens chamber was calculated by determining the diameter and the thickness of the spacer unit by assuming the PDMS membrane is flat. However, in reality, the PDMS membrane does not remain flat. First, the optical fluid (DI water) was pumped into the lens chamber until the chamber was filled and the membrane becomes flat. At this point, the volume of the fluid

( $v_1 = 0.289$  ml) necessary to fill the chamber without any noticeable curvature of the membrane was monitored. The small discrepancy between the calculated ( $v_c$ ) and measured values ( $v_1$ ) can be attributed to the sealing joints inside the chamber that would reduce the available space. As mentioned earlier, pumping more fluid into the lens chamber will make the lens structure behave like a DCX lens, whereas removal of the fluid from the lens chamber will make it behave like a DCV lens.

In the case of a DCX lens configuration, the maximum volume of fluid ( $v_2$ ) that can be pumped into the lens chamber without rupturing the lens membrane was measured. If we define  $v_3$  as the difference between  $v_2$  and  $v_1$  ( $v_3 = v_2 - v_1$ ), then  $v_3$  represents the volume of fluid that was actually used to cause the deflection of the membranes to form the DCX lens. Similarly, in the case of a DCV lens configuration, the maximum volume of fluid ( $v_5$ ) that can be pumped out from the already filled ( $v_1$ ) lens chamber was monitored. Theoretically,  $v_1$  and  $v_5$  are expected to be the same. The difference between  $v_1$  and  $v_5$  would represent the amount of fluid trapped in the chamber ( $v_1 - v_5$ ). The volume of fluid that is pumped-out to actuate the variable focal length lens structure as DCV lens is referred to as  $v_4$ .

The geometrical deflection of the membrane as a result of pumping fluid into the lens chamber is shown in Figure 4.10, and the associated volume of the lens chamber above the spacer chamber was calculated by using the formula for a spherical cap as given in Equation 4.1, where  $h$  is the membrane deflection height;  $r_1$  is base radius;  $v_3/2$  volume of the spherical cap which represents one side of the DCX lens. Since, the volume of fluid  $v_3$  is used to deflect the PDMS membranes on both sides, only half the volume of fluid pumped-in was considered.

$$\frac{V_3}{2} = \left(\frac{\pi}{6}\right)(3r_1^2 + h^2)h \quad (4.1)$$

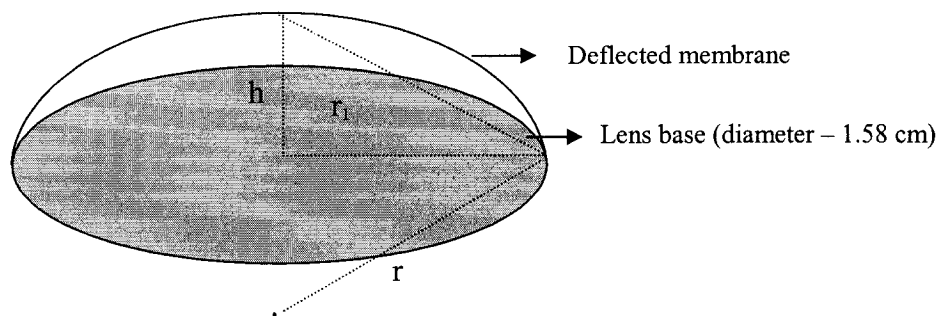


**Figure 4.10: Schematic diagram showing the deflection of the PDMS membrane above the spacer unit.**

Equation 4.1 is commonly derived using differential calculus, but, using volume of sphere and surface area of sphere, this equation can be derived geometrically. The spherical cap can be seen as the difference between a spherical sector and a cone, as shown in Figure 4.11.

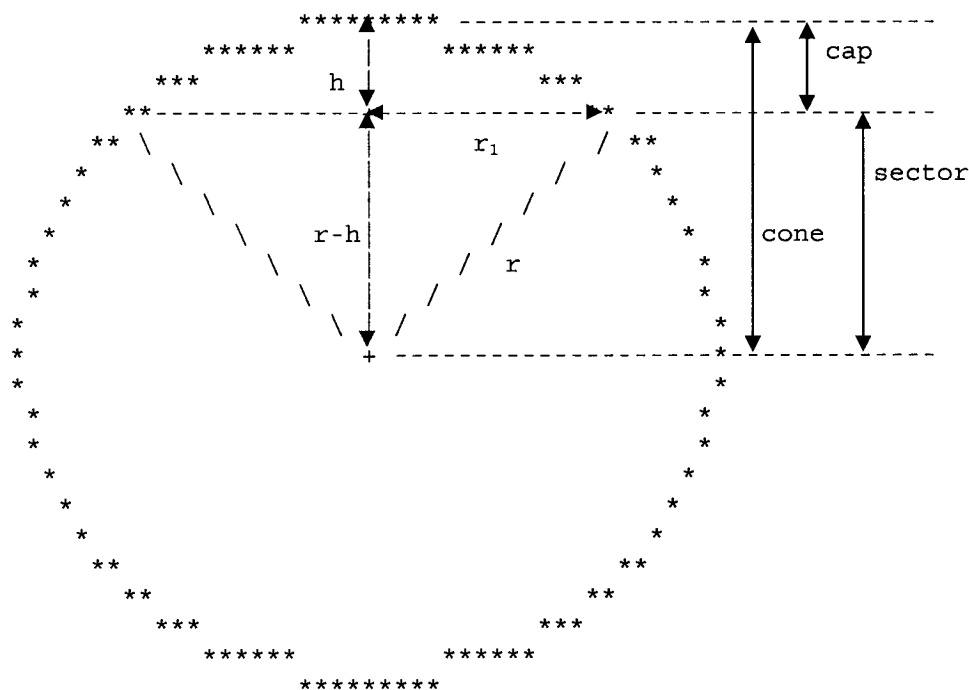


**Figure 4.11: Two-dimensional schematic of spherical cap [173].**



The volume of the sector is proportional to the surface area of the cap compared to that of the whole sphere. This can be observed from Figure 4.11 by assuming it as composed of many thin pyramids meeting at the center. Thus,

$$V_{SC} = \frac{A_C}{A_{SP}} \times V_{SP} = \frac{2 \cdot \pi \cdot r \cdot h \times (4/3) \cdot \pi \cdot r^3}{4 \cdot \pi \cdot r^2} \quad (4.2)$$

$$\Rightarrow V_{SC} = \frac{h \times (4/3) \cdot \pi \cdot r^3}{2 \cdot r} \quad (4.3)$$

$$V_{SC} = (2/3) \cdot \pi \cdot r^2 \cdot h \quad (4.4)$$

where  $V_{SC}$  is the volume of the sector,  $A_C$  is the area of the cap,  $A_{SP}$  is the area of the sphere,  $r$  is the radius of the sphere,  $h$  is the height of the cap, and  $V_{SP}$  is the volume of the sphere. Now, the volume of the cap  $V_C$  is given by Equation 4.5, where  $V_{Co}$  is the volume of the cone (Equation 4.6) and  $r_1$  is the radius of the circle (Equation 4.7) at which the cone and the cap meet (Figure 4.11).

$$V_C = V_{SC} - V_{Co} \quad (4.5)$$

$$V_{Co} = \frac{1}{3} \pi r_1^2 (r - h) \quad (4.6)$$

$$r_1^2 = r^2 - (r - h)^2 = 2rh - h^2 \quad (4.7)$$

Substituting Equation 4.4, 4.6, and 4.7 in Equation 4.5,  $V_C$  can be written as

$$V_C = \frac{2}{3} \pi r^2 h - \frac{1}{3} \pi (2rh - h^2)(r - h) \quad (4.8)$$

$$\Rightarrow V_C = \frac{2}{3} \pi r^2 h - \frac{1}{3} \pi (2r^2 h - 3rh^2 + h^3) \quad (4.9)$$

$$\Rightarrow V_C = \frac{1}{3} \pi h (3rh - h^2) \quad (4.10)$$

From Equation 4.7,  $rh$  can be written as

$$rh = (r_1^2 + h^2) / 2 \quad (4.11)$$

Therefore, from Equation 4.10 and 4.11,  $V_C$  can be formulated as

$$V_C = \frac{1}{3} \pi h \left[ \frac{3}{2} (r_1^2 + h^2) - h^2 \right] \quad (4.12)$$

$$\Rightarrow V_C = \frac{1}{6} \pi h [3r_1^2 + h^2] \quad (4.13)$$

Equation 4.13 and Equation 4.1 are similar with the only difference being that the volume  $v_3$  is taken as half because this volume deflects both the top and bottom membranes of the formed lens. So, only half of the volume is used to deflect the top membrane or the bottom membrane. From Equation 4.1, when the volume  $v_3$  and the radius of spacer unit  $r_1$  are known, then maximum deflection at the centre of the membrane  $h$  can be calculated. Once  $h$  is known, the radius of curvature of the lens  $r$  can be calculated using Equation 4.14 which is similar to Equation 4.11.

$$r = \frac{(h^2 + r_1^2)}{2h} \quad (4.14)$$

From the radius of curvature of the lens, the focal length ( $f$ ) can be calculated using the formula given in Equation 4.15, where  $n_1$  is the refractive index of air and  $n_2$  is the refractive index of DI water ( $n_2 = 1.33$ ). Figure 4.11 shows the variation of focal length with respect to the volume of fluid pumped-in when a lens unit with spacer of 7.9 mm radius is used.

$$f = \frac{r}{2(n_2 - n_1)} \quad (4.15)$$

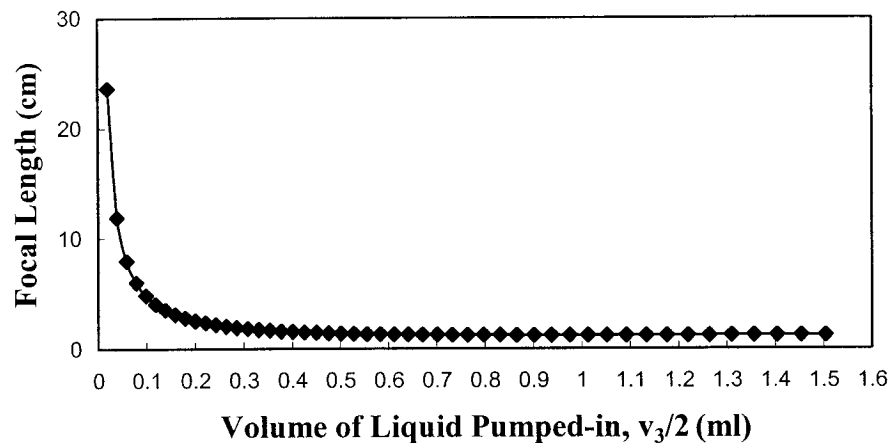


**Figure 4.12: Focal length ( $f$ ) vs. volume of fluid pumped-in ( $v_3/2$ ).**

The object was imaged with different combinations of dynamic lenses at different volumes of fluid pumped-in ( $v_3$ ) or pumped-out ( $v_4$ ). A syringe pump was used to increase or decrease the volume of fluid in the lens chamber, and the image of the object through the lens structure was captured for each fluid level.

First, a single dynamic lens was actuated as DCX lens by pumping fluid into the lens chamber (0.02 ml each time) to view the object. A static DCX glass lens ( $f = 10$  cm) was placed between the dynamic lens and the camera to image the object along with a dynamic lens configured as a DCX lens. The series of images captured by pumping different volumes of fluid into the lens chamber is shown in Figure 4.13. The FOV was calculated as shown in Chapter 3 using the formula given in Equation 3.1. The focal length of the DCX lens formed at each level of volume of fluid pumped-in was calculated using Equation 4.1. The variation of FOV and focal length with respect to the volume of fluid pumped-in are shown in Figure 4.14. It can be observed that, as the fluid was pumped into the lens chamber, the focal length of the lens decreases as a result of

decrease in the radius of curvature. It can also be observed that, as the focal length of this dynamic DCX lens decreases, the FOV increases as observed in the case of experiments conducted using a static glass lens in Chapter 3.

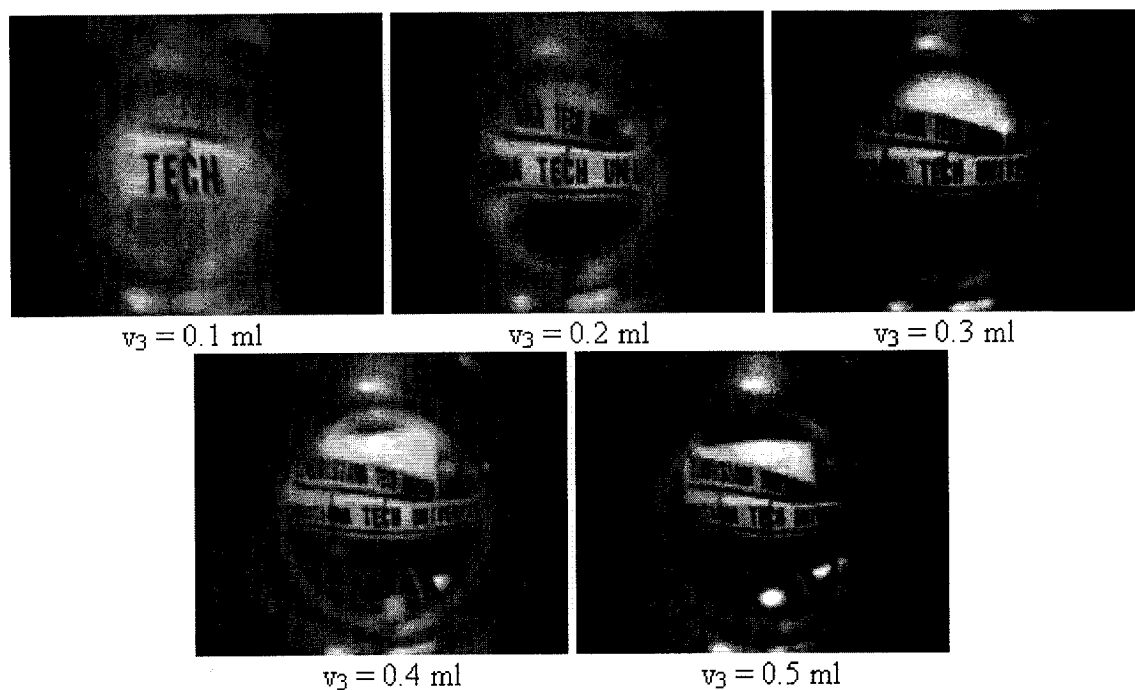


**Figure 4.13: Series of images captured at different volumes of fluid ( $v_3$ ) pumped into the lens chamber using single dynamic DCX lens system.**

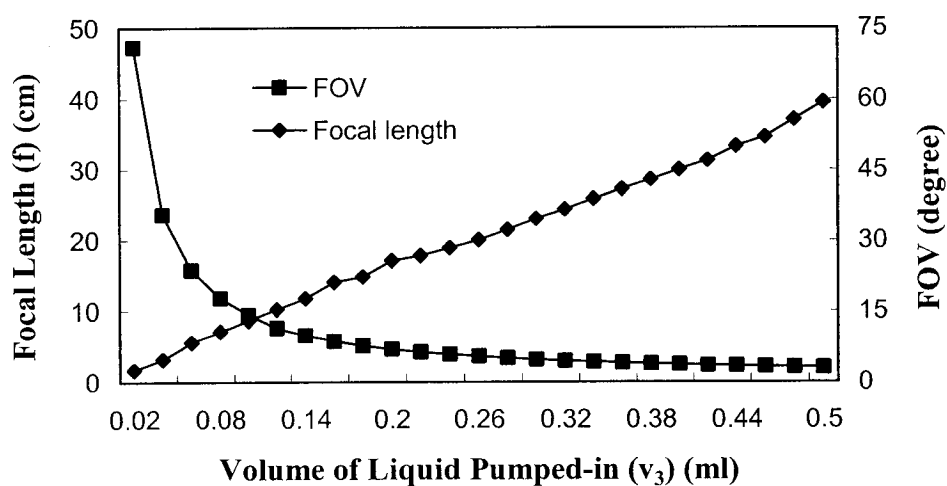


**Figure 4.14: Variation in the FOV and focal length as a function of the volume of fluid ( $v_3$ ) pumped-in achieved by using single dynamic DCX lens system.**

The variation of distance between the first fixed DCX lens and the single dynamic DCX lens system at every 0.02 ml volume of fluid pumped-in (focal length) to bring the fixed object into focus is shown in Figure 4.15.

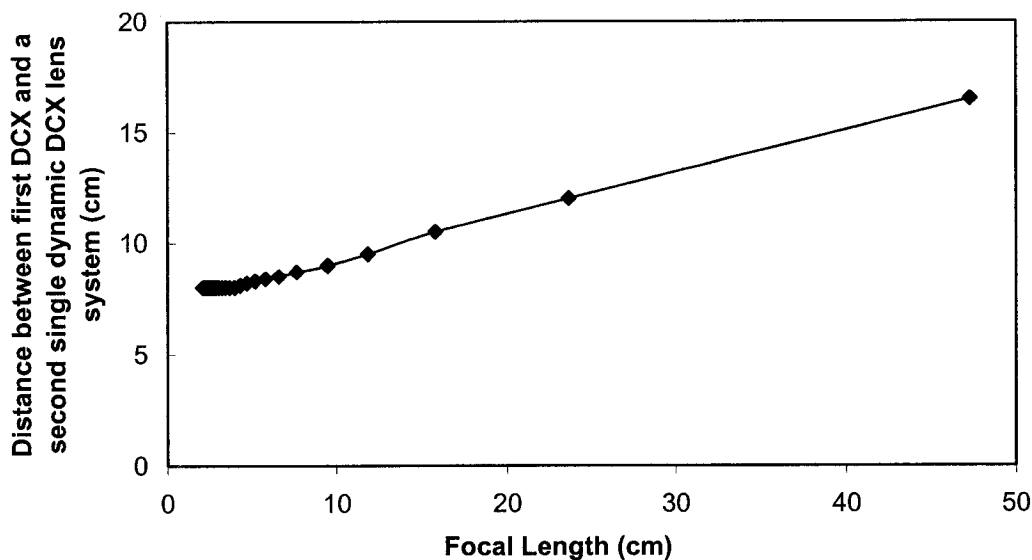


**Figure 4.15: Focal length vs. distance between the first fixed DCX and a second single dynamic DCX lens system.**

The f-number ( $f_{\#}$ ) and numerical aperture (NA) of the single dynamic DCX lens system with a radius of 7.9 mm are calculated using the formula given in Equation 4.16 and 4.17, respectively, where  $f$  is the focal length and  $D$  is the diameter of the lens.

$$f_{\#} = \frac{f}{D} \quad (4.16)$$

$$NA = \frac{\frac{1}{2}D}{\sqrt{\left(\frac{1}{4}D^2 + f^2\right)}} \quad (4.17)$$

The change in f-number and numerical aperture with respect to the volume of fluid pumped into the lens chamber of the single dynamic DCX lens system is shown in Figure 4.16. The smallest f-number achieved from the single dynamic DCX lens system

is 1.3 which corresponds to the numerical aperture of 0.35. The value of the numerical aperture achieved using the single dynamic DCX lens system is higher than the reported values to date using other types of variable focal length lenses (see Section 2.8.1).

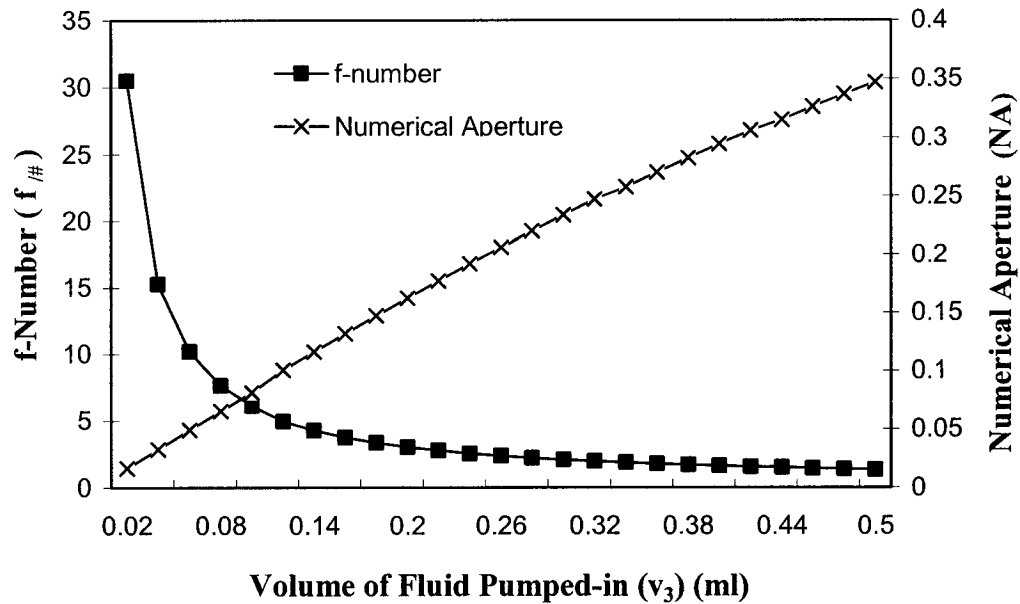


**Figure 4.16: The f-number ( $f_{\#}$ ) and numerical aperture (NA) with respect to the volume of fluid ( $v_3$ ) pumped-in for the single dynamic DCX lens system.**

In a different set of experiments, the single dynamic lens system was actuated as a DCV lens by pumping fluid out of the lens chamber (0.02 ml each time) to view the object. For comparison, the same static DCX lens ( $f = 10$  cm) was used in front of the camera to image the object. As it was found that two or three DCV lenses are essential for achieving wide FOV, the integrated dynamic lens system with two or three DCV lenses were fabricated by assembling similar single dynamic lens structures. The single dynamic lens system and integrated dynamic lens system with two and three DCV lenses are shown in Figure 4.17.

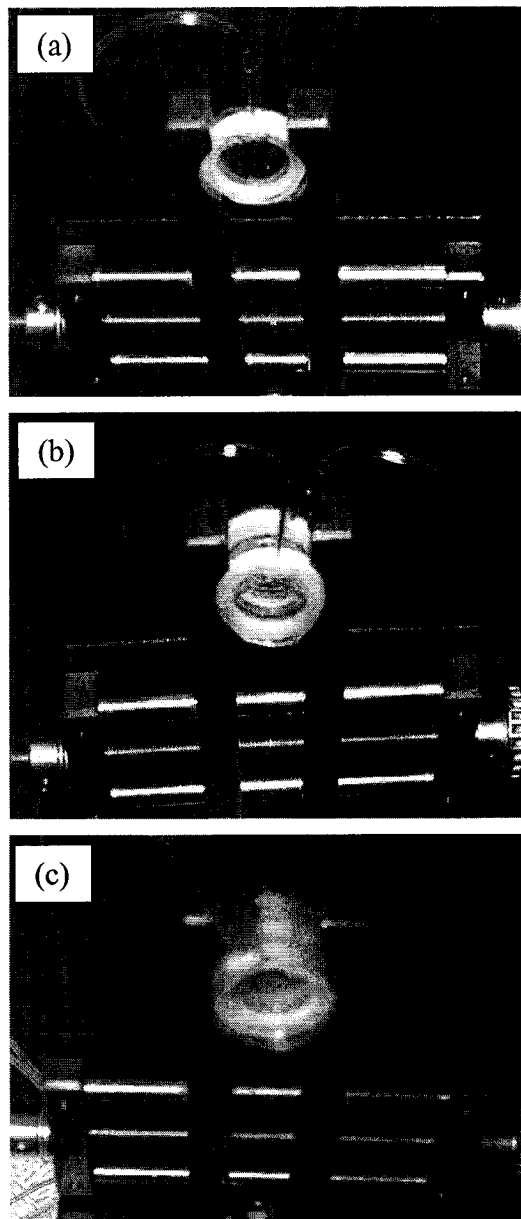


**Figure 4.17: (a) Single dynamic lens system, (b) Integrated dynamic lens system with (b) two DCV lenses, (c) three DCV lenses.**

The series of images captured when the dynamic lens system was actuated as a DCV lens at different volumes of fluid pumped out of the lens chamber are shown in Figure 4.18. It should be noted that, for this particular lens structure, a maximum of 0.18 ml could be pumped out. In the set of experiments that followed, the object was imaged using an integrated dynamic lens system with two or three DCV lenses by

pumping fluid out (0.02 ml each time) identically from all the lens chambers. Figures 4.19a and 4.19b show the series of images captured using an integrated dynamic lens system with two or three DCV lenses in contact, respectively. Here, the volume  $v_4$  represents the volume of fluid pumped-out from each lens chamber. It can be observed from Figures 4.19a and 4.19b that as the fluid was pumped out of the lens chamber, the focal length of the formed DCV lenses decreases and larger FOV can be achieved as observed in the case of static glass lenses. Figure 4.20 shows the image captured using the integrated three dynamic lens system by pumping-out the maximum volume of fluid (0.17 ml) before the lenses were ruptured. It can be observed that, when the FOV is increased, the image happens to be small and the intensity of the captured image decreases. So, further increasing the number of DCV lenses to increase the FOV will make the image smaller with lower intensity, which attenuates the finer details of the object imaged.

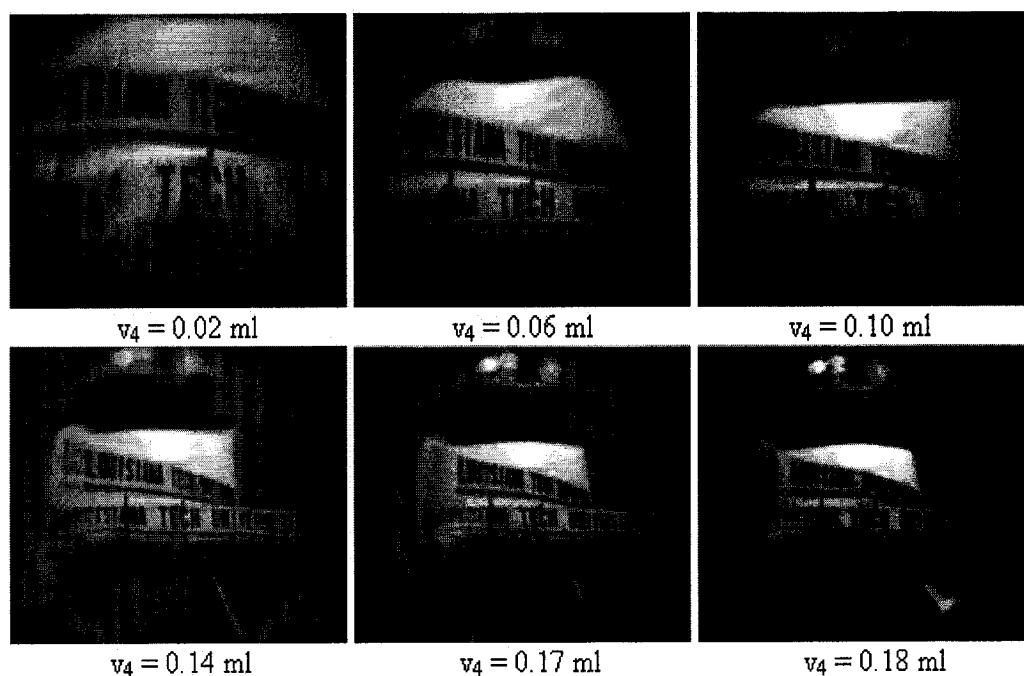


**Figure 4.18: Series of images captured using single dynamic DCV lens system.**



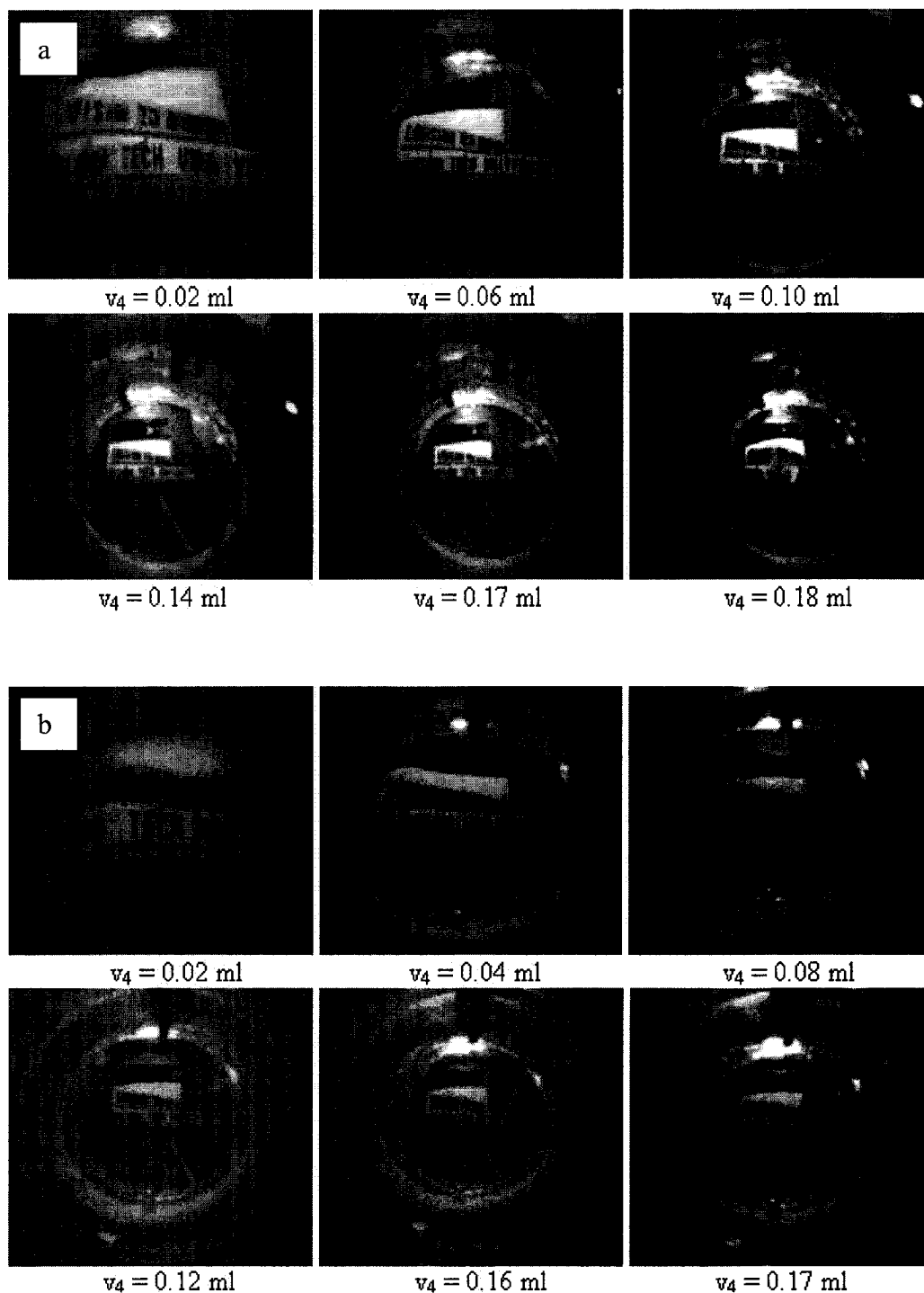


**Figure 4.19: Series of images captured using integrated dynamic lens system with (a) two DCV lenses, (b) three DCV lenses at different volumes of fluid ( $v_4$ ) pumped out of each lens chamber of the integrated system.**

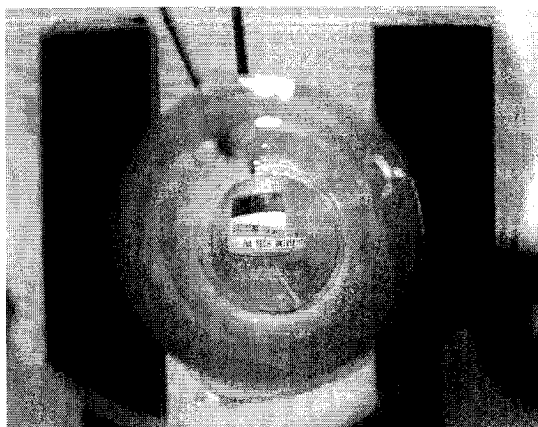


**Figure 4.20: Image of the object captured using integrated dynamic lens system with three DCV lenses.**

The FOV achieved using a single, integrated dynamic lens structure with two and three DCV lenses was measured at each level of volume of fluid pumped-out. The variation in the effective focal length and FOV with respect to the volume of liquid pumped out of the lens chamber of the single, integrated dynamic lens structure with two and three DCV lenses are shown in Figures 4.21a-c, respectively, where  $-f_1$  represents the focal length of the single dynamic DCV lens,  $-f_2$  represents the effective focal length of the two dynamic DCV lens system, and  $-f_3$  represents the effective focal length of the three dynamic DCV lens system. The maximum FOV achieved with the single dynamic DCV lens system was 50 degrees. It should be noted that the FOV increases (112 degrees) when two integrated DCV lenses are used to image the object compared to that of one DCV or DCX lens. The FOV further increases when three integrated dynamic DCV lenses are used to image the object compared to that of one or two integrated dynamic DCV lenses, and, by using this integrated lens system, the maximum FOV of 118.34 degrees was achieved. Figures 4.22a-c show the variation in the distance between the first fixed DCX lens and the single, two, and three dynamically DCV lens systems, respectively, to bring the object into focus with respect to the change in focal length.

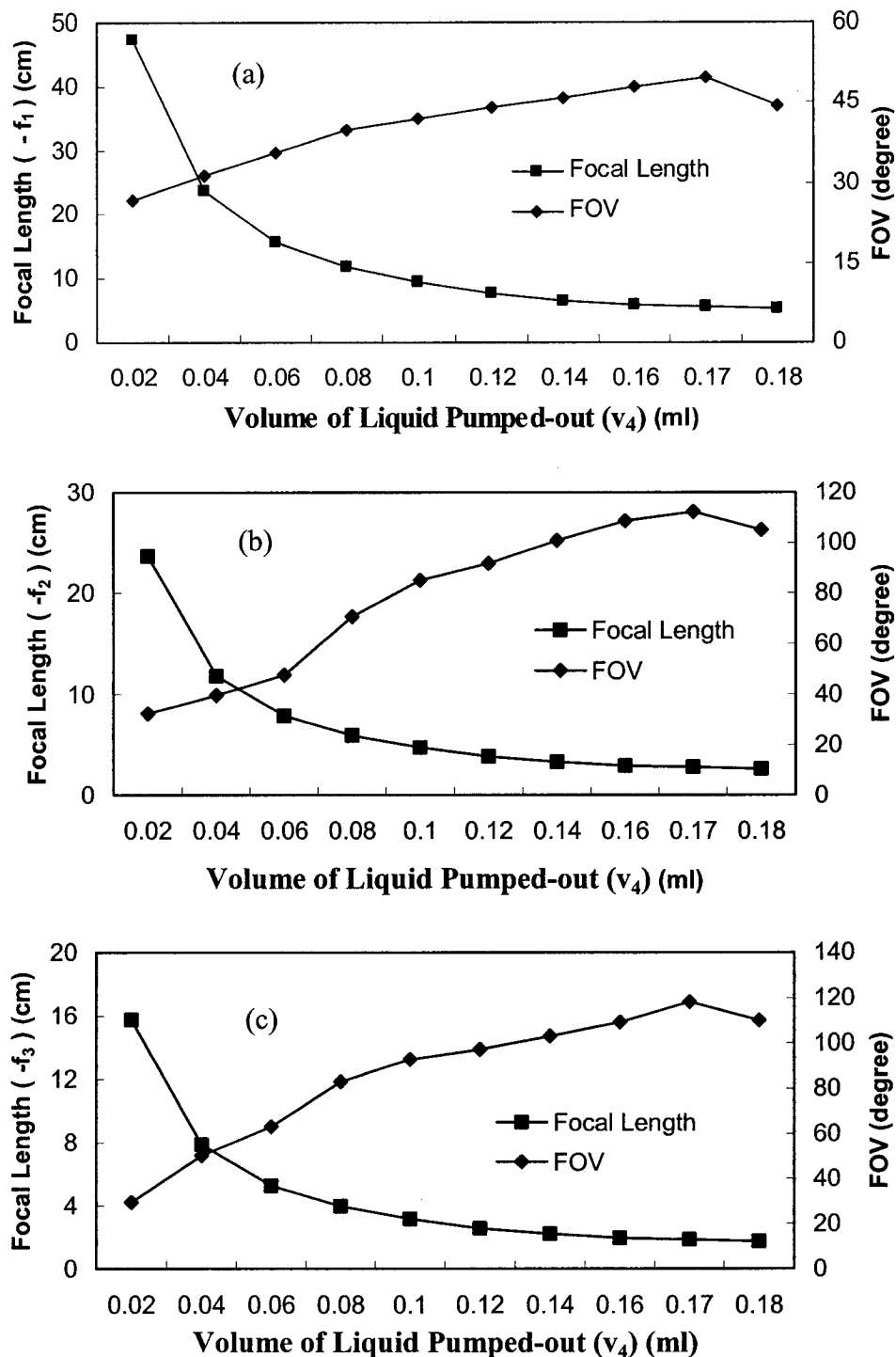
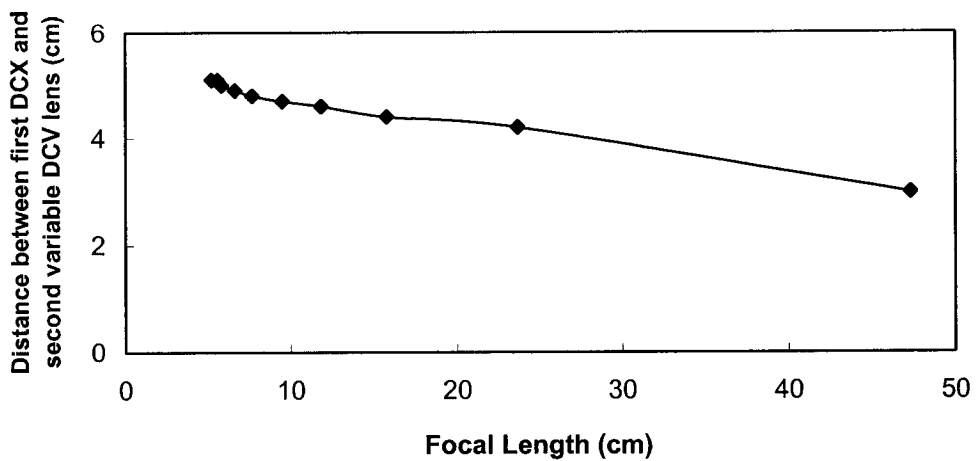
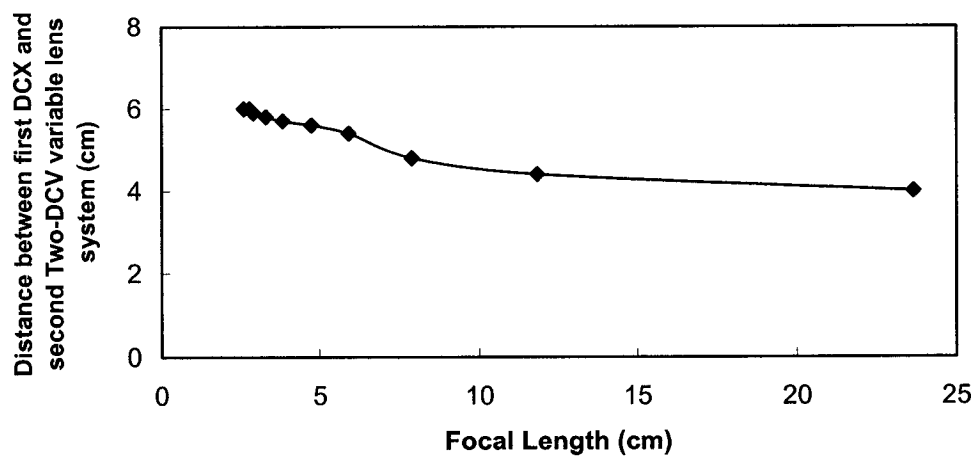


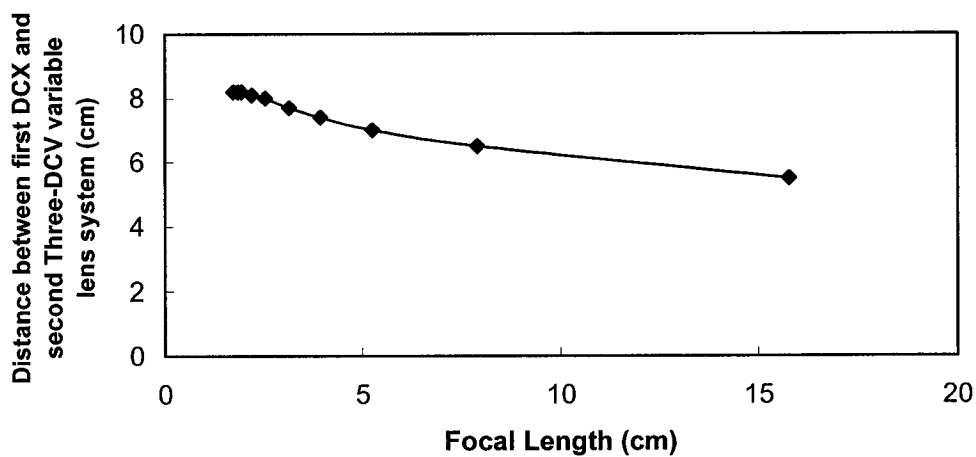
**Figure 4.21: Variation in the focal length and the field of view (FOV) with change in volume of liquid ( $v_4$ ) pumped out of each lens chamber using dynamic lens system with (a) single DCV lens, (b) two DCV lenses, (c) three DCV lenses.**



(a)



(b)



(c)

**Figure 4.22: Focal length vs. distance between the fixed DCX and dynamic lens system with (a) single DCV lens, (b) two DCV lenses, (c) three DCV lenses.**

Table 4.1 shows the summary of the change in focal length and field of view with change in the volume of fluid pumped-out of each lens chamber of the single dynamic DCV lens system and integrated dynamic two and three DCV lens systems. It can be noted from Table 4.1 that the integrated three DCV dynamic lens system has wide FOV (118.34 degree) with focal length ranging from -15.76 to -1.85 cm.

**Table 4.1: Change in focal length and field of view with volume of fluid pumped-out of different dynamic DCV lens systems.**

Volume of liquid pumped-out from each lens chamber ( $v_4$ )	Focal Length (-f)			Field of View		
	Single DCV	Two DCV	Three DCV	Single DCV	Two DCV	Three DCV
0.02	47.29	23.64	15.76	26.79	32.34	29.48
0.04	23.66	11.83	7.89	31.33	39.71	50.28
0.06	15.78	7.89	5.26	35.59	47.77	63.14
0.08	11.85	5.93	3.95	39.77	70.55	82.93
0.1	9.49	4.75	3.16	41.82	85.00	92.83
0.12	7.67	3.84	2.56	43.85	91.69	97.27
0.14	6.62	3.31	2.21	45.86	100.80	103.16
0.16	5.83	2.91	1.94	47.83	108.61	109.18
0.17	5.56	2.78	1.85	49.57	112.20	118.34
0.18	x	x	x	x	x	x

x – DCV lens ruptured at this point

## CHAPTER 5

### POLYMER-BASED WIDE-ANGLE DYNAMIC MICRO-OPTIC LENS SYSTEM

#### 5.1 Overview

For the next generation of customer products such as mobile phones, security cameras, and surgical instruments in medical field, lenses with dynamic features and high resolution have become an important feature. After designing and fabricating the macro-scale variable focal length, the same design is followed to fabricate micro-scale lenses with variable focal length. In this chapter, design, fabrication and testing of novel micro-scale variable focal length optical lens systems will be demonstrated. The flexible polymer (PolyDiMethyl Siloxane) PDMS membrane, used to form the lens shape, is actuated by fluidic pressure built by a syringe pump. The diameter of the fabricated lens is 4000  $\mu\text{m}$ , and the thickness is 500  $\mu\text{m}$ . The thickness of the PDMS membrane was measured to be 60  $\mu\text{m}$ . The total volume of the fabricated lens chamber was measured to be 21.28  $\mu\text{l}$ . The dimensions of the lens assembly are 10 mm x 10 mm x 1.5 mm. The variable focal lens structure thus fabricated is capable of forming dual mode, double convex (DCX) lens when the fluid is pumped into the lens chamber and double concave (DCV) lens when the fluid is pumped out of the lens chamber. Two or three variable focal length lenses are integrated, and a single wide-angle variable focal length lens is

fabricated and tested for its wide field of view (FOV). Similarly, this method can be adopted to fabricate smaller sized (500  $\mu\text{m}$ ) diameter lenses. The fabrication of dynamic microlens systems, presented in this research, involves standard photolithography and silicon micromachining techniques which will be demonstrated in detail in this chapter. The fabrication of PDMS membrane and its optical characteristics using a UV-Vis spectroscope will be demonstrated in detail. The bonding of PDMS membrane to the silicon substrate, with a lens chamber, to form flexible membrane has also been investigated and will be demonstrated in this chapter. The relation between the variation of focal length and FOV with the volume of fluid pumped into or out of the lens chamber has also been investigated and will be presented in this chapter. A complete characterization of the variable focal length lens system for its imaging and optical properties will be demonstrated in detail. The imaging and optical characteristics of the integrated dynamic microlens system with two or three DCV lenses have also been investigated and will be presented in the latter part of this chapter.

## **5.2 Design and Fabrication of Variable Focal Length Microlens System**

### **5.2.1 Fabrication Process Steps**

The process steps involved to fabricate the variable focal length microlens system are shown in Figure 5.1. First, a mask is designed for photolithography and ICP (Inductive Coupled Plasma) etching. This mask is transferred onto the wafer by using AZ 4903 photoresist. The oxide layer under the photoresist is protected to get better bonding between the silicon wafer and PDMS film, as discussed in Chapter 2. After forming a circular pattern (through hole) in the silicon wafer and bonding the PDMS membrane,

two such units are taken and bonded together with a spacer having similar size of the circular lens chamber and microchannel to pass optical fluid. The shape and the focal length of this single microlens structure can be varied by pumping fluid in or out of the lens chamber, as shown in Figure 5.1.

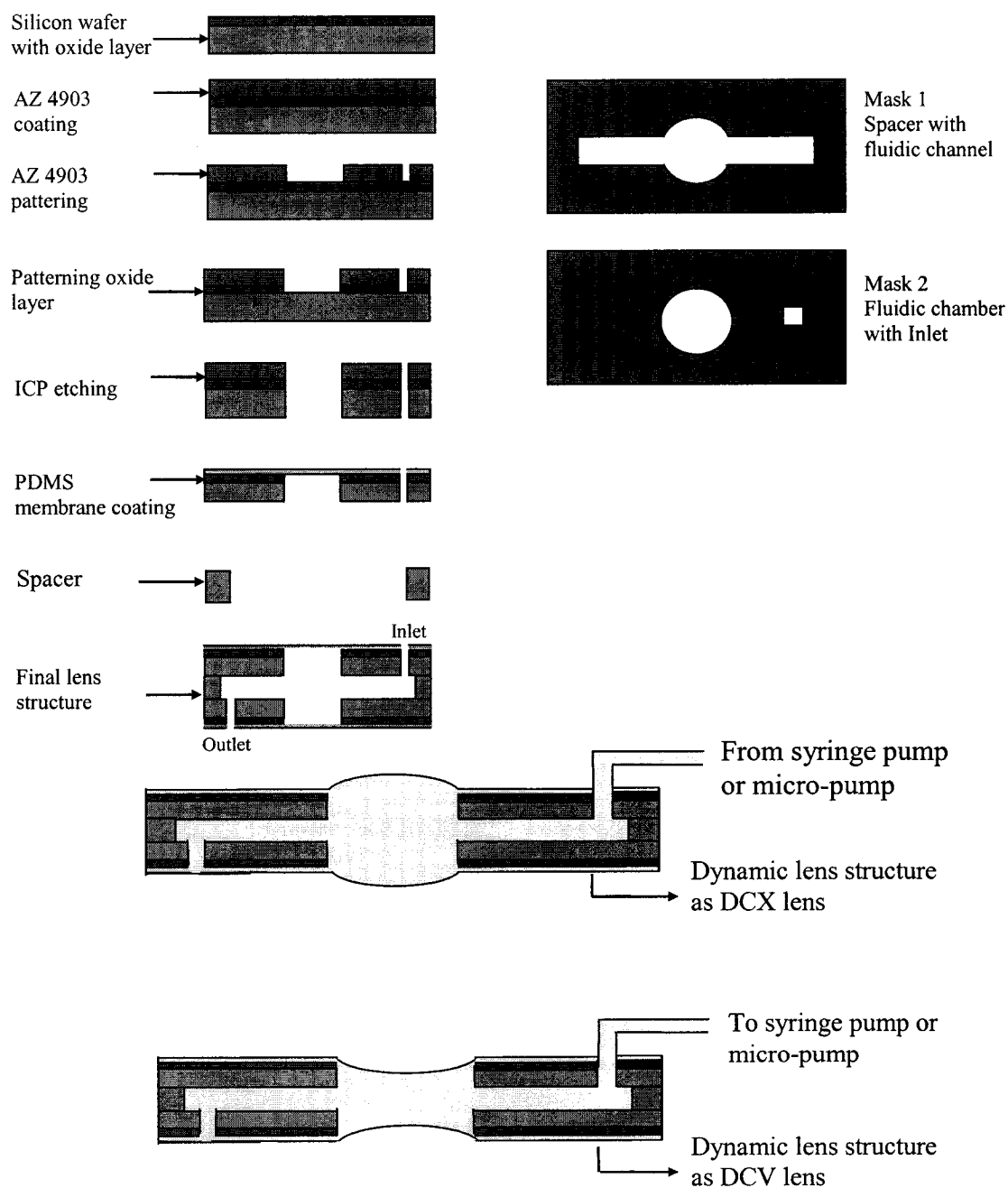


**Figure 5.1: Fabrication steps for variable focal length microlens systems.**



### 5.2.2 Mask Design

Using L-edit micro designing software, a mask was designed to fabricate lens chambers and fluidic channels of different dimensions. L-Edit mask designing software is a part of complete integrated circuit design tools suite offered by Tanner Research Inc. It is a low-level, fully customized mask editor. It does not perform automatic layer transformations. That is, there is no automatic wee or selected generation for CMOS processes. Although wells and selects must be generated manually, this can be done more quickly than with other "high-level" tools because of L-Edit's intuitive user interface. In addition, using L-Edit one can construct special structures to utilize a technology without worrying about problems caused by automatic transformations. Figure 5.2 shows the layout of the lens chamber and spacer with fluidic channels of different dimensions.

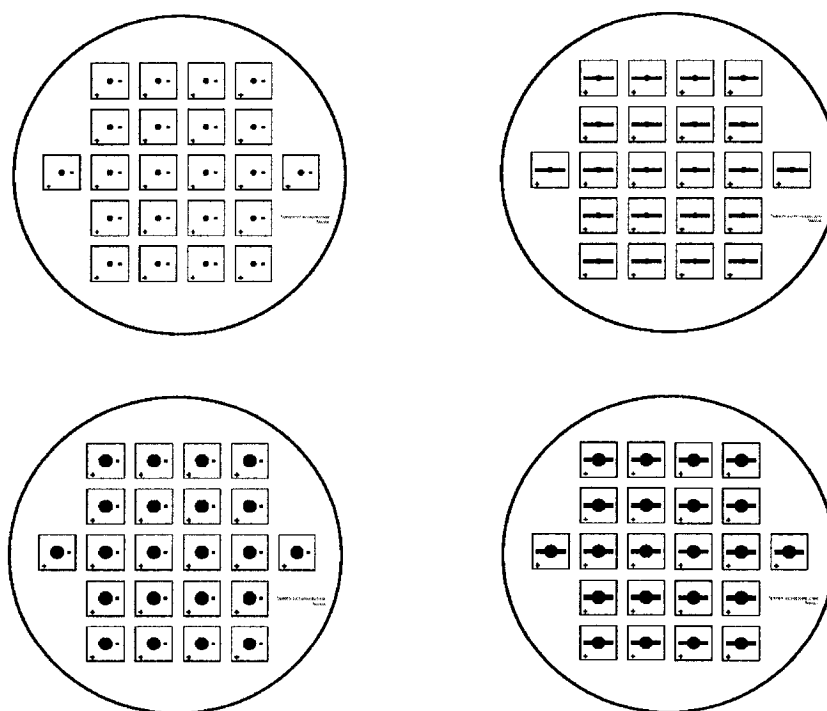


**Figure 5.2: Mask layout for different dimensions of lens chambers with inlet and spacer with microfluidic channels.**

### **5.2.3 Lithography and Silicon Micromachining**

A silicon wafer <100> with 2  $\mu\text{m}$  thick oxide layer was used for the fabrication of fluidic microchannels and the fluidic lens chamber. The oxide layer is found to be very useful, as it can serve as a masking layer as well as can bond to PDMS membrane with high quality bond strength. A positive photoresist is used for masking the oxide layer during both BOE etching (to pattern the oxide layer) and ICP etching (to etch through the silicon). The pattern transfer was performed using the UV photolithographic process. Photolithography is an optical means of transferring patterns from a mask to the surface of a silicon wafer. The steps for photolithography process involve

- Wafer cleaning
- Prebaking
- Photoresist coating
- Softbaking
- Alignment and exposure
- Development
- Hardbaking
- Etching

A commercially available AZ 4903 positive resist was used in this process for pattern transfer. As this resist is quite viscous, it can be spun into thick layers on silicon wafers over a spin range of 700-2000 rpm. As a first step, the substrate (silicon <100> 2  $\mu\text{m}$  oxide coated wafer) used for lithography was chemically cleaned prior to photoresist coating to remove any traces of particulate matters, organic, inorganic, and metallic impurities. The substrate was then prebaked at a high temperature

(115°C for 10 min) to ensure that it was completely dry. After the substrate reached room temperature, it was coated with an adhesion promoter Hexamethyldisilazane (HMDS) which increases the adhesion of the photoresist on the wafer surface. The spin curve for coating HMDS is given in Figure 5.3. Approximately 4 ml of AZ 4903 photoresist was dispensed on the wafer and spun according to the spin curve shown in Figure 5.4.

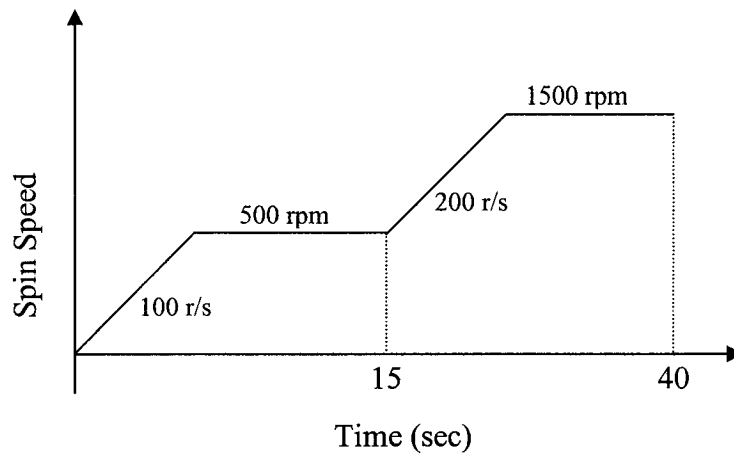


**Figure 5.3: Spin curve for coating the HMDS adhesion promoter.**

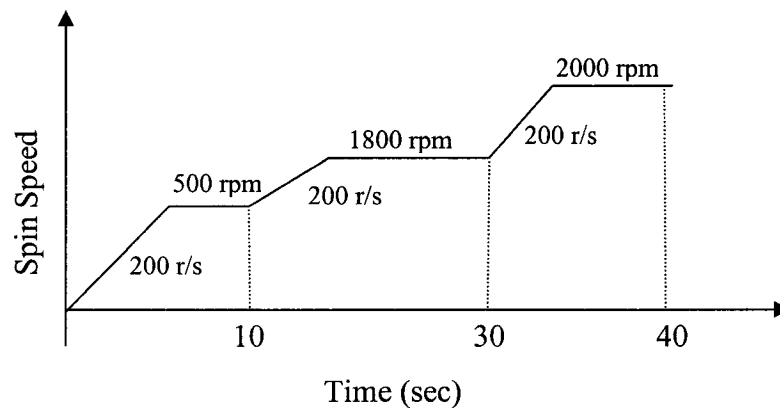


**Figure 5.4: Spin curve for coating AZ 4903 resist.**

After spin coating the photoresist, softbaking was done at 60 degrees for 4 min, 70 degrees for 1 min, 90 degrees for 2 min, and 110 degrees for 3 min to evaporate the solvent from the photoresist without leaving any air bubbles trapped inside. Softbaking

plays an important role in subsequent exposure and development steps. Under-softbaking will prevent light from reaching the photoactive compound; as a result, considerable solvent remains after developing. Conversely, over-softbaking will degrade the sensitivity of resist by destroying a part of the sensitizer. After alignment with a photomask, the resist-coated substrate was exposed to UV-light for 80 sec. Exposing the resist to the UV light (I-line of Hg lamp, with wavelength of 410 nm) induces the photochemical reaction in the resist sensitizer which allows the resultant product to dissolve in the solvents.

For the resist samples developed in commonly used MF 319 positive photoresist developer, the patterns were not well-developed leaving residues on the developed area. Whereas, the patterns on those samples developed with AZ 400K positive photoresist developer were found to be fully developed. The developed patterns were inspected under an optical microscope for undeveloped resist or residues in the developed area. The thickness of the resist layer was measured using a step profilometer, and patterned structures were examined by a scanning electron microscope (SEM- see Figure 5.5). SEM micrographs of the microfluidic inlet pattern after the lithography process are shown in Figure 5.6a.

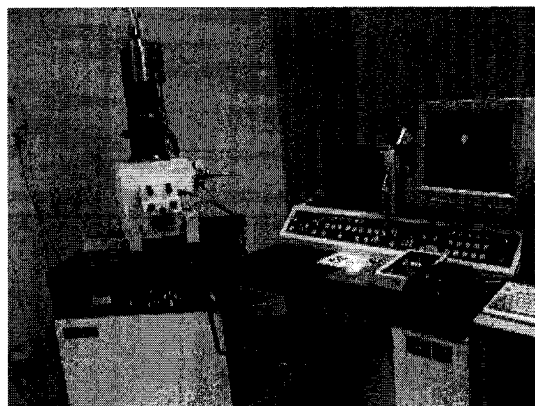
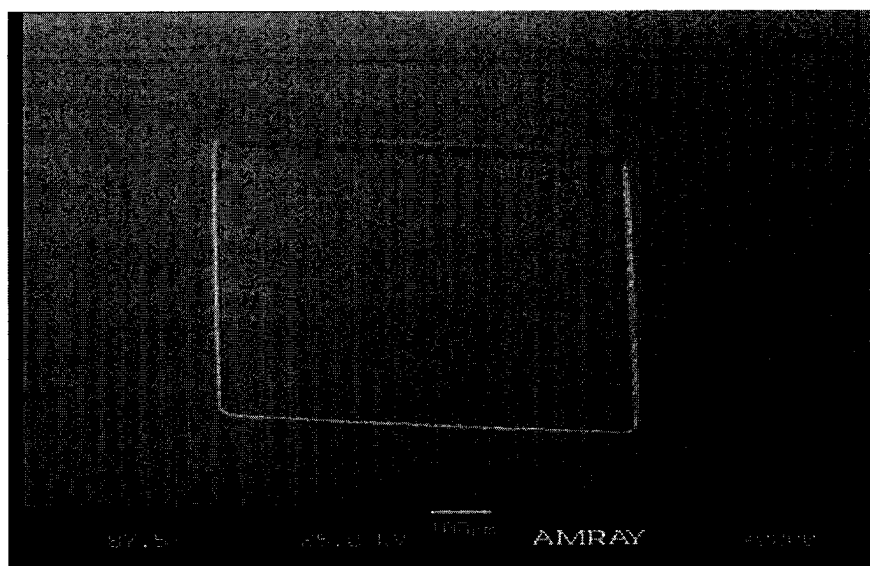
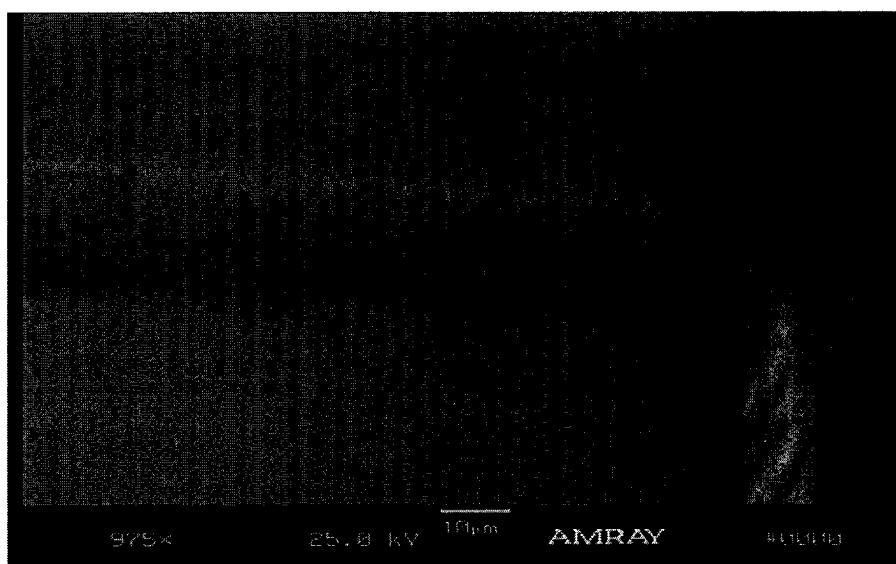


**Figure 5.5: Scanning Electron Microscope at IfM.**



(a)



(b)

**Figure 5.6: SEM micrographs of the patterned AZ 4903 resist (a) Microfluidic inlet pattern, (b) Close-up of the sidewalls of microfluidic inlet pattern.**

The magnified SEM micrograph of the sidewalls is shown in Figure 5.6b. It can be noted that the sidewalls of the pattern are nearly vertical and rough. Figure 5.7 shows the step profile of the resist pattern measured using surface profilometer (Tencor). The average thickness of the AZ 4903 resist patterns was measured to be 22.79  $\mu\text{m}$

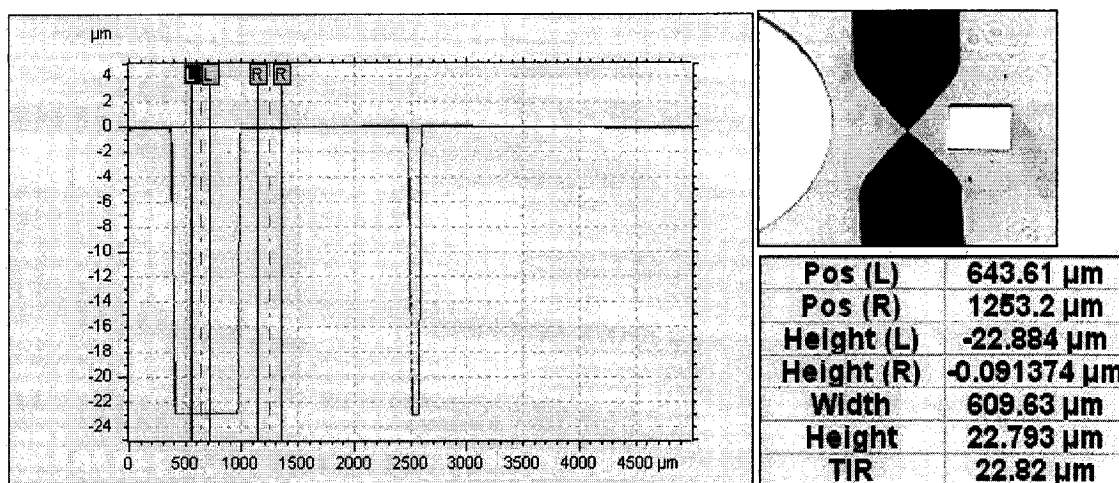


**Figure 5.7: Step profile of the AZ 4903 pattern measured using surface profilometer (Tencor).**

After the lithography process, the sample was subjected to BOE etching to remove the oxide layer from the patterned structures. Then, the sample was subjected to Inductively Coupled Plasma (ICP) etching. The ICP dry etching method is used as it gives higher etch rates, high selectivity and well-defined sidewalls. The Alcatel 601 E ICP machine at Institute for Micromanufacturing (IfM) shown in Figure 5.8 was used to perform the etching process.

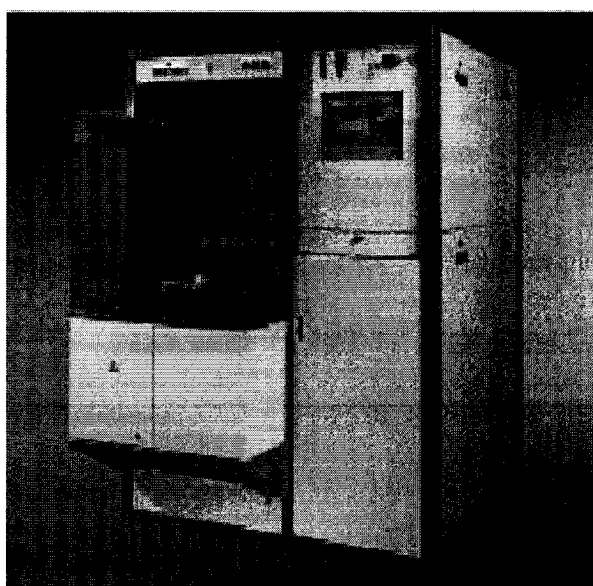


**Figure 5.8: Alcatel 601E ICP Etching system.**

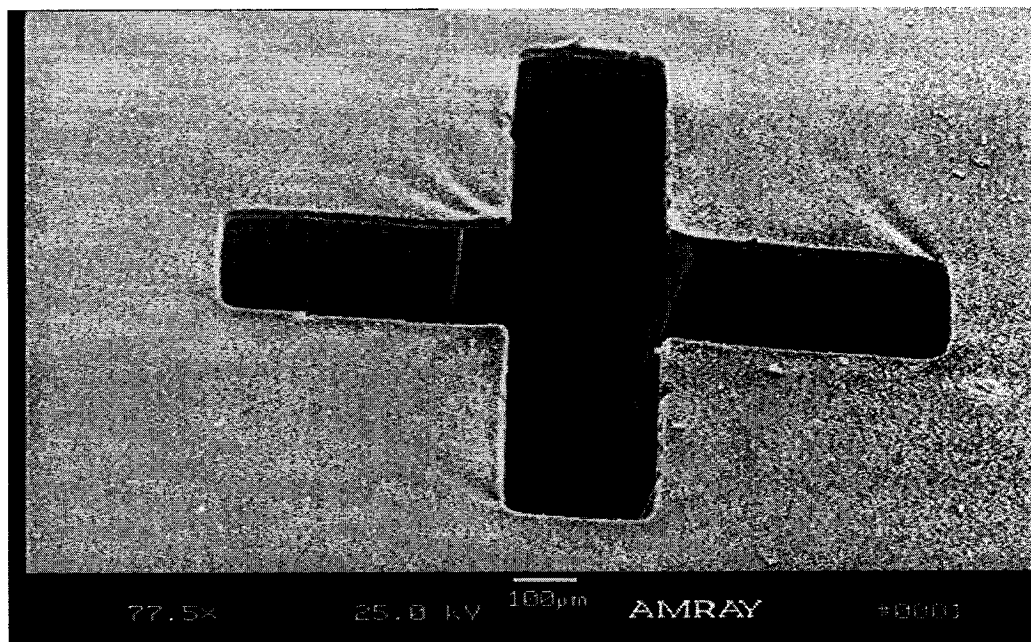
A standard Bosch process was used for ICP etching, in which the wafer is exposed with alternative sequence of SF<sub>6</sub> gas for etching and C<sub>4</sub>F<sub>8</sub> for passivation. The SF<sub>6</sub> gas, together with ions produced from high density inductively coupled plasma, etches the silicon substrate. The passivation layer prevents etching of silicon from the sidewalls to give straight side walls with very high anisotropy and high aspect ratios. The processing conditions used during ICP etching to etch through ( $\approx 525 \mu\text{m}$ ) the patterns in the silicon wafer are given in Table 5.1.

**Table 5.1: Parameters used for ICP etching.**

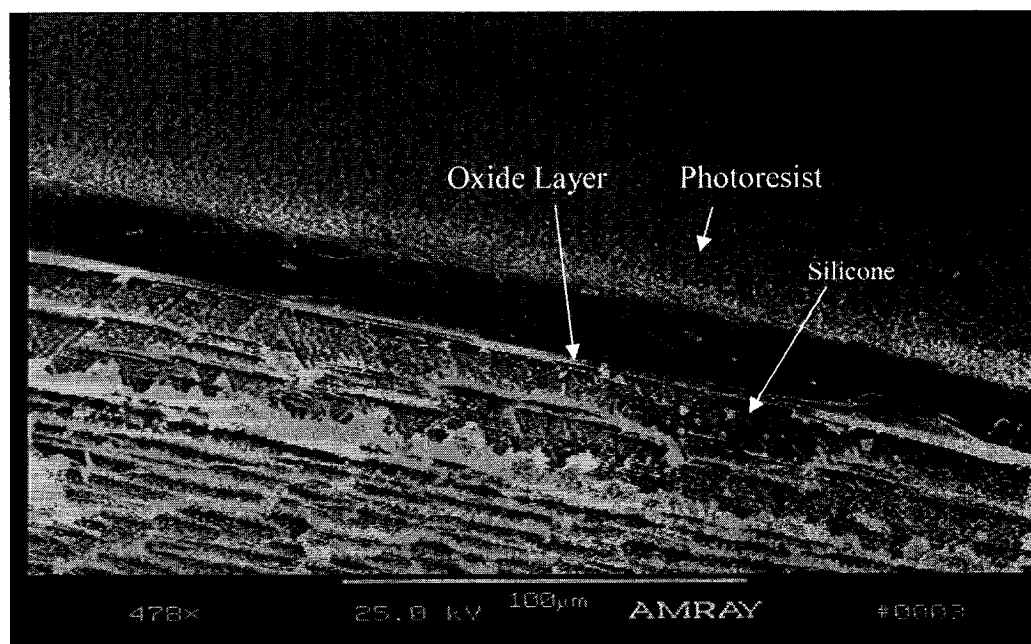
Parameters	Values
Power	1800 W
Bias	30 W
SF <sub>6</sub> flow rate	300 ccm/sec for 7 sec
C <sub>4</sub> F <sub>8</sub> Flow rate	50 ccm/sec for 3 sec
He regulation	7.5 E +03
Etching time	75 to 90 min

The alignment mark and the sidewall of the fluidic inlet pattern after ICP etching are shown in Figure 5.9. It can be clearly observed from Figure 5.9b that the AZ 4903 photoresist was able to withstand in ICP thereby protecting the oxide layer under it. Figure 5.10 shows the thickness profile of the leftover AZ 4903 photoresist after ICP etching. The thickness of the leftover resist layer was measured to be 18.51  $\mu\text{m}$ , that is only 3  $\mu\text{m}$  of the AZ 4903 layer was etched during ICP process. These results indicate

that the AZ 4903 resist has a very low etch rate in ICP and that it can be used as a good masking layer.



(a)



(b)

**Figure 5.9: SEM micrographs of the patterns after ICP etching (a) Alignment mark, (b) Close-up micrograph of the ICP etched side wall.**



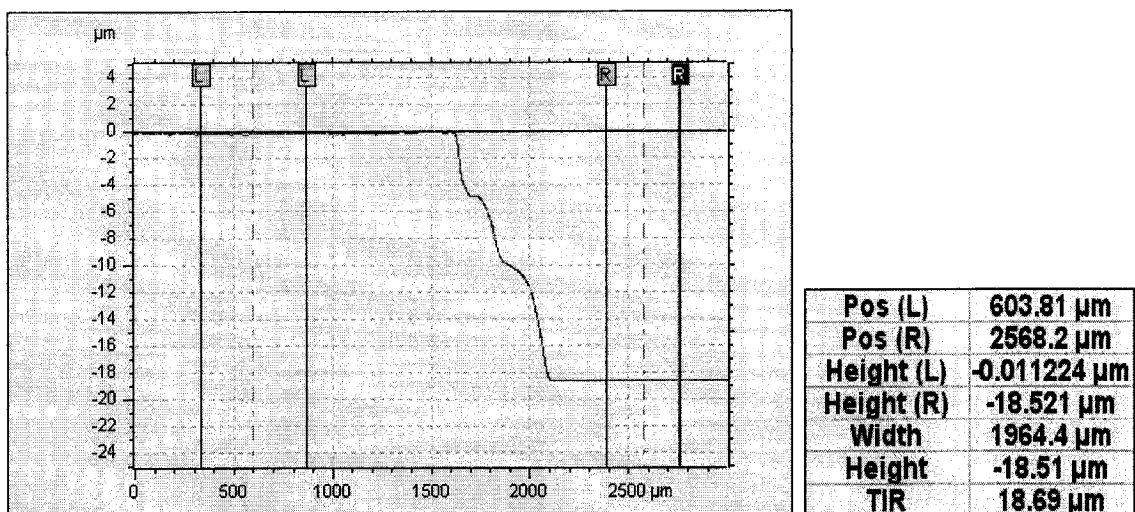


**Figure 5.10: Step profile of AZ 4903 after ICP etching process.**

The optical images of the lens chamber with fluidic inlet after the ICP etching process are shown in Figure 5.11. It can be observed from Figure 5.11a that the photoresist did not have any sign of degradation or burn during the ICP etching process. The optical image of the pattern after complete ICP etching and removal of the photoresist is shown in Figure 5.11b. The SEM micrographs of the lens chamber with fluidic inlet and spacer with fluidic microchannel are shown in Figure 5.12.

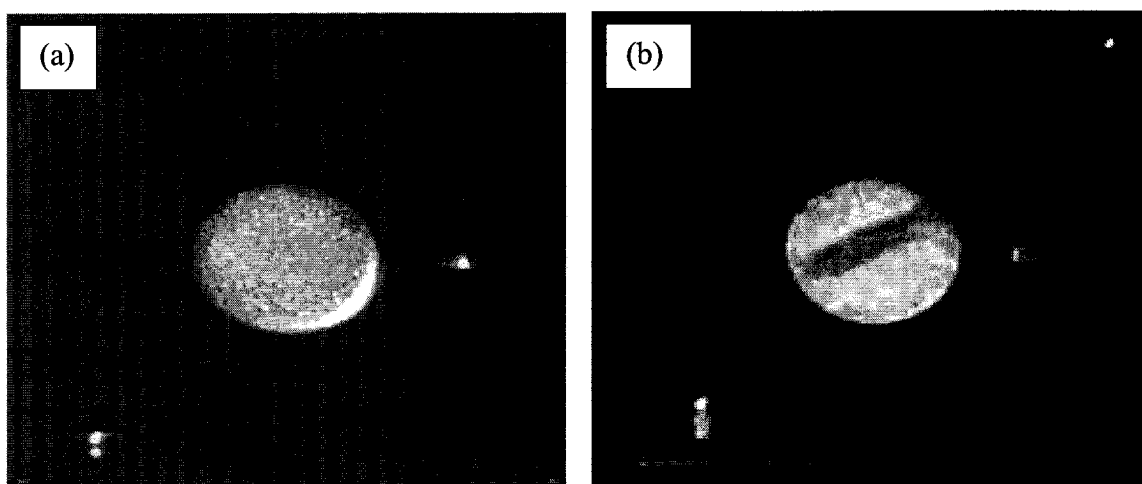


**Figure 5.11: (a) Lens chamber with fluidic inlet after ICP etching with photoresist, (b) Lens chamber and fluidic inlet after complete ICP etching and removing photoresist.**

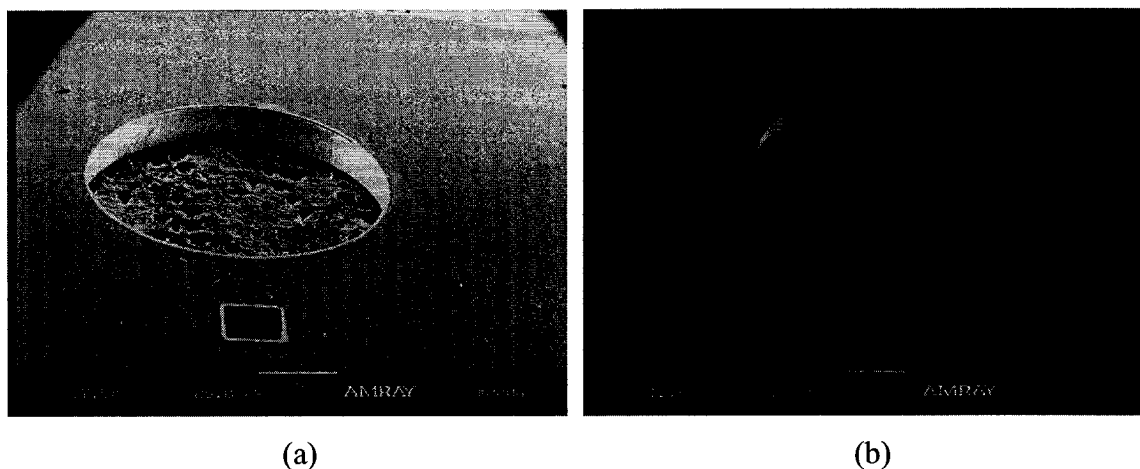


**Figure 5.12: SEM micrographs of (a) Lens chamber with fluidic inlet, (b) Spacer with microfluidic channel and lens chamber.**

#### **5.2.4 Integration and Packaging**

PDMS has very low glass transition temperatures and, hence, is a fluid at room temperature. However, it can be easily converted into solid form by cross-linking. The Sylgard™ 184 PDMS elastomer kit, obtained from Dow Corning, was used to fabricate the PDMS membrane. The kit consists of two-components, a liquid elastomer and a curing agent. Once these two components are mixed and heated, the liquid mixture becomes a solid because of the cross-linking of elastomer induced by the curing agent. The silicon sample was first silanized by exposing it to the vapor of Trichlorosilane in vacuum desiccators for two hours. This step helped in easy peeling of PDMS membrane from the silicon wafer after curing. Approximately 8.8 g of PDMS (a mixture of 8 g of PDMS and 0.8 g of curing agent) was dispensed on the Trichlorosilane treated wafer and spun according to the spin curve shown in Figure 5.13.

PDMS membrane thus formed was cured at 50 °C for 30 min and at 90 °C for 15 min. The next step is to activate the surfaces of the PDMS membrane and the ICP etched sample with the lens chamber in oxygen plasma so that they will permanently

bond. A strong covalent siloxane (Si – O – Si) bond is formed when the two plasma oxidized surfaces are brought into contact. The activation was done with a Micro Reactive Ion Etching (Micro-RIE) unit shown in Figure 5.14.

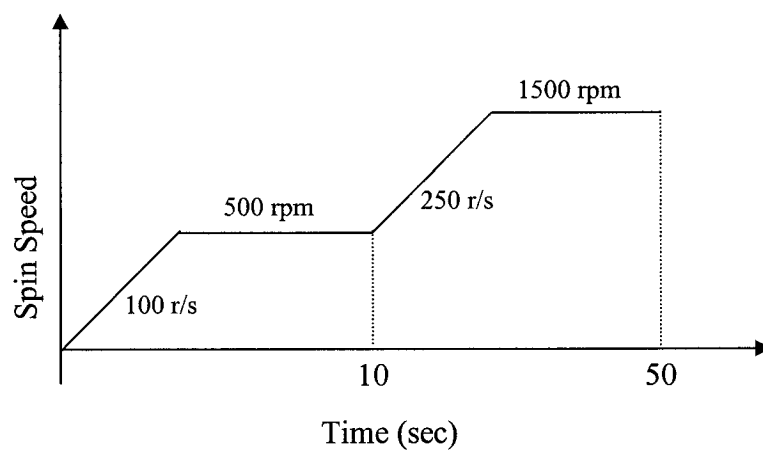


**Figure 5.13: Spin curve to form PDMS membrane.**

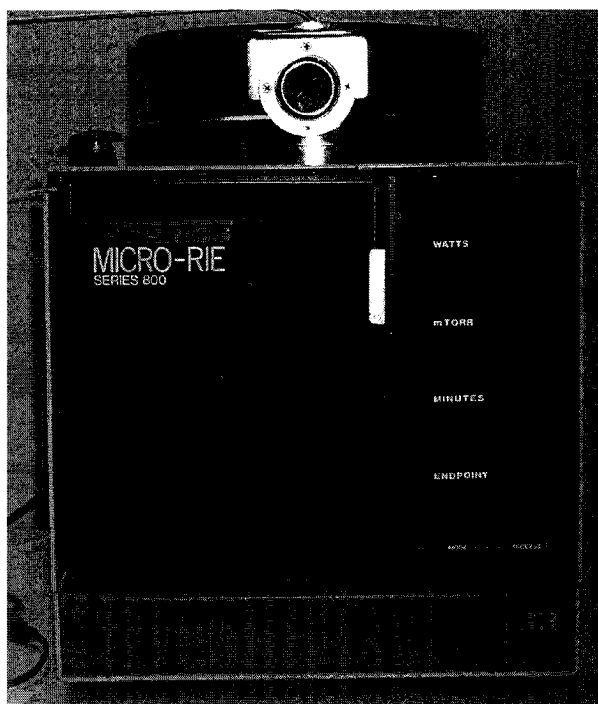


**Figure 5.14: Micro-RIE (Series 800) Instrument from Technics.**

The ICP etched silicon sample with the lens chamber and the sample with spin coated PDMS membrane were loaded into the top chamber of the Micro-RIE unit. After pumping down the chamber to 50 mtorr, the RF power was turned on (320 W), establishing a pale blue plasma. The inlet valve on the chamber was then slowly opened to let in a small stream of oxygen (5.5 sccm), turning the plasma pink. It was found that a 30 second exposure to the oxygen plasma (after it has turned pink) consistently yielded strong bonds. After 30 seconds, the RF power was turned off, and the chamber was vented; the samples were removed. It should be noted that after two to three minutes of surface activation, the silicon substrate and PDMS pieces must be brought into contact to form a permanent bond between them. The PDMS membrane was transferred to the ICP etched sample with the lens chamber to form a flexible membrane within two or three minutes after activating the surfaces with oxygen plasma, as shown in Figure 5.15.

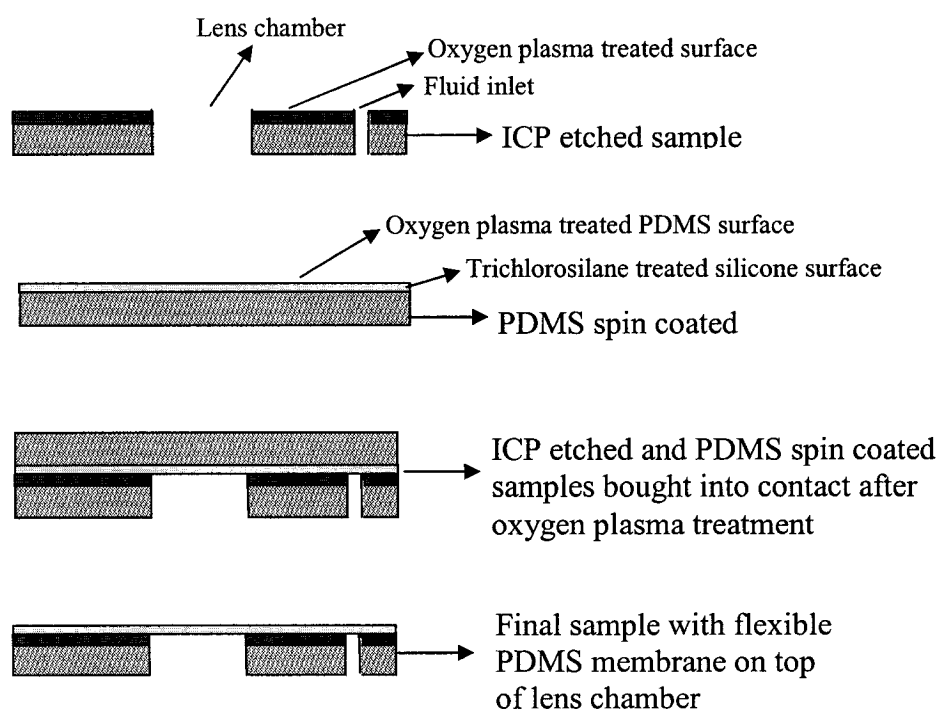


**Figure 5.15: Fabrication process steps to fabricate flexible PDMS lens membrane.**

When two lens chambers with PDMS membrane were formed, they were glued together with a spacer having a microchannel and a fluidic chamber. To protect the PDMS membrane, an extra piece of silicon sample with a lens chamber was fixed on either side of the lens structure. The optical photographs of the completely assembled variable focal length microlens system with fluidic connection are shown in Figure 5.16. The dimensions of this microlens system are 10 mm x 10 mm x 1.5 mm with a lens diameter of 4 mm.

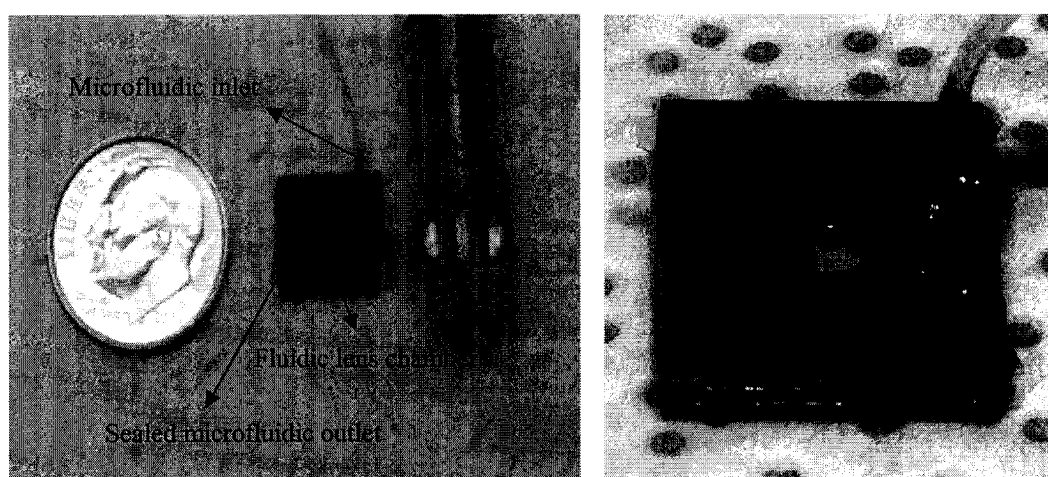


**Figure 5.16: Single variable focal length microlens structures with microfluidic chamber and inlet connection.**

### **5.2.5 Fabrication of Integrated Wide-Angle Dynamically Variable Focal Length Microlens System**

As discussed in Chapter 4, an integrating dynamic microlens system can be fabricated with two or three DCV lenses by combining two or three single variable focal length microlenses. This integrated dynamic microlens system can view objects at wider FOV compared to a single variable focal length microlens system. The fabrication steps for the integrated microlens system with two variable focal length DCV lenses are shown in Figure 5.17. An integrated dynamic microlens system with two dynamic DCV lenses is

fabricated using the same fabrication principle applied for single variable focal length microlens systems. To fabricate this system, two single variable focal length microlenses were fabricated and glued together with a spacer in between by using epoxy material. The optical images of the integrated dynamic microlens system with two DCV lenses are shown in Figure 5.18.

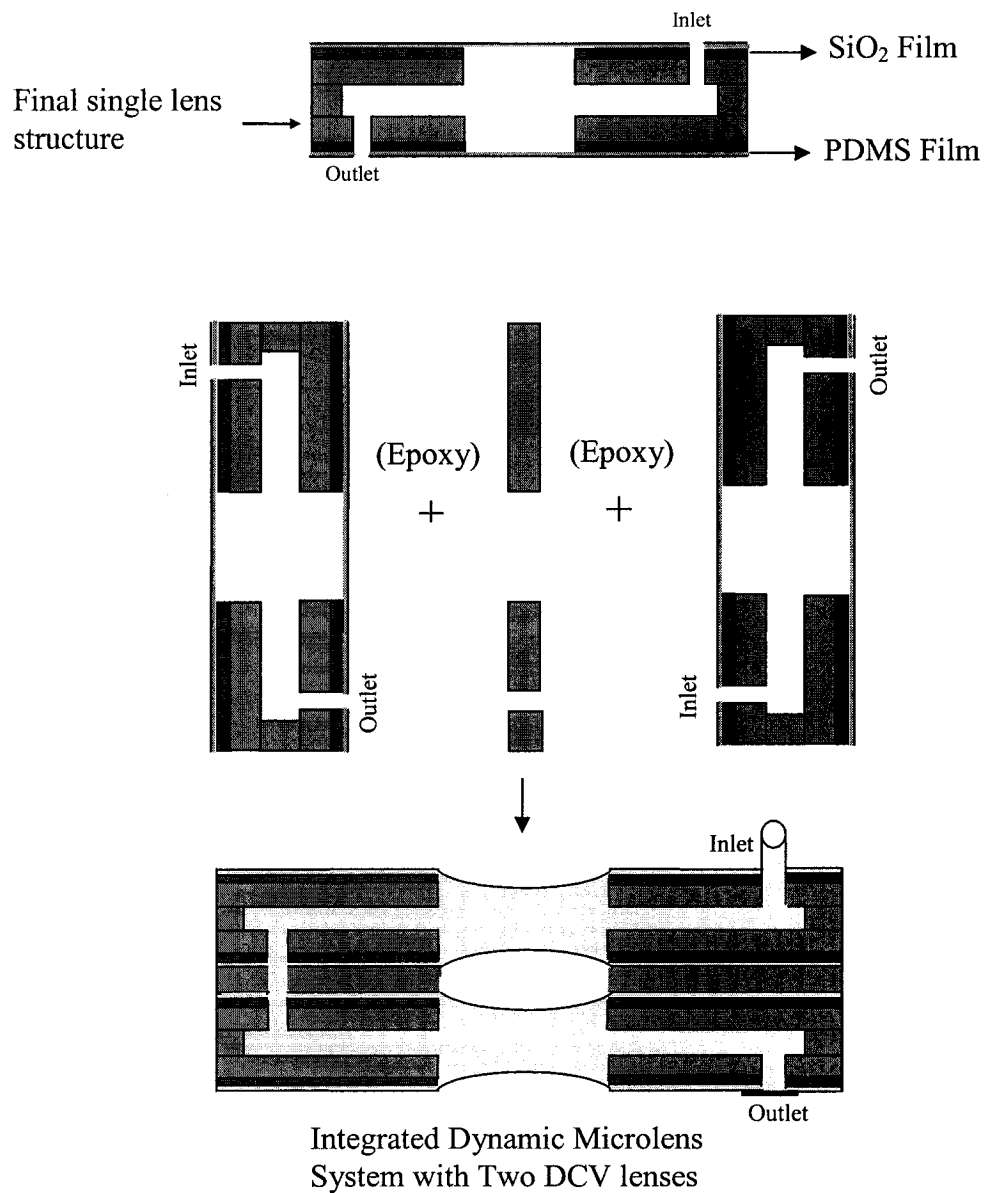


**Figure 5.17: Fabrication steps for integrated dynamic microlens system with two DCV lenses.**

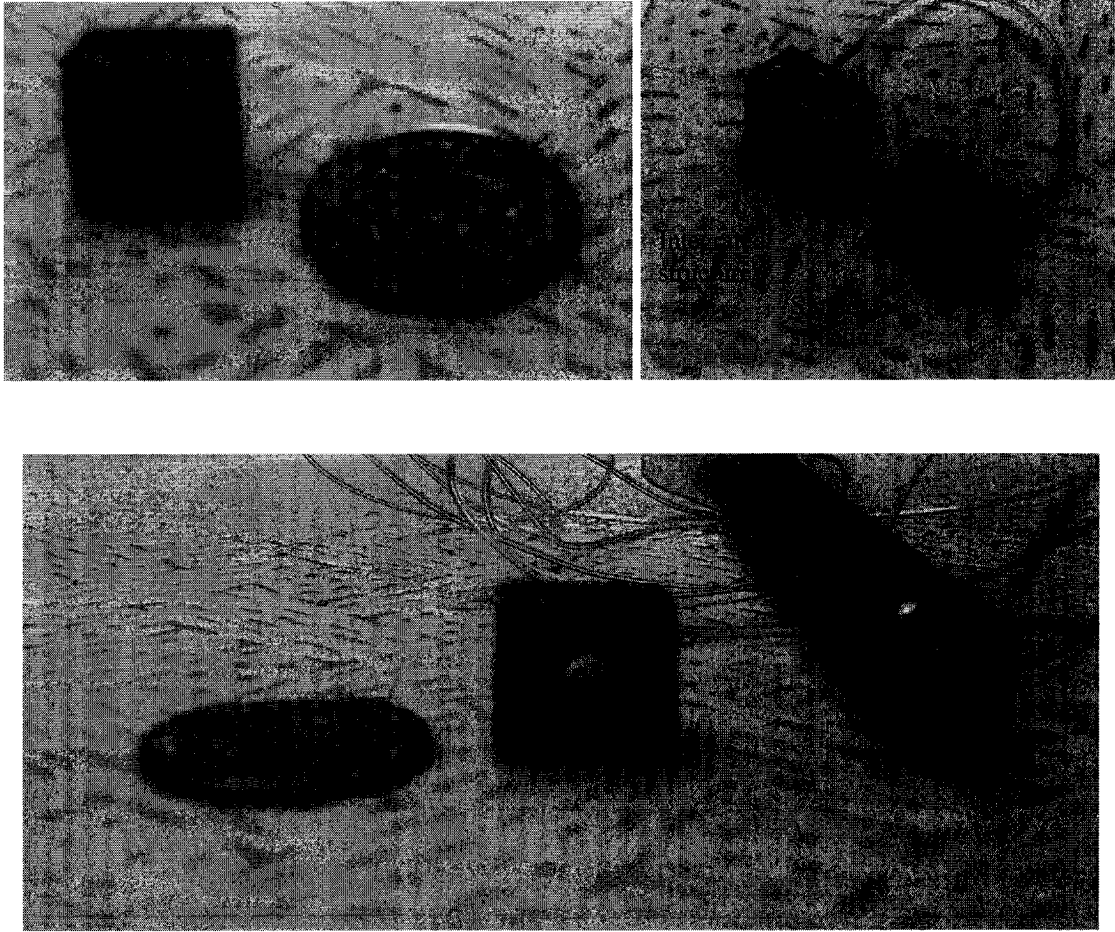


**Figure 5.18: Optical images of integrated dynamic microlens system with two DCV lenses.**

The integrated dynamic microlens system with three DCV lenses is fabricated to further increase the field of view using the same fabrication principle applied for single variable focal length microlens systems. Figure 5.19 shows the fabrication steps for an integrated microlens system with three variable focal length DCV lenses. Three single variable focal length microlenses were fabricated and glued together with a spacer in between by using epoxy.

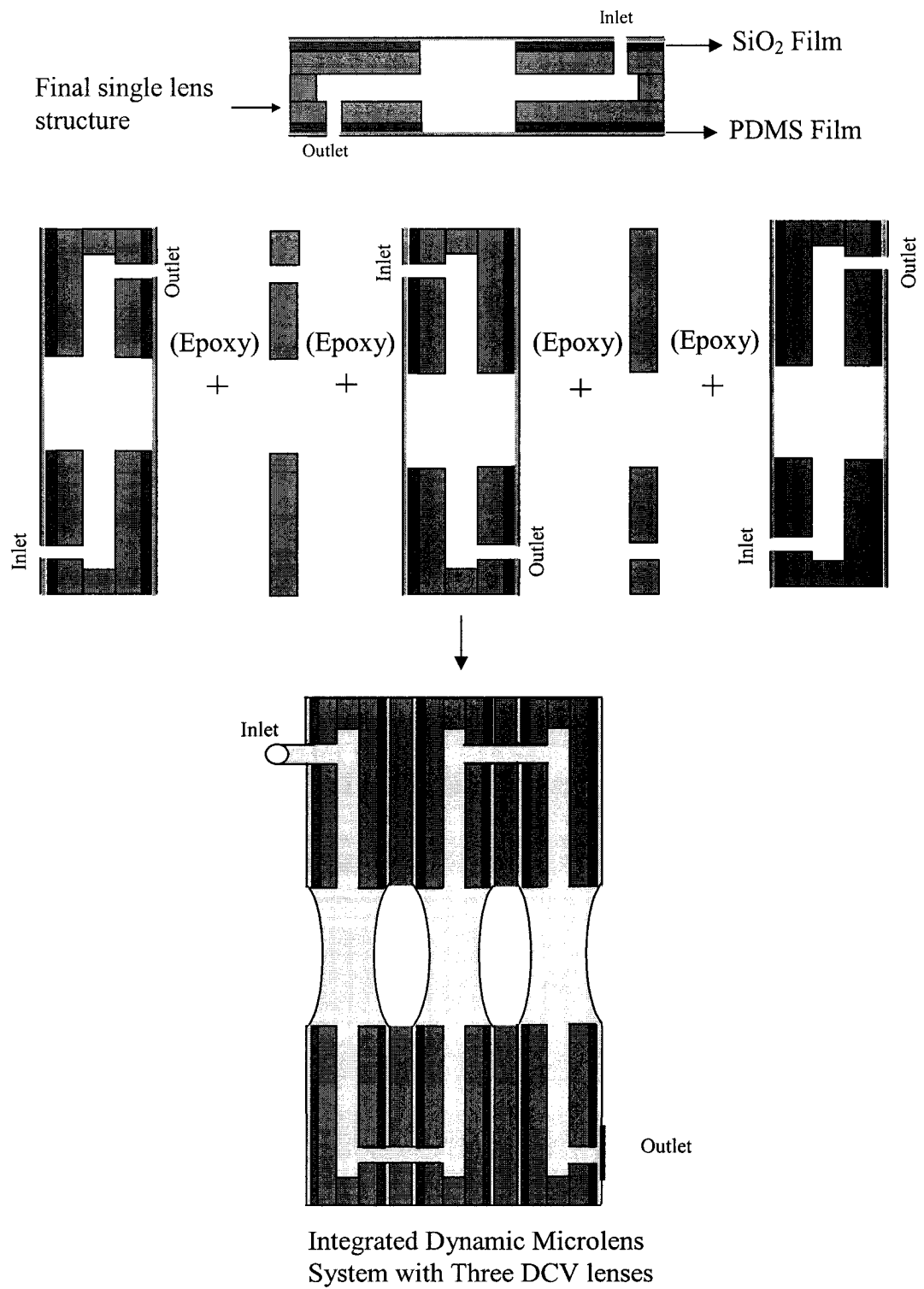
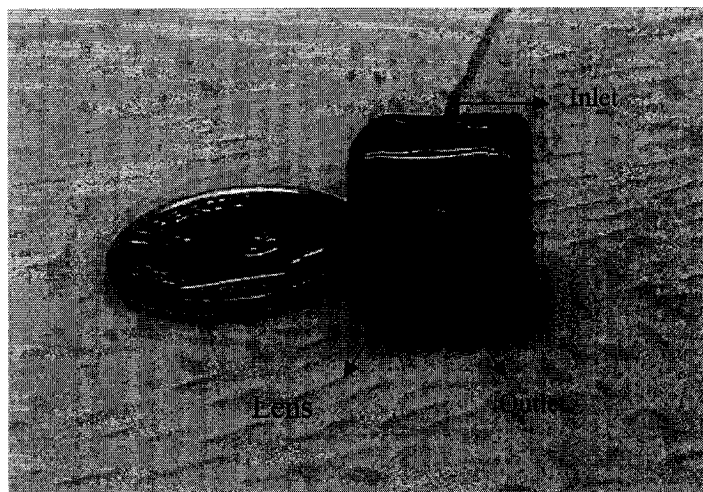


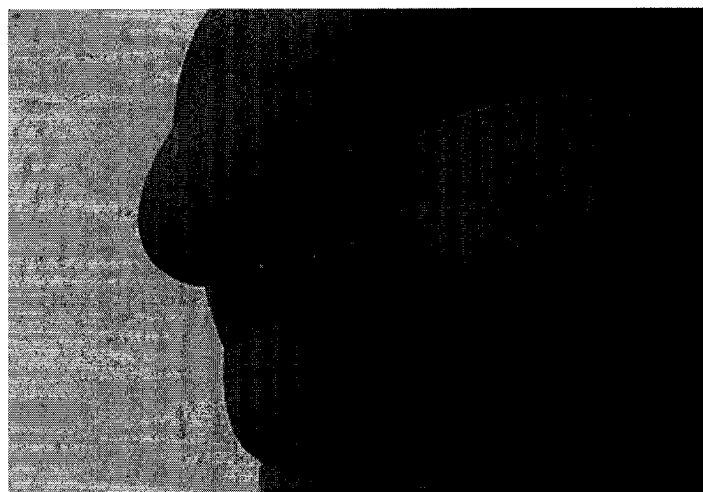
**Figure 5.19: Fabrication process steps for integrated dynamic microlens system with three DCV lenses.**



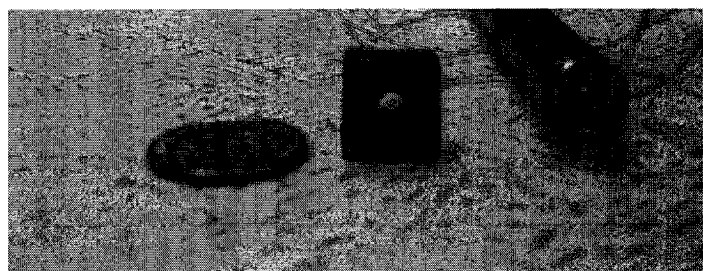
The optical images of the integrated dynamic microlens system with three variable focal length DCV lenses are shown in Figure 5.20.



(a)



(b)



(c)

**Figure 5.20: Optical images of the integrated dynamic microlens system with three DCV lenses, (a) & (b) Three lens system, (c) Three lens system with syringe used to deflect the lens membranes.**

## 5.3 Results and Discussions

### 5.3.1 PDMS Membrane Characteristics

The PDMS membrane formed as discussed in Section 5.2 was tested for different characteristics.

**5.3.1.1 Roughness of PDMS Membrane.** The roughness of the PDMS membrane was tested using the Atomic Force Microscope (AFM) and Roughness Step Tester (RST) profilometer. The 3D image of the PDMS membrane surface measured using AFM is shown in Figure 5.21. It can be observed from Figure 5.21 that the surface is smooth with no sign of deformities.

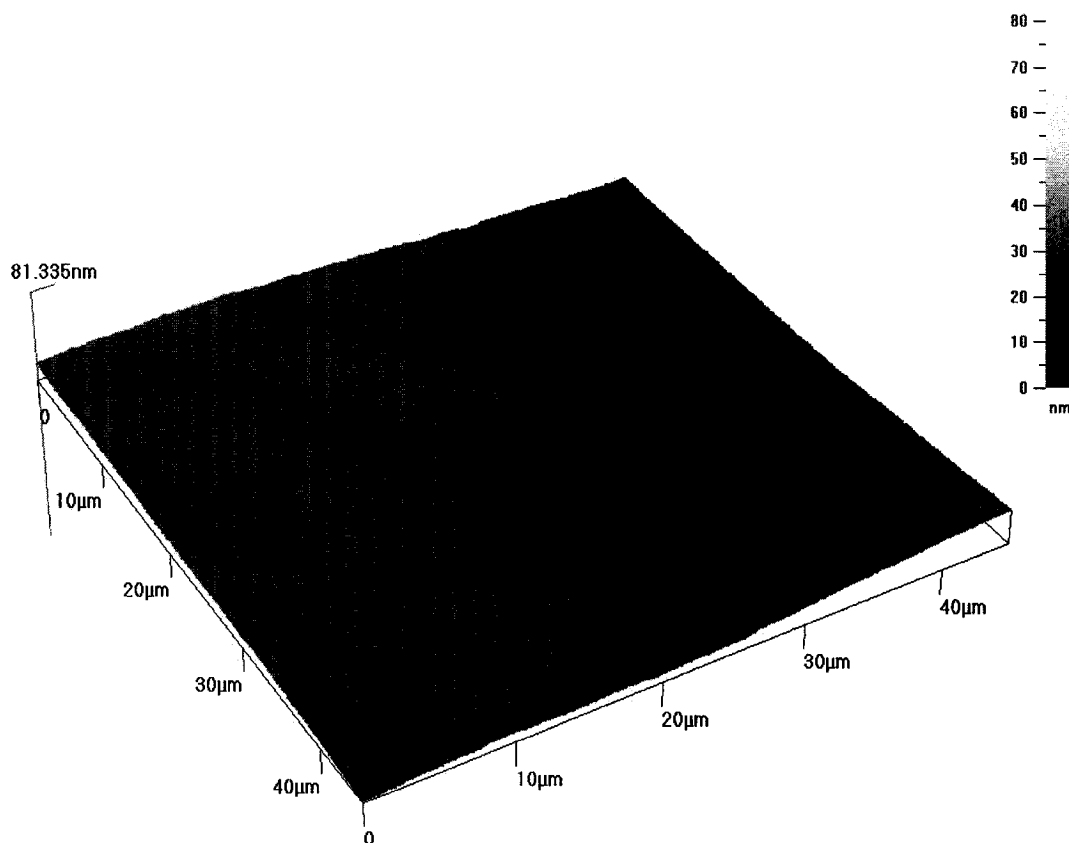


**Figure 5.21: 3D profile of the PDMS membrane measured using AFM.**

The 2D profile of the PDMS membrane surface measured using AFM is shown in Figure 5.22. The average roughness of the PDMS membrane is measured to be 31.23 nm from AFM. It can be noted from Figure 5.22 that there are no sharp peaks and slopes indicating any deformities on the PDMS membrane which is very important for optical quality membranes.

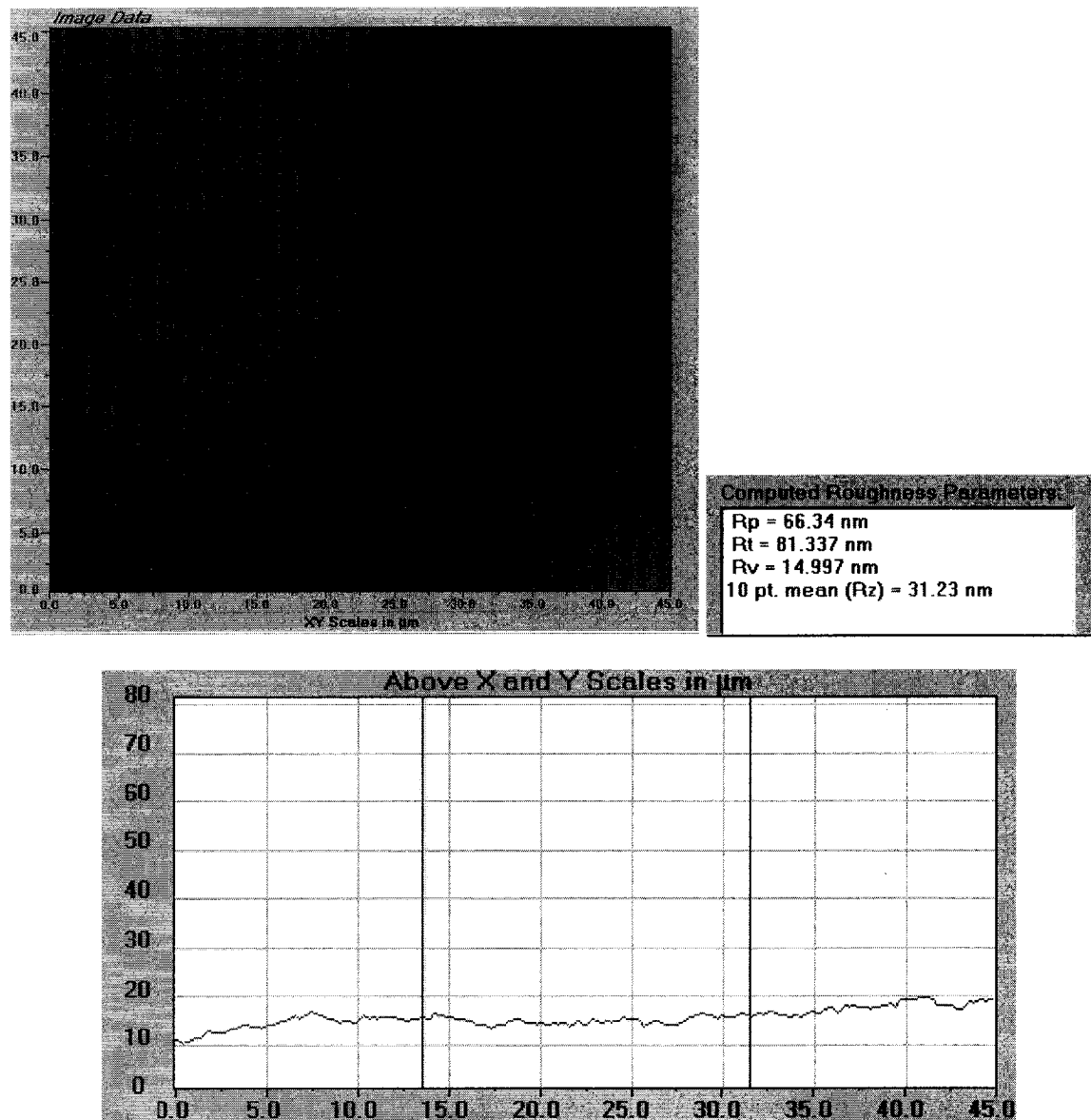
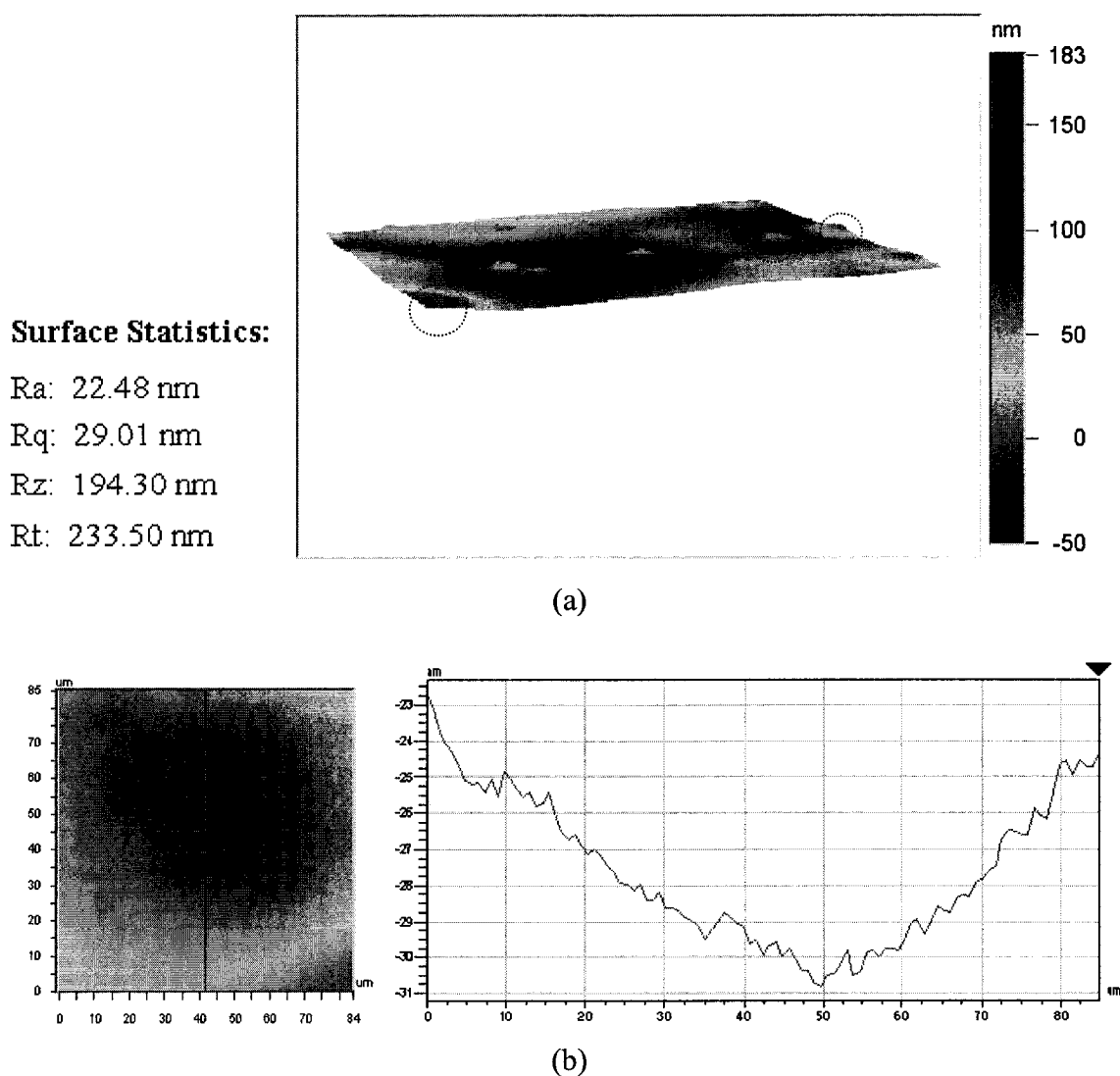


Figure 5.22: 2D profile of the PDMS membrane measured using AFM.

The membrane was coated with thin metallic film in order to use RST to analyze the surface. Figures 5.23a and 5.23b shows the 2D and 3D surface profile of the PDMS membrane measured using RST, respectively. The average roughness was measured to be 22.48 nm. The peaks, as marked in Figure 5.23a, on the surface of the PDMS membrane are metal particles caused by micro sputtering prior to the analysis of the sample. Table 5.2 shows the average roughness value and the roughness values measured using AFM and RST.



**Figure 5.23: (a) 3D profile of the PDMS surface, (b) 2D profile of the PDMS surface measured using RST.**

**Table 5.2: Average roughness value and the roughness values of the PDMS membrane measured using AFM and RST.**

Roughness measured using RST	31.23 nm
Roughness measured using AFM	22.48 nm
Average roughness	26.85 nm

Figure 5.24 shows the micrograph of the PDMS surface taken using a scanning electron microscope (SEM) under 19,400 X magnification. It can be observed that the surface is smooth and there are no sign of cracks or deformities on the PDMS surface.

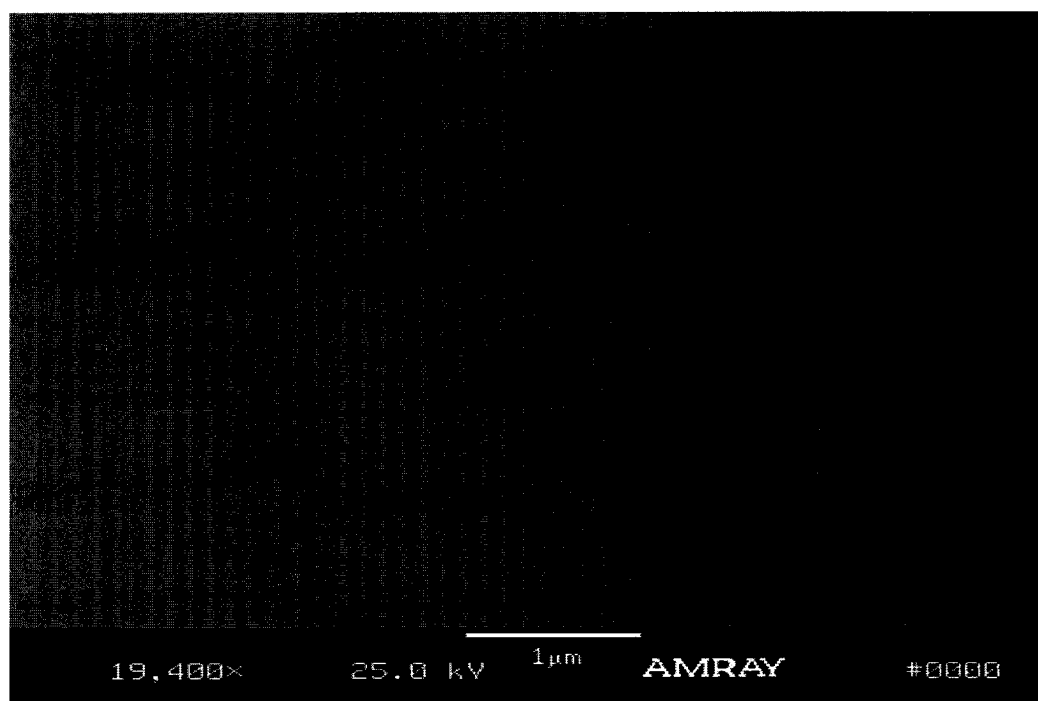
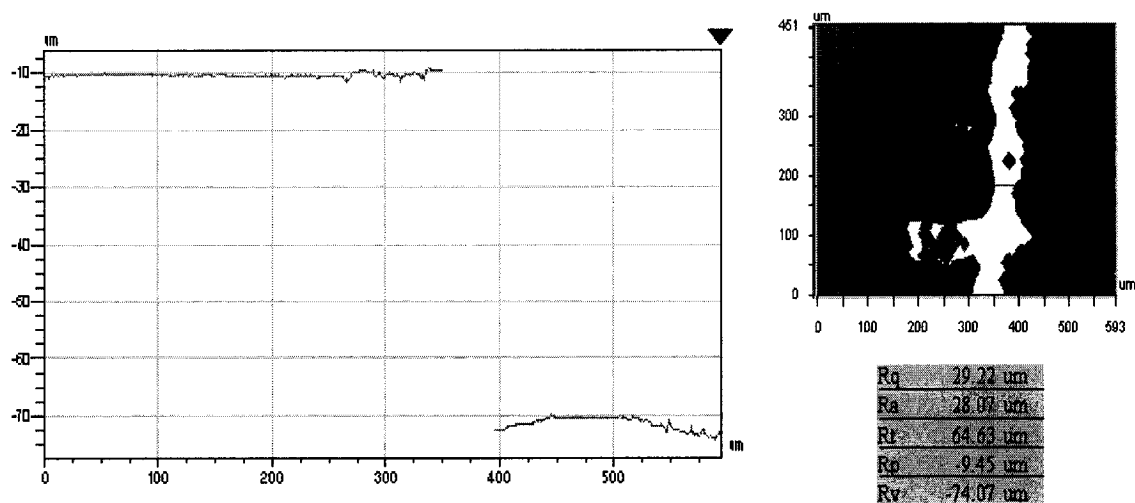


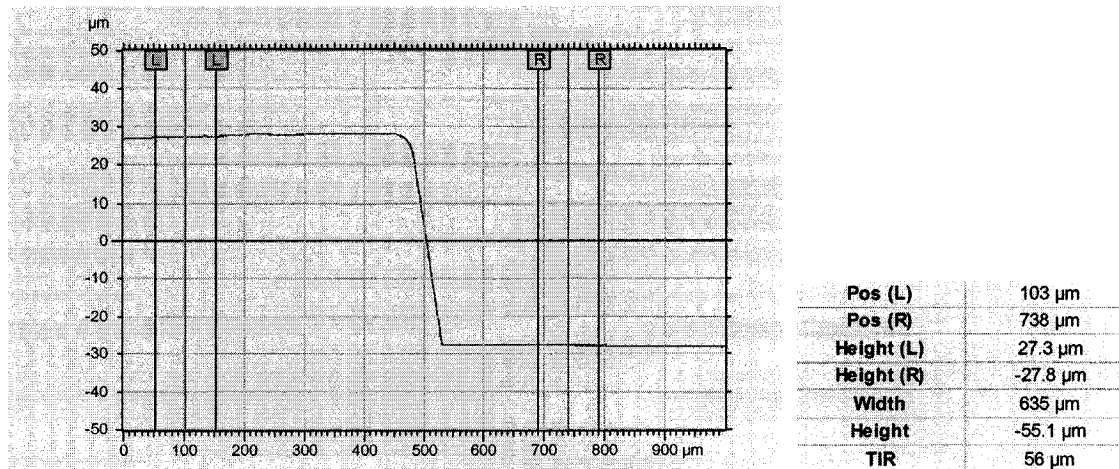
**Figure 5.24: SEM micrograph of the PDMS surface.**

**5.3.1.2 Thickness of PDMS Membrane.** The thickness of the spin-coated PDMS membrane at 1500 rpm for 40 sec was measured using an RST and Tencor surface profilometer. Figures 5.25a and 5.25b show the step profile of the PDMS membrane measured using an RST and Tencor surface profilometer, respectively. Table 5.3 list the

average thickness value and the thickness values measured using an RST and Tencor surface profilometer.



(a)



(b)

**Figure 5.25: 2D step profile of the PDMS membrane measured using (a) RST, (b) Tencor surface profilometer.**

**Table 5.3: Average roughness value and the roughness values of the PDMS membrane measured using RST and Tencor surface profilometer.**

PDMS thickness measured using RST	65 $\mu\text{m}$
PDMS thickness measured using Tencor	55 $\mu\text{m}$
Average PDMS thickness	60 $\mu\text{m}$

**5.3.1.3 Transmittance and Absorption Characteristics.** The transmittance for a film of thickness  $d$  and refractive index  $n$ , at any wavelength  $\lambda$ , and for condition where interference effects are negligible or average out is given by Equation 5.1 [174], where  $\alpha$  is the absorption coefficient at wavelength  $\lambda$ .

$$T = \frac{I}{I_o} = \frac{16n^2 e^{-\alpha d}}{(n+1)^4 - (n-1)^4 e^{-2\alpha d}} \quad (5.1)$$

Equation 5.1 is the ratio of the total emergent energy to the total incident energy. The expression takes into account multiple reflections; some of the radiation reflected from the back face is re-reflected from the front face. Unless the film is parallel and the angle of incidence is  $0^\circ$ , the multiple reflected radiations will not be exactly coaxial with the “main beam.” The total incident energy  $I$  in Equation 5.1 includes all the transmitted radiation. Therefore, the exact formula in Equation 5.1 is only used if the refractive index is high ( $>2$ ) and the internal transmittance,  $e^{-\alpha d}$ , is between 0.2 and 0.9. The alternate formula to calculate transmittance is given by Equation 5.2.

$$T = \frac{2n}{(n^2 + 1)} e^{-\alpha d} \quad (5.2)$$

For highly transparent thin substrate,  $e^{-\alpha d} = 1$ , so Equation 5.2 can be modified as

$$T = \frac{2n}{(n^2 + 1)} \quad (5.3)$$

Using Equation 5.3, the transmittance of PDMS membrane in the visible region can be calculated theoretically. The refractive index of PDMS (10:1) from literature was found to be 1.4. This gives the transmittance of PDMS membrane to be 94.5%.

The transmittance and absorption characteristics of the 60  $\mu\text{m}$  thick PDMS membrane were also measured experimentally using Agilent's UV-Vis spectrophotometer 8453 (Figure 5.26).

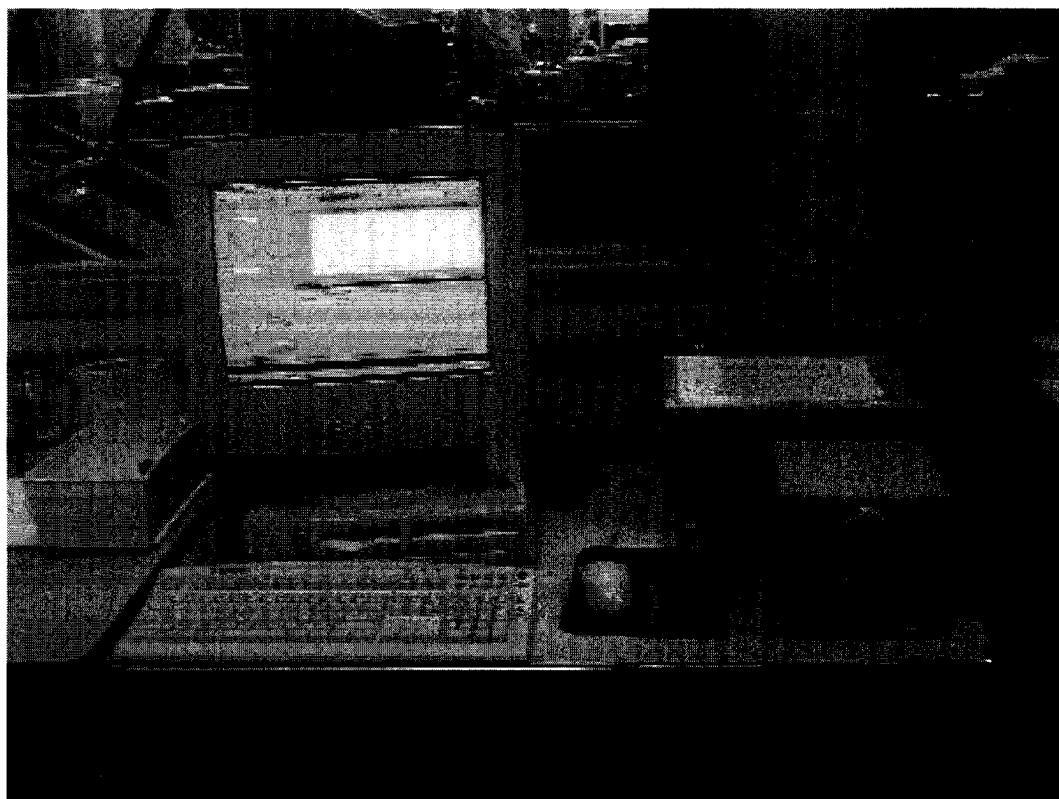


**Figure 5.26: UV-Vis spectrophotometer 8453 from Agilent at IfM.**

The transmittance characteristic of the PDMS membrane of thickness 60  $\mu\text{m}$  at different wavelengths is shown in Figure 5.27. It can be noted that PDMS membrane showed excellent transmittance characteristics from near ultraviolet to near infrared light. Average transmittance of 92% was observed in the visible range of light which closely matches with theoretically calculated transmittance value using Equation 5.3.



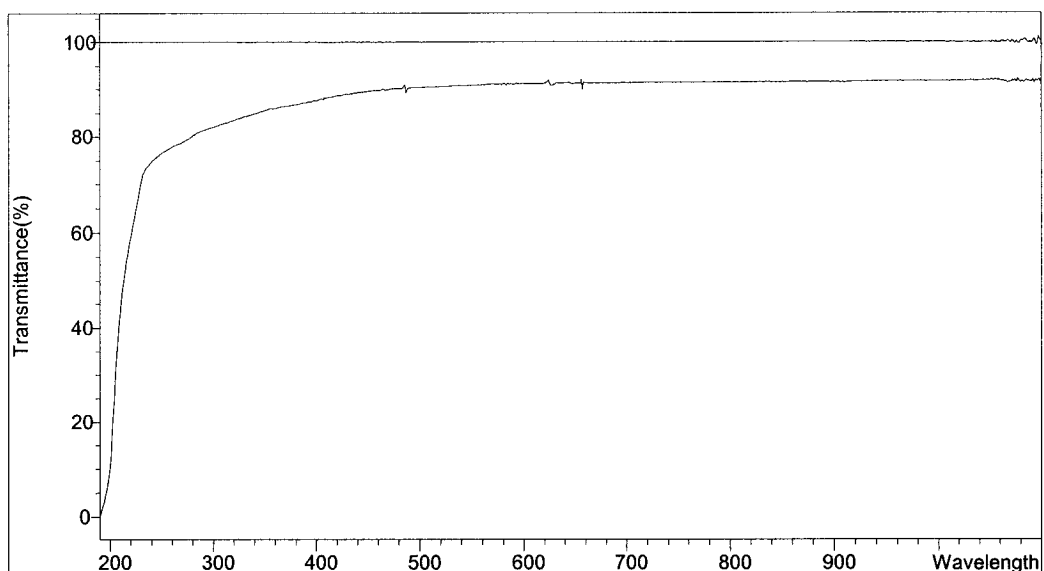


**Figure 5.27: Transmittance of 60  $\mu\text{m}$  thick PDMS membrane measured using UV-Vis spectrophotometer.**

Similarly, the absorption characteristic of the 60  $\mu\text{m}$  thick PDMS membrane using UV-Vis spectrophotometer is given in Figure 5.28. For the measurement, air was taken as the blank, and direct PDMS film was used to transmit the light of different wavelength.

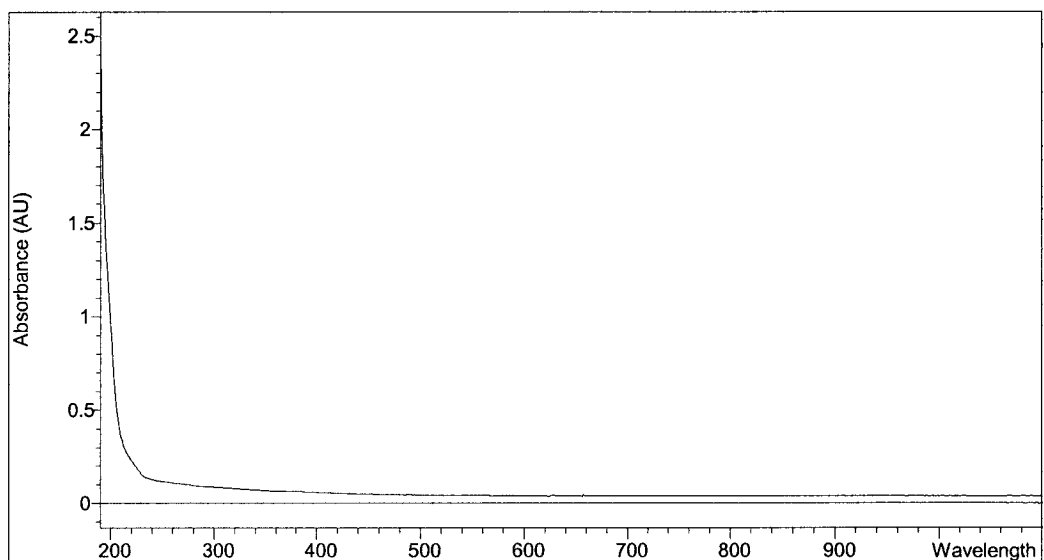


**Figure 5.28: Absorption of 60  $\mu\text{m}$  thick PDMS membrane measured using UV-Vis spectrophotometer.**

### **5.3.2 Variable Focal Length DCX and DCV Microlens System**

The experimental setup used for pumping fluid in the variable focal length lens system is shown in Figure 5.29. The setup consists of a syringe pump on which a 1 ml syringe is mounted.

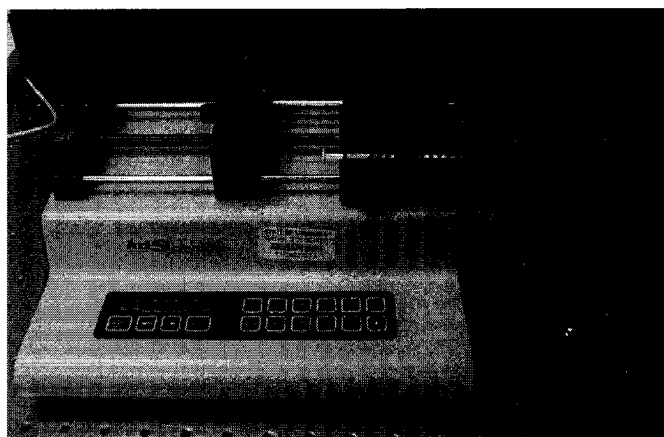


**Figure 5.29: Single variable focal length microlens system with syringe pump.**

**5.3.2.1 Imaging Characteristics.** The single variable focal length microlens structure was first actuated as a DCX lens by pumping optical fluid (DI water) into the lens chamber by means of a syringe pump. Initially, the lens chamber was filled with fluid of volume  $v_0 \approx 22 \mu\text{l}$  (flat lens volume). The theoretically calculated volume ( $v_1$ ) of the lens chamber was  $21.28 \mu\text{l}$ . The flat lens volume is slightly more than the theoretically calculated volume, which may be due to the fluid trapped in the joints or corners of the lens. The fluid was pumped into the lens chamber at a rate of  $3 \mu\text{l}/\text{min}$ , and the images were captured every 10 sec, that is at every  $0.5 \mu\text{l}$  ( $v_2$ ) of fluid pumped into the lens chamber, by directly viewing the object through the lens assembly. Next, the variable microlens system was actuated as a double concave (DCV) lens by pumping fluid out of the lens chamber from the initial reference point ( $v_0$ ). The fluid was pumped-

out at the same rate of  $3 \mu\text{l}/\text{min}$ , and the images were captured every 10 sec, that is at every  $0.5 \mu\text{l}$  ( $v_3$ ) of fluid pumped out of the lens chamber. Figures 5.30 and 5.31 show series of the images taken by actuating the single variable focal length microlens as DCX and DCV lenses, respectively.

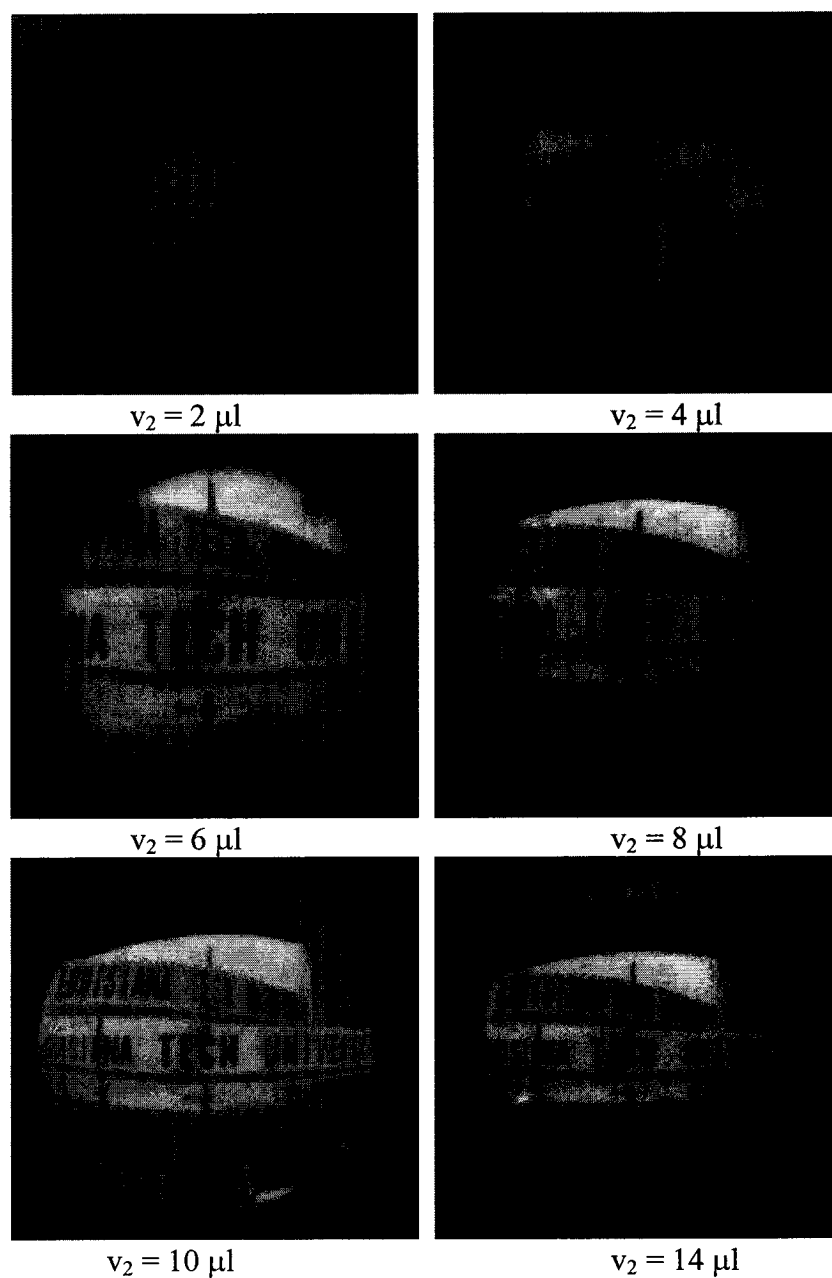


**Figure 5.30: Series of images taken at different volume of fluid by actuating the single variable focal length microlens system as DCX lens.**

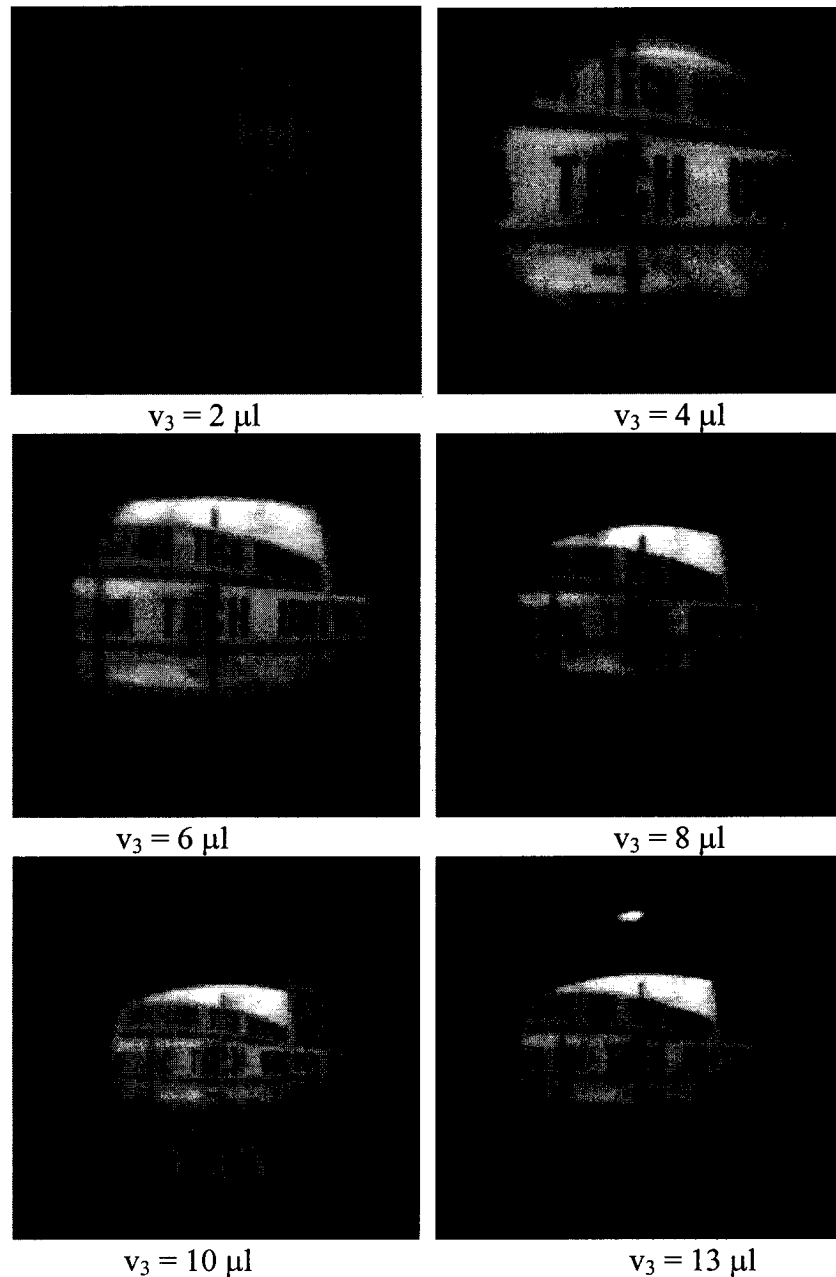


**Figure 5.31: Series of images taken at different volume of fluid by actuating the single variable focal length microlens system as DCV lens.**

It can be observed from Figure 5.30 and Figure 5.31 that the DCV lens has higher FOV compared to DCX lens at the same level of fluid pumped in or pumped out of the lens chamber. The FOV was calculated using the procedure similar to that shown in Chapter 3. Further, to demonstrate the relationship between the FOV and the focal length

of the formed lenses, the radius of curvature of the deflected PDMS lens membrane is theoretically calculated with respect to the volume of fluid pumped in or out ( $v_2$  or  $v_3$ ) of the lens chamber using the formulas given in Equations 5.4 and 5.5 which are similar to the formulas derived in Chapter 4. It should be noted that fluidic volume  $v_2$  or  $v_3$  is used to deflect membranes on both side of the lens, so only half the volume is considered. In Equation 5.1, the volume  $v_2$  and the radius  $r_1$  of the lens (2mm) are known, so the maximum deflection ( $h$ ) at the centre of the membrane can be calculated. Once  $h$  is known, the radius of curvature of the lens  $r$  can be calculated using Equation 5.5.

$$\frac{v_2}{2} = \left(\frac{\pi}{6}\right)(3r_1^2 + h^2)h \quad (5.4)$$

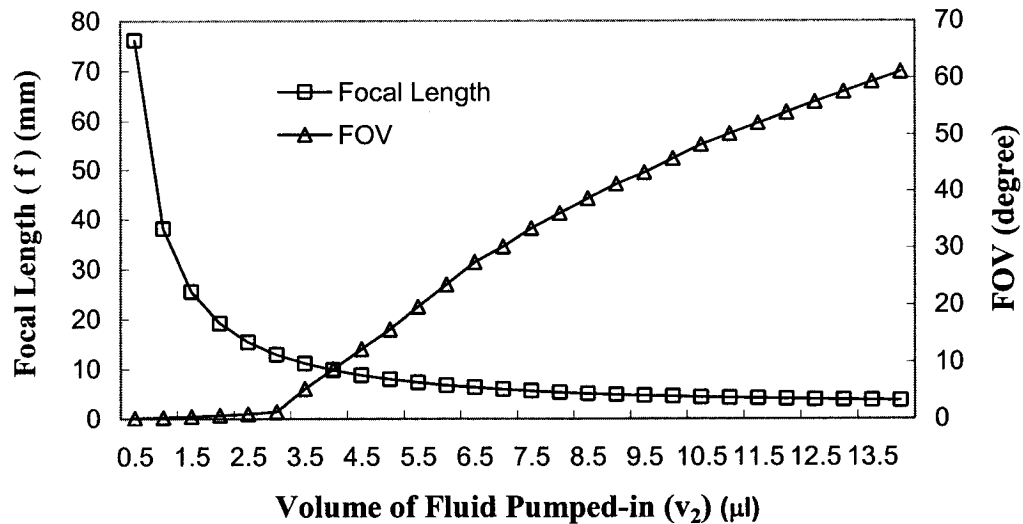
$$r = \frac{(h^2 + r_1^2)}{2h} \quad (5.5)$$

From the radius of curvature of the lens, the focal length ( $f$ ) can be calculated using the formula given in Equation 5.6, where  $n_1$  is the refractive index of air and  $n_2$  is the refractive index of the optical fluid (DI water,  $n_2 = 1.33$ ) inside the lens chamber.

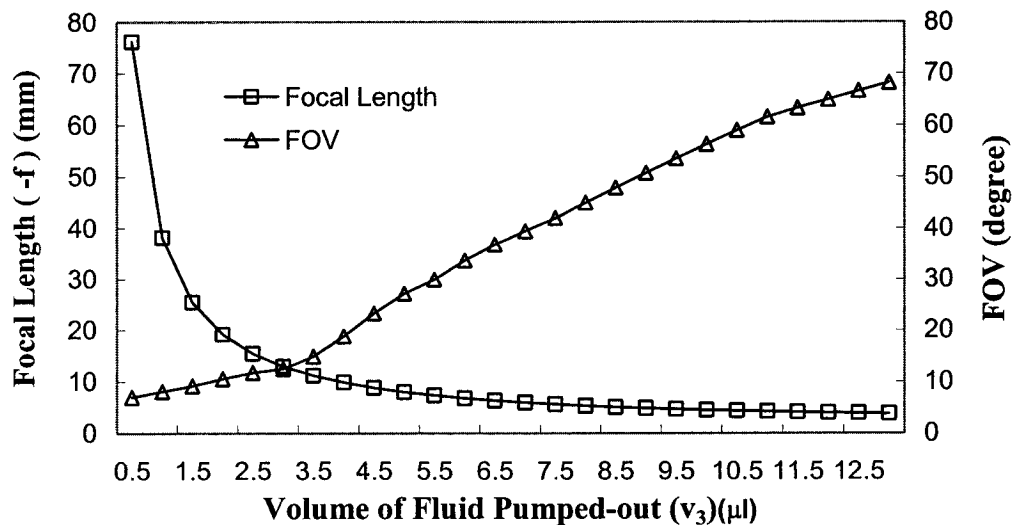
$$\frac{1}{f} = \frac{n_2 - n_1}{n_1} \left(\frac{2}{r}\right) \quad (5.6)$$

The relationship between the focal length and FOV with respect to the volume of fluid pumped in and out of the variable focal length microlens chamber is shown Figures 5.32a and 5.32b, respectively. It can be noted that, as the fluid is pumped into or out of the microlens chamber, the focal length of the corresponding DCX or DCV lens decreases as a result of the decrease in the radius of curvature. It can also be noted that, as the focal length of the dynamic DCX or DCV microlens decreases, the FOV increases. The maximum FOV achieved with a single variable focal length microlens system when actuated as DCX and DCV lenses is 61.8 and 68.2 degrees, respectively. The tuning

range of focal length achieved using the single variable focal length microlens when actuated as DCX and DCV microlenses is 76.15 mm to 3.73 mm and -76.18 mm to -3.88 mm, respectively. Figure 5.33a and 5.33b show the variation of distance between the single variable focal length microlens and the camera for each volume of fluid pumped in and pumped out of the lens chamber, respectively, to bring the fixed object into focus.

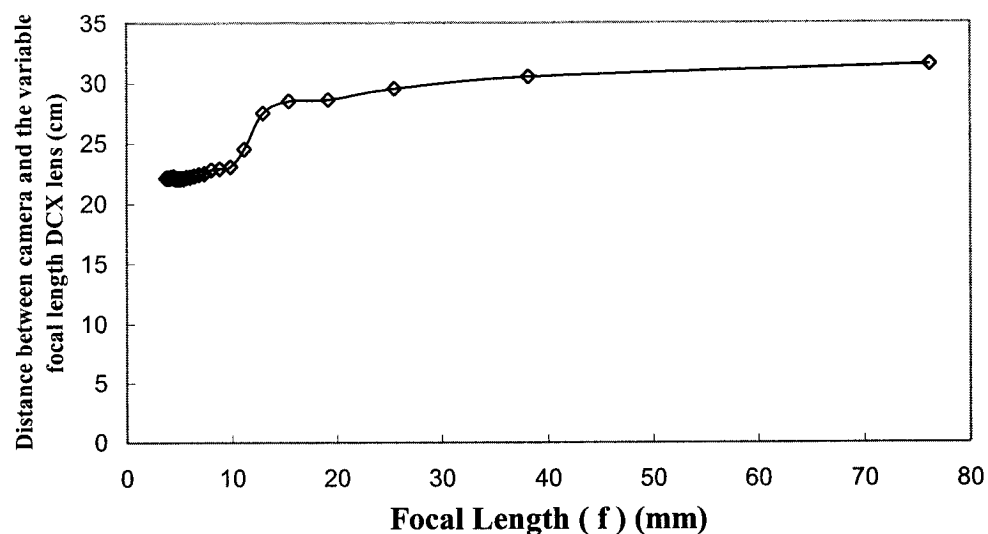


(a)

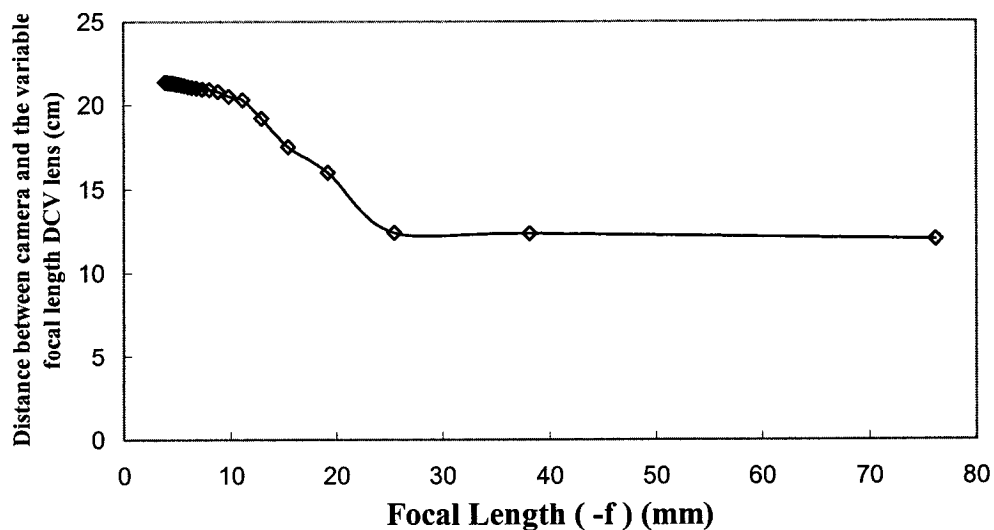


(b)

**Figure 5.32: Variation in the focal length and the field of view achieved as a function of the volume of fluid (a) Pumped-in (DCX microlens), (b) Pumped-out (DCV microlens).**



(a)



(b)

**Figure 5.33: Focal length vs. distance between the camera and the single variable focal length microlens system as (a) DCX lens, (b) DCV lens.**

It can be observed from Figure 5.33a that the distance between the camera and the variable focal length microlens decreases as the focal length decreases showing the DCX lens effect and from Figure 5.33b that the distance between the camera and the single variable focal microlens increases as the focal length decreases showing the DCV lens effect.

**5.3.2.2 Transmittance Characteristics.** The transmittance characteristic of the single variable focal length microlens system was first derived by measuring the transmittance characteristics of the working fluid (DI water) used to deflect the PDMS membrane. The transmittance characteristics of DI water are shown in Figure 5.34. It can be noted that the transmittance of DI water in the visible range is 86% which is less than the transmittance of PDMS membrane (90%). Therefore, the optical characteristics of the variable focal length microlens system are affected by the type of fluid used to deflect the PDMS membrane. Different types of optical fluids and their refractive index which can be used in this type of variable focal length lens system are given in Chapter 6.

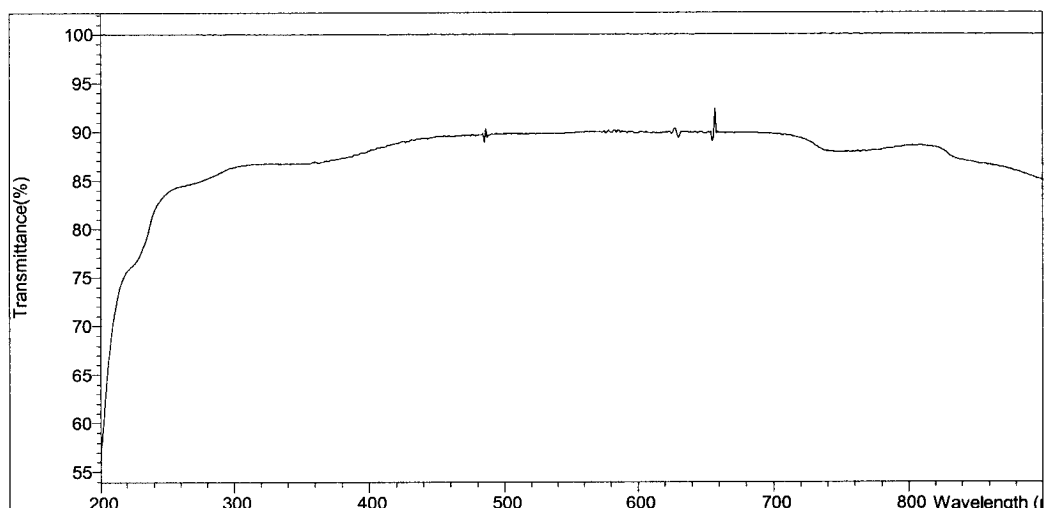


**Figure 5.34: Transmittance characteristics of working fluid (DI water).**

The transmittance characteristics measurement of the single variable focal length microlens system was also done using an Oriel spectrometer. The setup for the measurement is shown in Figure 5.35. The optical power of the light was measured using a photodiode. The initial optical power  $P_o$  of the light at different wavelengths focused on the photodiode without the variable focal length microlens was measured and is given in Figure 5.36. The optical power  $P$  of light with the single variable focal length microlens



filled with DI water (no deflection of membrane) placed in between the light source and the photodiode was also measured and is given in Figure 5.36.

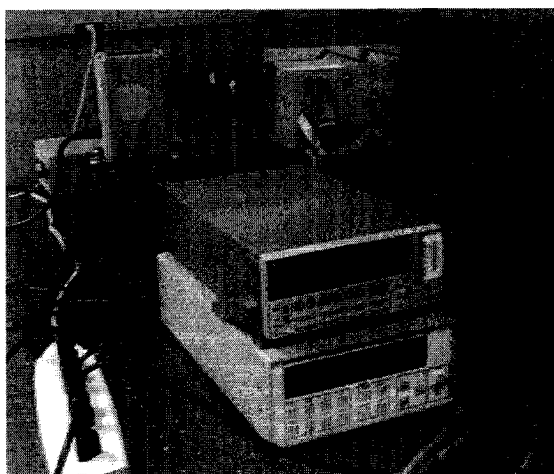


**Figure 5.35: The setup used to measure transmittance of single variable focal length microlens system.**

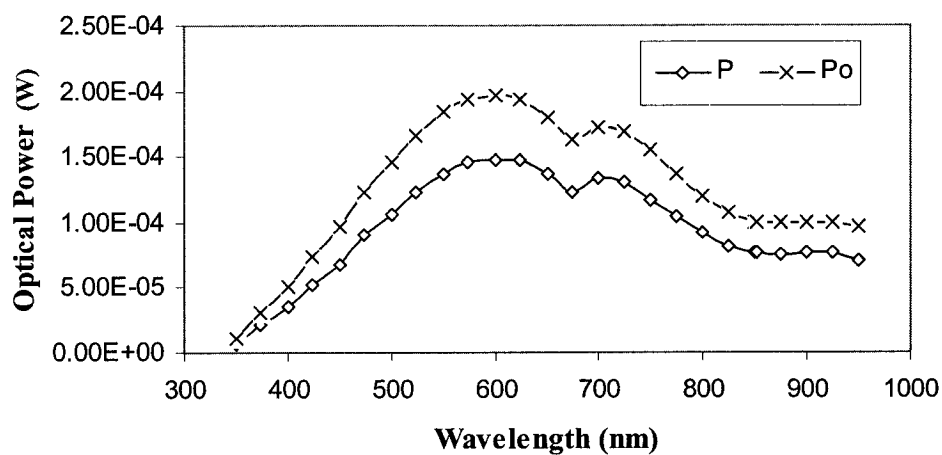


**Figure 5.36: Optical power of the light (with and without variable focal length microlens system) at different wavelengths of light measured using Oriol spectrometer and photodiode.**

From the optical power measurements obtained as shown in Figure 5.36, the transmittance of a single variable focal length microlens system can be calculated using Equation 5.7, where  $I_0$  is the initial intensity of the light,  $I$  is the intensity of light through the variable focal length microlens, and  $A$  is the area of the photodiode. The transmittance

characteristics of a single variable focal length microlens system filled with DI water without deflecting the PDMS membrane at different wavelengths are shown in Figure 5.37.

$$T = \frac{I}{I_0} = \frac{P/A}{P_o/A} = \frac{P}{P_o} \quad (5.7)$$

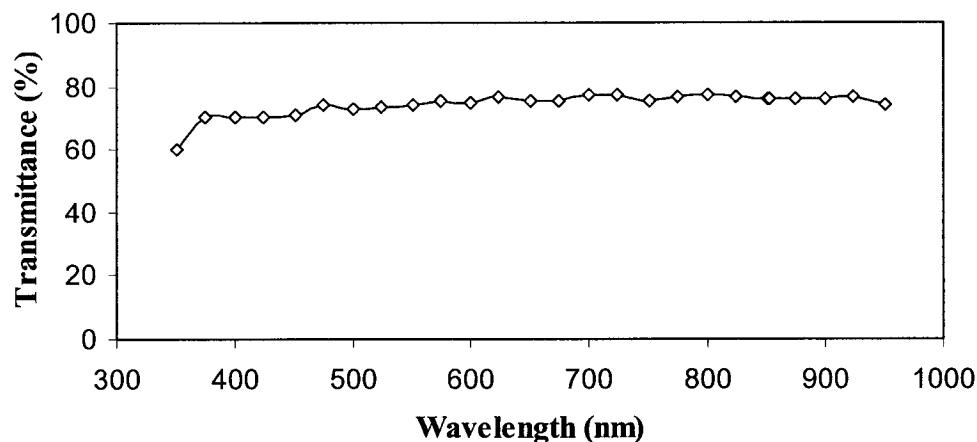


**Figure 5.37: Transmittance characteristic of single variable focal length microlens system filled with DI water without deflecting the PDMS membrane.**

It can be noted from Figure 5.37 that 75% to 80% of the light is transmitted from the single variable focal length microlens system without actuating the PDMS membrane. This value is lower than that from individual transmittance values of PDMS membrane (90%) and DI water (86%) which shows that the PDMS membrane and DI water produce a combined effect in the transmission of light from the single variable focal length microlens system.

**5.3.2.3 Contact Angle Measurements.** To determine the change in focal length of the single variable focal length microlens system experimentally, a contact angle measurement system was used. The contact angle measurement system and the series of images with contact angle values captured from this system at different volumes of fluid

pumped into the lens chamber of a single variable focal length microlens system are shown in Figures 5.38a and 5.38b. Half the total volume ( $v_2$ ) of the fluid pumped-in is taken into account because only one surface of the DCX lens is considered. Figure 5.39 depicts the measured profile of the outer lens surface at different volumes of fluid pumped-in.

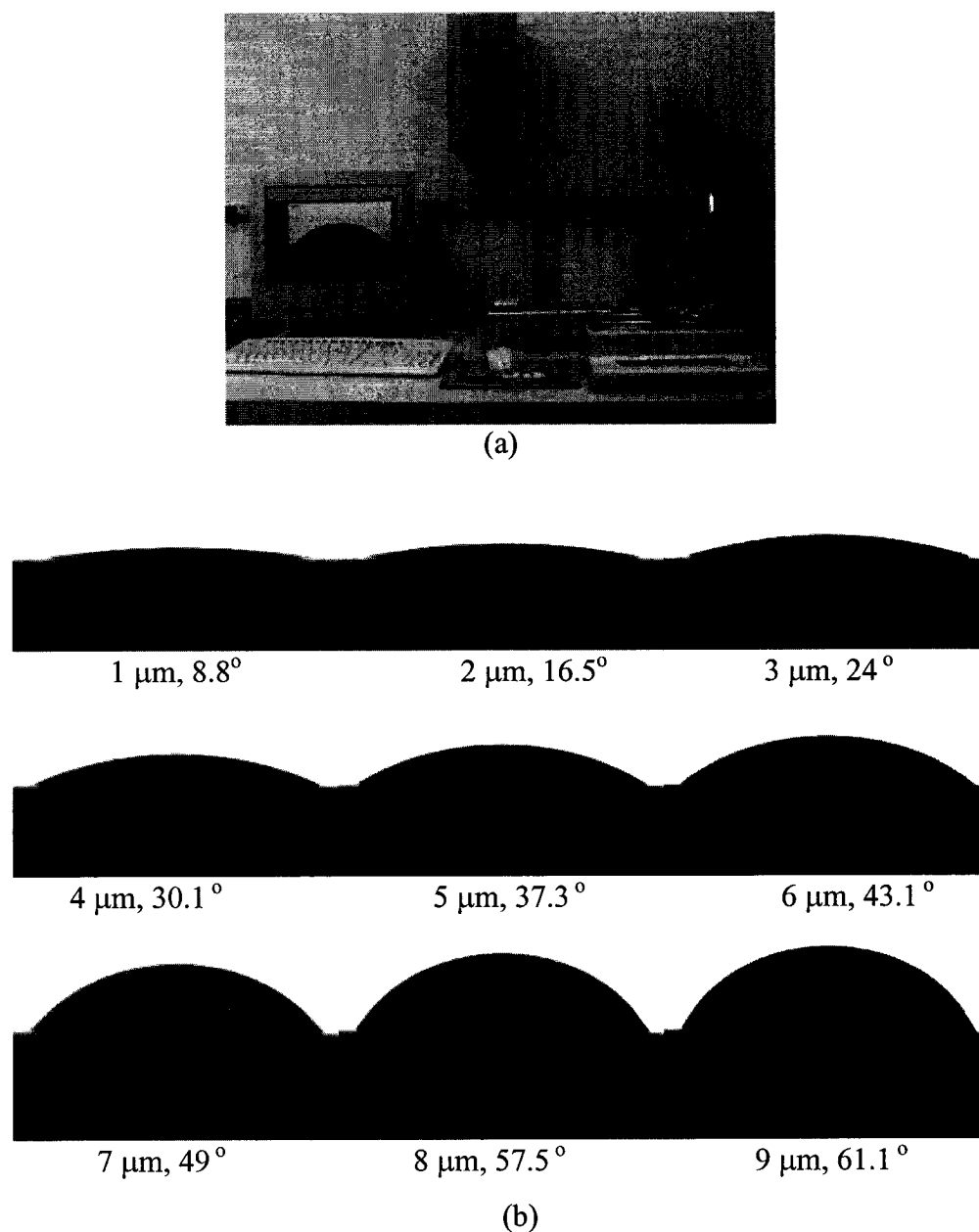


**Figure 5.38: (a) Contact angle measurement system, (b) Images of the dynamic microlens captured at different volumes of fluid pumped-in.**

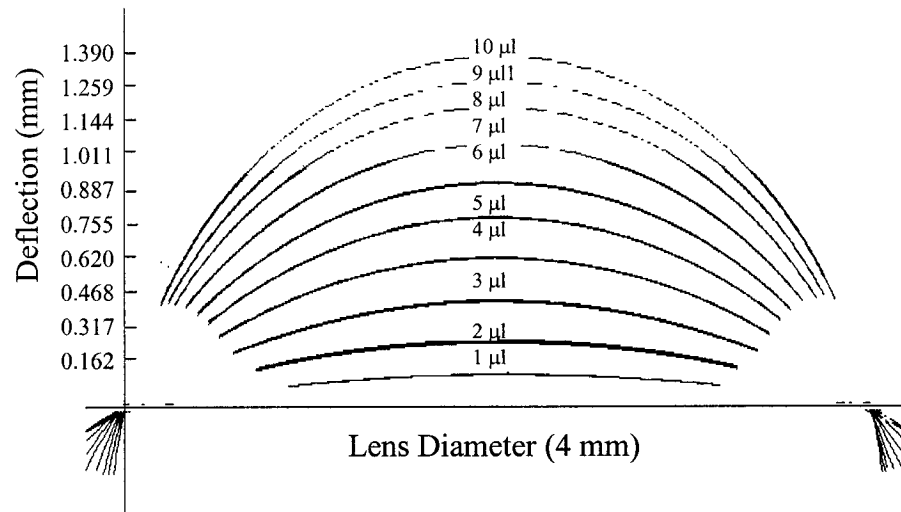


**Figure 5.39: Measured profile of the PDMS membrane of the single variable focal length microlens at different volumes of fluid pumped-in.**

From the contact angle, the radius of curvature of the lens surface at different volumes of fluid pumped into the lens chamber can be calculated using the formula given in Equation 5.8 [175], where  $R$  is the radius of curvature,  $v_2$  is the total volume of fluid pumped-in, and  $\phi$  is the contact angle.

$$R = \left[ \frac{3(v_2/2)}{\pi(2 + \cos \phi)(1 - \cos \phi)^2} \right]^{1/3} \quad (5.8)$$

For the lens diameter of 4 mm, the radius of curvature  $R$  of the variable focal length lens by different volumes of fluid pumped-in was calculated. The variation in contact angle and radius of curvature with respect to the volume of fluid pumped into the lens chamber is shown in Figure 5.40. The focal length  $f$  of the lens formed with the radius of curvature  $R$  was calculated using the formula given in Equation 5.9, where  $n_l = 1.33$ .

$$f = \frac{R}{2(n_l - 1)} \quad (5.9)$$

The comparison of the theoretically calculated focal length from Equation 5.6 and the experimentally derived focal length from Equation 5.9 is shown in Figure 5.41. It can be observed from Figure 5.41 that there is a close agreement between the theoretically and experimentally calculated focal lengths. It can be inferred that there was very close control of the volume of fluid pumped in or pumped out of the microlens chamber.

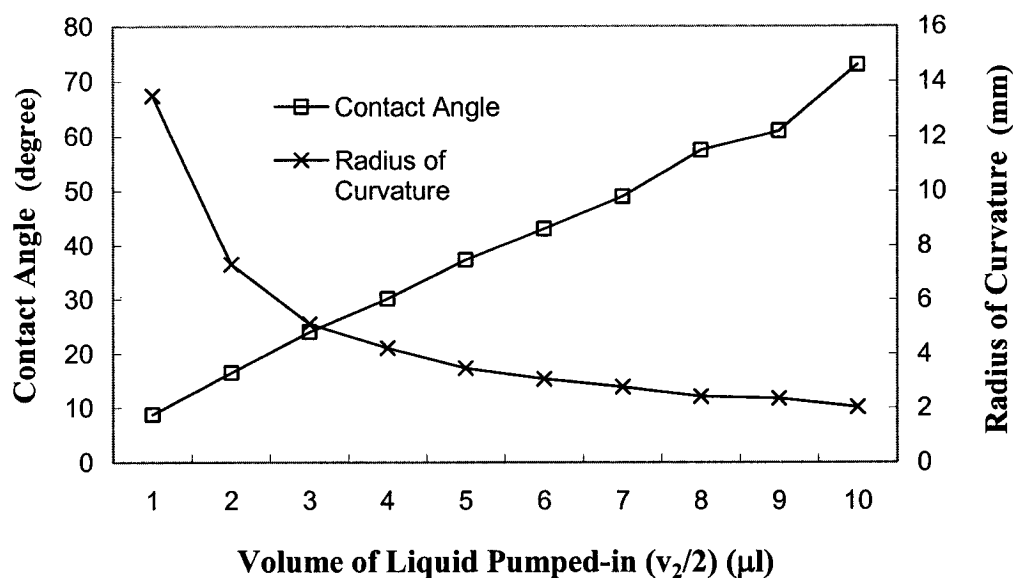


**Figure 5.40: Contact angle ( $\phi$ ) and radius of curvature ( $R$ ) of the single variable focal length microlens with change in the volume of fluid pumped-in.**

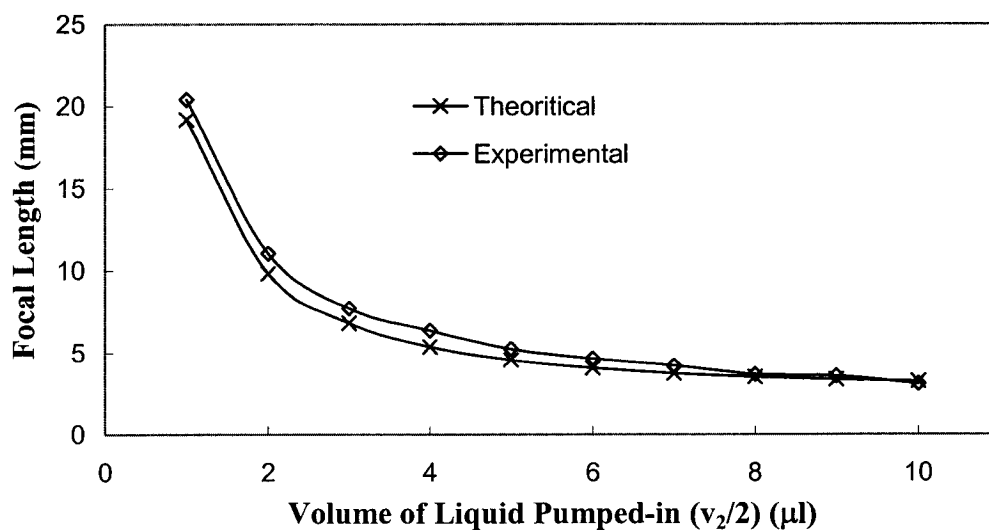


**Figure 5.41: Comparison of theoretical and experimental values of focal length with change in the volume of fluid pumped into the lens chamber.**

**5.3.2.4 The f-number and Numerical Aperture.** The f-number ( $f_{\#}$ ) and numerical aperture (NA) of the single variable lens system were calculated using the formula given in Equations 4.16 and 4.17 (Chapter 4), respectively. The change in f-number and numerical aperture with respect to the volume of fluid pumped into the lens chamber is shown in Figure 5.42. The smallest f-number achieved in this single variable focal length microlens system is 0.76 which corresponds to the numerical aperture of 0.55 (at  $v_2/2 = 10 \mu\text{l}$ ).

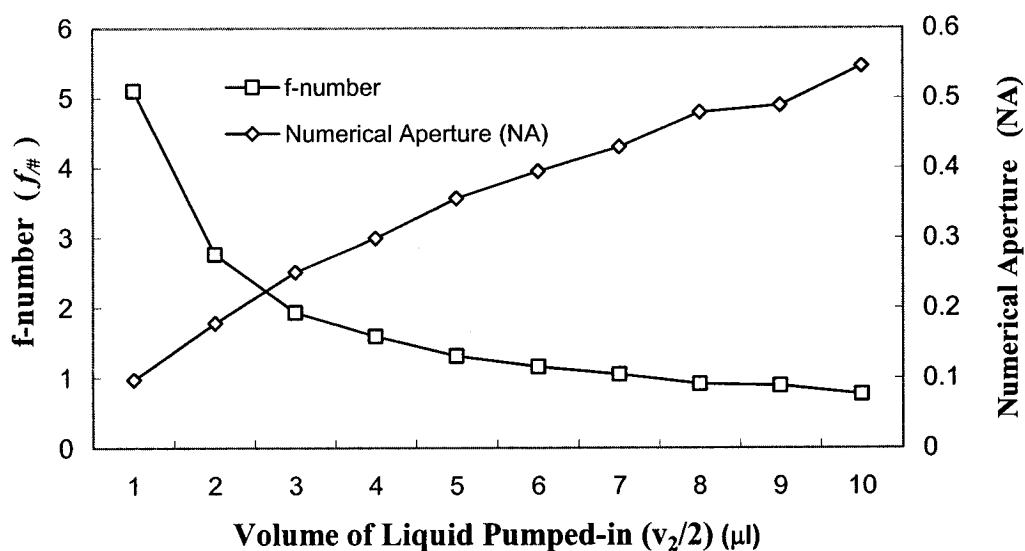


**Figure 5.42: The f-number ( $f_{\#}$ ) and numerical aperture (NA) of the single variable focal length microlens system with change in the volume of fluid pumped-in.**

Table 5.4 lists the various optical properties measured using the single variable focal length microlens system. The numerical aperture achieved using the single variable focal length microlens presented in this work is far better than that achieved from different types of variable focal length lenses fabricated to date (see Table 2.2).

**Table 5.4: Optical properties of single variable focal length microlens system at different volumes of fluid pumped-in.**

Pumped-in Volume ( $v_2/2$ ) (ml)	Contact Angle $\phi$ (degree)	Curvature R (mm)	Focal Length f (mm)	f-number f/#	Numerical Aperture
1	8.8	13.17	20.41	5.10	0.09
2	16.5	7.55	11.06	2.76	0.18
3	24	5.26	7.72	1.93	0.25
4	30.1	4.20	6.38	1.59	0.30
5	37.3	3.46	5.25	1.31	0.36
6	43.1	3.07	4.65	1.16	0.40
7	49	2.77	4.20	1.05	0.43
8	57.5	2.49	3.66	0.92	0.48
9	61.1	2.42	3.56	0.89	0.49
10	73	2.19	3.07	0.76	0.55

### **5.3.3 Integrated Wide-Angle Dynamically Variable Focal Length Microlens System**

Initially, the lens chambers of an integrated dynamic microlens system with two DCV lenses were filled with fluid ( $v_0 \approx 43 \mu\text{l}$ ). The lenses were then actuated as DCV by pumping fluid out of the lens chambers from the initial reference point ( $v_0 \mu\text{l}$ ). The fluid was pumped-out at a rate of  $6 \mu\text{l}/\text{min}$ , and images were captured every 10 sec, that is at every  $1 \mu\text{l}$  ( $v_4$ ) of fluid pumped out of the lens chambers. The volume pumped out of each lens chamber ( $v_3$ ) is half the total volume pumped out of the integrated microlens system ( $v_4$ ). The series of images taken by actuating an integrated dynamic microlens system with two DCV lenses at different volumes of fluid pumped-out are shown in

Figure 5.43. It can be noticed from the figure that the FOV increases as the volume of the fluid inside the lens chamber reduces. Also, the intensity of light collected by the integrated dynamic microlens system decreases as the volume inside the lens chamber reduces. The total attenuation in the light intensity could be due to the combined effect of attenuation of light intensity by each variable focal length microlens system.

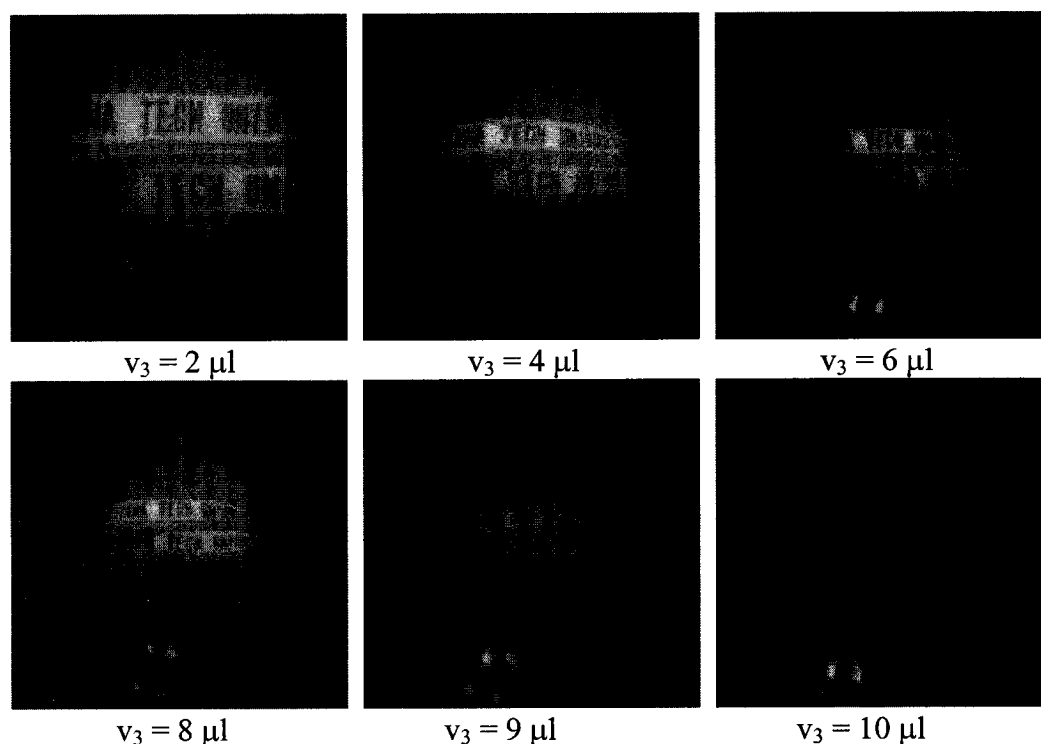


**Figure 5.43: Images of the object captured with integrated dynamic microlens system with two DCV lenses at different volumes of fluid pumped out of the lens chambers.**

The decrease in the resolution of the image, as the effective focal length of the integrated dynamic microlens system with two DCV lenses decreases, may also be due to the limitation of the CCD camera used to image the object and can be explained from Figure 5.44. As the focal length decreases, the light ray coming out of the dynamic microlens system becomes more divergent. These divergent light rays at wider angles (ray 1,2,3,4 in Figure 5.44) are not captured by the CCD camera lens and hence do not



contribute to the image formation. Therefore, the resolution of the image decreases as the focal length of the lens decreases.

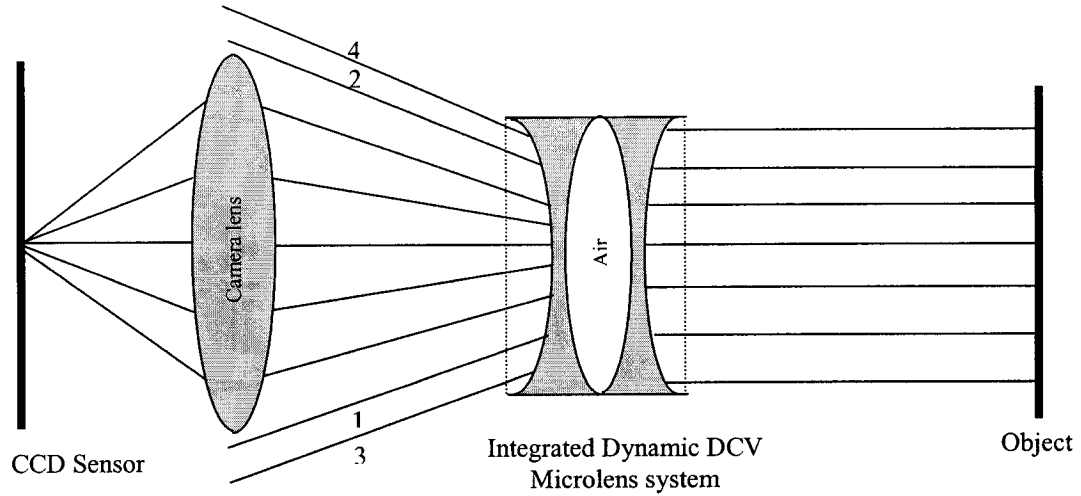


**Figure 5.44: Schematic ray diagram from integrated dynamic microlens system with two DCV lenses.**

The effective focal length  $f_{eff2}$  of an integrated dynamic microlens system with two DCV lenses can be derived from the formula given in Equation 5.10, where  $f_1$  and  $f_2$  are the individual focal lengths of the two dynamic DCV lenses combined to form an integrated microlens system. It is assumed that there is equal pressure developed inside each lens chamber and, hence, the membrane in each lens chamber deflects equally. Therefore, the focal lengths of the individual variable focal length DCV lenses  $-f_1$  and  $-f_2$  are equal.

$$\frac{1}{f_{eff2}} = \frac{-1}{f_1} + \frac{-1}{f_2} \quad (5.10)$$

Figure 5.45 shows the relationship between the focal length and FOV with respect to the volume of fluid pumped out of the lens chambers. It can be observed that as the fluid is pumped out of the lens chambers, the effective focal length of the integrated dynamic microlens decreases as a result of the decrease in the radius of curvature. It can

also be observed that, as the effective focal length decreases, the FOV increases. The maximum FOV achieved with an integrated dynamic microlens system with two DCV lenses is 76.78 degrees. The tuning range of effective focal length achieved using this system is -38.09 mm to -2.28 mm.

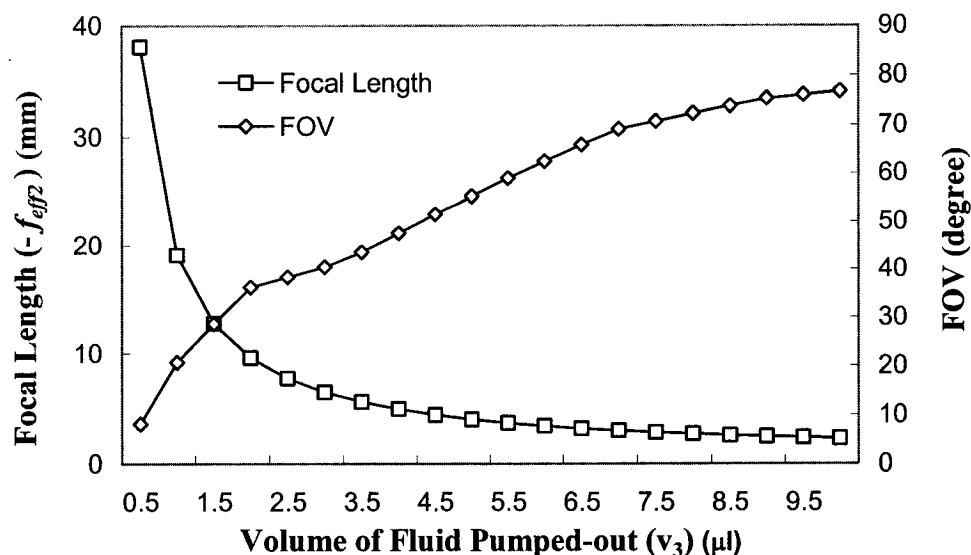


**Figure 5.45: Variation in the focal length and the field of view (FOV) achieved as a function of the volume of liquid ( $v_3$ ) pumped out of each lens chamber of the integrated dynamic microlens system with two DCV lenses.**

It can also be noticed from Figure 5.45 that the average volume of liquid pumped out per lens chamber of the integrated dynamic microlens system with two DCV lenses is less than that of the single variable focal length DCV microlens system. This effect can be due to the back pressure exerted by the PDMS membranes on the syringe which limits the flow (pumping-out) of fluid from the lens chamber on account of the membrane's elastic limit. It can also be observed that, as the focal length of the integrated dynamic microlens system decreases, the FOV increases initially and tries to saturate. The saturation of the FOV may be due to the fact that the light rays coming at a wider angle are attenuated by the lens structure as shown in Figure 5.46. It can be observed from

Figure 5.46 that the light rays 1 and 2 coming at wider angles are not accounted for imaging. Also, this effect may be due to the fact that light rays coming at wider angles diverge at wider angles and, hence, these rays are not captured by the CCD sensor or CCD camera lens used to image the object.

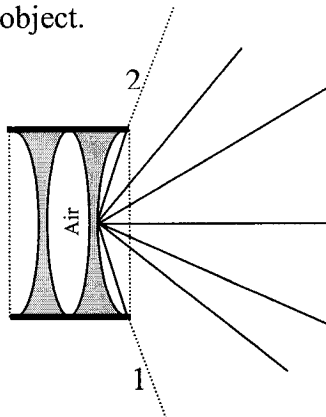


**Figure 5.46: Schematic diagram of the light ray coming at wider angle from the object.**

In an integrated dynamic microlens system with three DCV lenses, the lenses were actuated as DCV by pumping fluid out of each of the lens chambers from the initial reference point ( $v_0 \approx 65 \mu\text{l}$ ). The fluid was pumped-out at a rate of  $3 \mu\text{l}/\text{min}$ , and images were captured every 30 sec, that is at every  $1.5 \mu\text{l}$  ( $v_4$ ) of fluid pumped out of each of the lens chambers. The total volume of fluid pumped out is given by  $v_4$ , and it is equal to three times the volume  $v_3$  (volume of fluid pumped out from each lens chamber). The series of images taken by actuating the integrated dynamic microlens system with three DCV lenses at different volumes of fluid pumped-out are shown in Figure 5.47.

It can be noticed from Figure 5.47 that the FOV increases as the volume of the fluid inside the lens chamber reduces. Also, the intensity of light collected by the three lens system further decreases from that of the two lens system as the volume inside the lens chamber reduces indicating that the light is absorbed by each layer and intensity decreases as the number of layer increases. Also, as explained for the integrated dynamic

microlens system with two DCV lenses, the decrease in the light intensity and resolution may also be due to the limitation of the CCD camera which does not capture the incoming rays at wider angles.

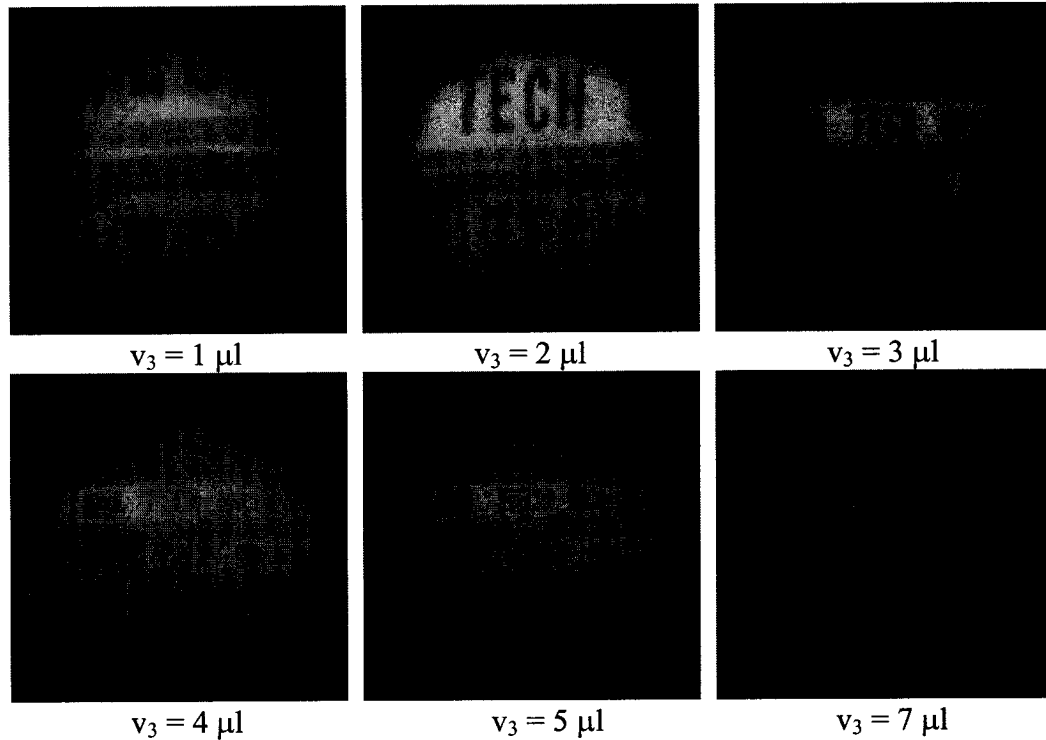


**Figure 5.47: Images of the object captured with an integrated dynamic microlens system with three DCV lenses at different volumes of fluid pumped out of the lens chambers.**

The effective focal length  $f_{eff3}$  of an integrated dynamic microlens system with three DCV lenses can be derived from the formula given in Equation 5.11, where  $-f_1$ ,  $-f_2$  and  $-f_3$  are the individual focal lengths of the three DCV lenses integrated to form a compound lens system.

$$\frac{1}{f_{eff3}} = \frac{-1}{f_1} + \frac{-1}{f_2} + \frac{-1}{f_3} \quad (5.11)$$

It is assumed that there is equal pressure developed inside each lens chamber and, hence, the membranes in all the three lens chambers deflect equally. Therefore, the focal

lengths of the individual variable focal length DCV lenses  $-f_1$ ,  $-f_2$  and  $-f_3$  are equal. The relationship between the effective focal length and the FOV achieved from the integrated dynamic microlens system with three DCV lenses with respect to the volume of fluid pumped-out of the lens chambers is shown in Figure 5.48.

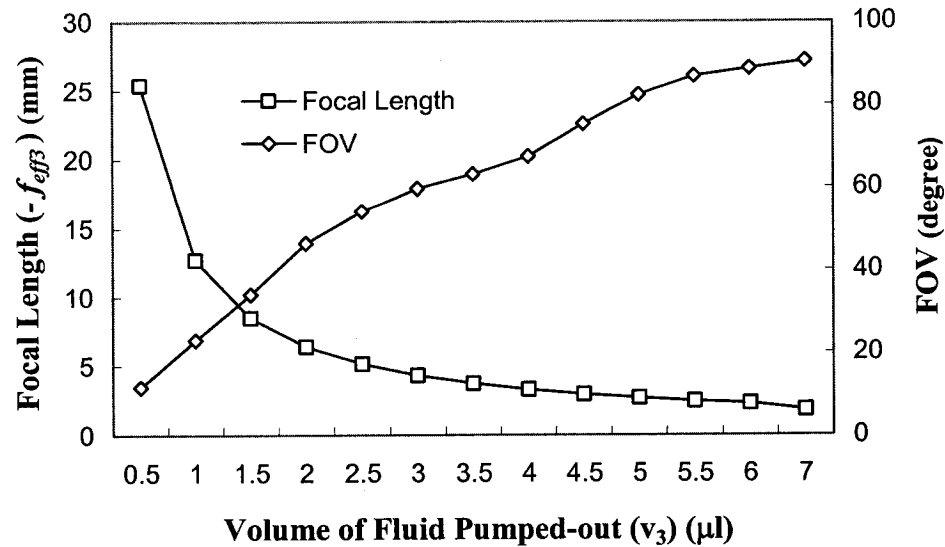


**Figure 5.48: Variation in the focal length and the field of view (FOV) achieved as a function of the volume of liquid ( $v_3$ ) pumped out of each lens chamber of the integrated dynamic microlens system with three DCV lenses.**

It can be observed from Figure 5.48 that, as the fluid is pumped out of the lens chambers, the effective focal length of the integrated dynamic microlens system with three DCV lenses decreases. This behavior is due to the decrease in the radius of curvature of each membrane. Also, as the effective focal length decreases, the FOV increases. The maximum FOV achieved with an integrated dynamic microlens system with three DCV lenses is 90.45 degrees. The tuning range of the effective focal length achieved using this lens system is -25.39 mm to -1.80 mm.

It can also be noticed from Figure 5.48 that the average volume of liquid pumped out per lens chamber of the integrated three lens system is less than that of a one or two lens system. This effect is due to the back pressure exerted by the PDMS membranes on

the syringe which limits the flow of fluid out of the lens chamber. The summary of the change in focal length and FOV with the change in volume of fluid pumped out ( $v_3$ ) of the single variable focal length DCV microlens and integrated dynamic microlens system with two or three DCV lenses are given in Table 5.5 and Figure 5.49.

**Table 5.5: Change in focal length and field of view with the change in volume of fluid pumped out of different dynamic DCV microlens systems.**

Volume of liquid pumped out of each of the lens chamber ( $v_3$ )	Focal Length (-f)			Field of View		
	Single DCV lens	Two DCV lens	Three DCV lens	Single DCV lens	Two DCV lens	Three DCV lens
1	37.88	19.08	12.71	8.09	20.66	22.90
2	18.94	9.60	6.39	10.52	36.18	46.41
3	12.63	6.47	4.31	12.47	40.41	59.59
4	9.47	4.92	3.27	18.81	47.53	67.30
5	7.58	4.01	2.67	27.17	55.27	82.22
6	6.32	3.41	2.27	33.64	62.49	88.66
7	5.41	2.82	1.80	39.40	69.14	90.44
8	4.74	2.69	x	44.97	72.29	x
9	4.21	2.45	x	50.78	75.31	x
10	3.79	2.28	x	56.33	76.05	x
11	3.45	x	x	61.6	x	x
12	3.16	x	x	64.97	x	x
13	2.92	x	x	68.22	x	x

x – fluid could not be pumped-out because of back pressure

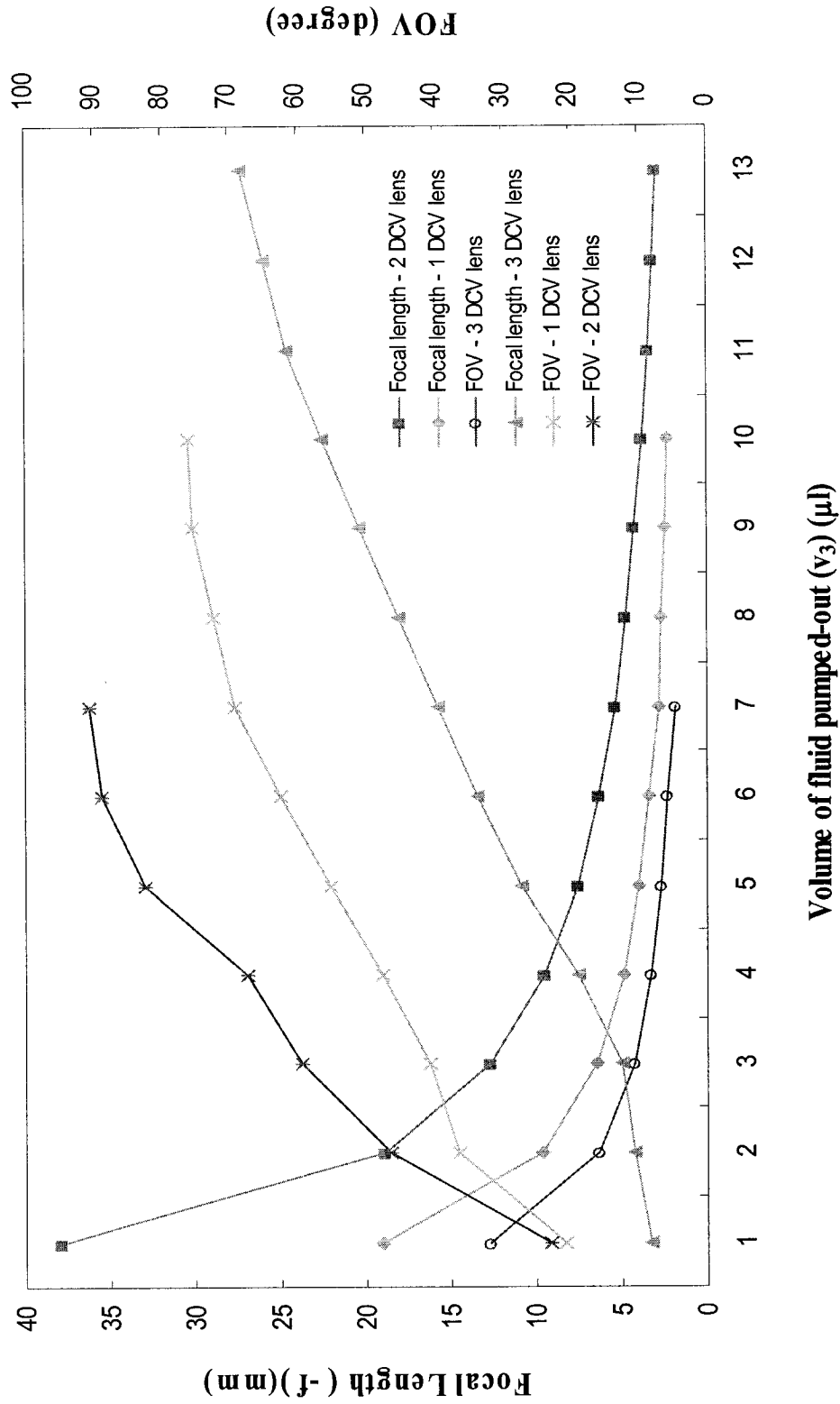


Figure 5.49: Change in focal length and field of view with the change in volume of fluid pumped out of different integrated dynamic DCV microlens systems.

## CHAPTER 6

### CONCLUSIONS AND RECOMMENDATIONS

#### 6.1 Conclusions

In the present work, a novel fluid-controlled polymer-based wide-angle micro-optical lens system with variable focal length and field of view (FOV) has been designed and fabricated. A fluidic actuation mechanism was used to deflect the flexible PDMS membranes to achieve the variable focal length. The curvature of the lens (PDMS membrane) changes because of the fluidic pressure built by the syringe pump and produces the change in focal length and FOV. Comparative imaging experiments were performed to obtain the relationship between the focal length and FOV for different types of lenses and lens configurations using both static glass lenses of fixed focal length and dynamic PDMS lens systems of variable focal length.

Preliminary experiments were conducted using different sets of double concave (DCV) and double convex (DCX) lenses of different focal lengths to understand the relationship between the field of view and focal length of the lenses, and to find out the specific combination of lenses that can provide a wider FOV. These lenses were chosen because they are relatively easy to fabricate and make the polymer lens system adapt to one of these configurations. From the experiments conducted using static glass lenses, it was found that the FOV increases with the decrease in the focal length of DCX lenses or



DCV lenses used to image the object and wider FOV could be achieved with the DCV lens compared to the DCX lens of the same focal length. In the other experiments conducted using a primary DCX lens and a secondary DCV lens or a set of DCV lenses, it was found that the focal lengths of both primary and secondary lenses determine the FOV. The FOV of the compound lens system increases with the decrease in the focal length of secondary DCV lenses. It was also observed that increasing the number of DCV lenses leads to an increased FOV. It is demonstrated that wide FOV could be achieved when three DCV lenses are used to image the object compared to single or two DCV lenses.

A macro-scale fluid controlled optical lens system that is capable of displaying dynamic variation of its focal length and FOV was first designed, fabricated, and tested successfully. It was demonstrated that the focal length of a single dynamic lens system, when actuated as DCX and DCV lenses, can be tuned in the range of 47.28 to 2.09 cm and -47.28 to -5.56 cm, respectively. It was also demonstrated that the FOV achieved using this lens system is in the range of 2.56 to 59.31 degrees and 26.79 to 49.57 degrees, respectively. Also, the FOV achieved using integrated variable focal length lens systems with two DCV lenses and three DCV lenses is in the range of 32.34 to 112.2 degrees and 29.48 to 118.34 degrees, respectively. The smallest f-number achieved from the single DCX variable focal length lens system is 1.3 which corresponds to the numerical aperture of 0.35. The maximum FOV achieved by using a fluid-controlled macro-optical lens system with three DCV lenses was 118.34 degrees.

Further, the design, fabrication, and testing of a novel micro-scale variable focal length lens system have been demonstrated. Standard photolithography and silicon

micromachining techniques were used to fabricate fluidic microchannels and lens chambers. A new process to etch through the silicon wafer in Inductive Coupled Plasma (ICP) etching using positive photoresist (AZ 4903) as the masking layer has been successfully attempted and demonstrated in this research. The diameter of the fabricated lens is 4000  $\mu\text{m}$ , and the dimensions of the lens assembly are 10 mm x 10 mm x 1.5 mm. An integrated two or three variable focal length DCV microlens system with wide FOV has also been fabricated and tested. The average thickness of the PDMS membrane, used to form the lens surface and fabricated using a spin coating technique, was measured to be 60  $\mu\text{m}$  using a surface profilometer (Tencor) and a Roughness Step Tester (RST). The surface characteristics of the PDMS membrane were also determined using an Atomic Force Microscope (AFM) and RST, and the results obtained indicate that a smooth PDMS membrane (roughness = 26 nm) can be fabricated using a spin coating technique.

The focal length of the single variable focal length microlens system as a DCX lens and a DCV lens can be tuned over the range of 76.15 to 3.73 mm and -76.18 to -3.88 mm, respectively. A comparative study between the theoretically calculated focal length and experimentally determined focal length has been performed and analyzed. A close match between these two values indicates that the volume of fluid pumped in or out of the fluidic lens chamber can be precisely controlled using the syringe pump. The FOV characteristic of these types of variable focal length lens systems has been investigated and demonstrated for the first time in this work. It has been demonstrated that the FOV that could be achieved using a single variable focal length microlens system as DCX and DCV lenses is in the range of 0.12 to 61.08 degrees and 7 to 68.22 degrees, respectively. The smallest f-number of 0.76 which corresponds to a numerical aperture of 0.55 can be

achieved using a single variable focal length microlens system. This shows that the present variable focal length microlens system, developed in this research work, has excellent optical properties compared to that of other types of variable focal length lens systems reported to date (see Table 2.2). The effective focal length of the integrated dynamic microlens system with two and three DCV lenses can be tuned in the range of the -38 to -2.28 mm and -25 to -1.8 mm, respectively. The field of view achieved using integrated two and three variable focal length DCV microlens systems are in the range of 8 to 79.65 degrees and 11.49 to 90.44 degrees, respectively. Similar design and fabrication processes can be used to fabricate even smaller diameter (500  $\mu\text{m}$ ) variable focal length lens systems. However, it should be noted that, as the diameter of the lens decreases because of diffraction effects, the resolution and image finesse would reduce drastically. It should also be noted that other types of lenses such as positive and negative meniscus lens, doublet with double convex and meniscus lens, and any other combination of lenses could be fabricated using the integrated dynamic microlens system presented in this work.

An essential characteristic of the present wide-angle variable focal length microlens system is its bio-inspired architecture similar to that found in the human eye lens with a large flexibility and versatility. The method of changing focus by changing the shape of the lens has no parallel in photography. Focus is changed in cameras by moving the position of the entire lens with respect to the film. The wide-angle microlens system designed and fabricated in this research work can be applied to a wide range of optical imaging applications such as components for optical communication, biomedical instruments, digital cameras, camera phones, endoscopes, home security systems, optical

storage drives, micro-air vehicles (MAVs), bio-medical diagnostic and surgical devices, vertical scanners, optical holography devices, surveillance systems and other diverse micro-optical systems.

## **6.2 Recommendations for Future Research**

In the present work, DI water ( $n= 1.33$ ) was taken as the working fluid to deflect the lens membrane. Different types of high refractive index fluid (e.g., immersion oil,  $n = 1.55$ ) can be used as working fluid in the present variable focal length microlens system [167]. As the refractive index increases, it can be demonstrated from Equation 5.9 that the focal length of the DCX or DCV lenses decreases. The decrease in focal length further enhances the chances of increasing the FOV, as demonstrated in Chapters 4 and 5. The types of available optical fluids with their physical, chemical, and optical properties are listed in the *Handbook of Optical Materials* by M. J. Weber [168,169].

The human eye lens is made of transparent fibers in a thin membrane as shown in Figure 6.1, and has a non-uniform index of refraction (GRIN structure). The exact distribution of the refractive index of the human eye lens is not yet well known [170-172].

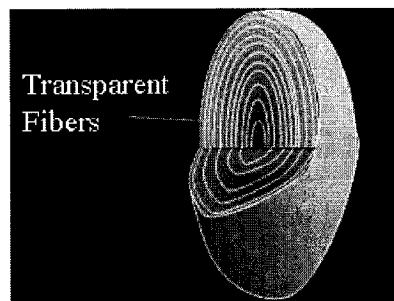


**Figure 6.1: Cross-section of human eye lens.**

It is known that the GRIN lens in real eyes permits an increase in the refractive power of the crystalline lens, which otherwise would be too low on account of the small differences in refractive index between adjacent biological media that have a high water content [171]. Thus, the GRIN structure permits an increase in the effective refractive index of the lens and, hence, its power [171]. Similar types of fluids could be developed with a controllable and distributive refractive index, such as found in the human eye lens, and can be used as working fluid in the variable focal length microlens systems presented in this research to increase the refractive power as well as other optical characteristics. In the present integrated dynamic microlens system, the gap between the two or three DCV microlenses is air. This gap, if filled with other fluids with properties similar to that of vitreous humor and aqueous humor fluids found in the human eye [170], could help to improve the optical properties of the integrated microlens system presented in this work. Also, the lens chambers of an integrated dynamic microlens system with two or three DCV lenses filled with different working fluids of different optical properties can be further investigated and tested for wide FOV.

*Integration with Micro-pump:* The designed variable focal length microlens system can further be improved by integrating the overall system with a micro-pump avoiding the currently used syringe pump to deflect the PDMS membrane. Different types of micro-pumps are available commercially which can be used to integrate with the present microlens system. One such piezoelectrically actuated micro-pump from Fraunhofer-IMS is shown in Figure 6.1.

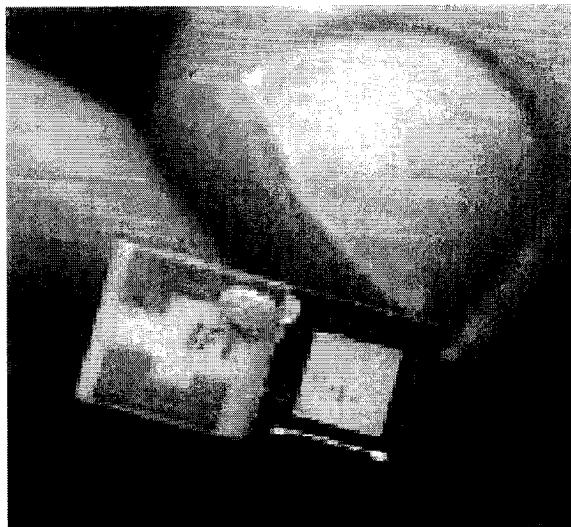


**Figure 6.2: Piezoelectrically actuated micro-pump from Fraunhofer-IMS [173].**

The technical specifications of this micro-pump are given in Table 6.1. It can be noticed from Table 6.1 that this micro-pump could be adopted with the present variable focal length microlens system developed in this research work to deflect the PDMS membrane.

**Table 6.1: Technical specification of micro-pump from Fraunhofer-IMS [173].**

chip dimensions	7 mm x 7 mm x 1 mm
maximum pump rate (H <sub>2</sub> O)	1500 - 3000 $\mu$ l/min
maximum pump rate (air)	3000 $\mu$ l/min
maximum back pressure	500 mbar (for liquids)
power consumption	typically 135 mW
pump media	water, aqueous solutions, viscose oils, various gases

*Monolithic All-Polymer Variable Focal Length Lens System:* The schematic design of the mold to fabricate monolithic integrated variable focal length lens system with three DCV lenses is demonstrated in Figure 6.3. The process steps to fabricate monolithic wide-angle variable focal length lens systems are shown in Figure 6.4. The

mold for a monolithic microlens can be fabricated by using hot embossing techniques, electroplating processes, or other silicon etching techniques.

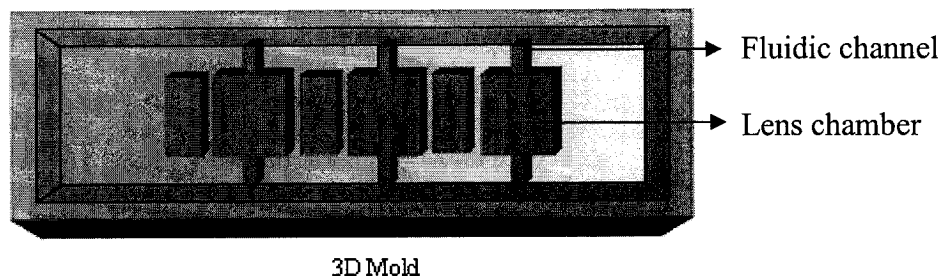


**Figure 6.3: 3D schematic of the mold to fabricate monolithic wide-angle variable focal length lens system.**

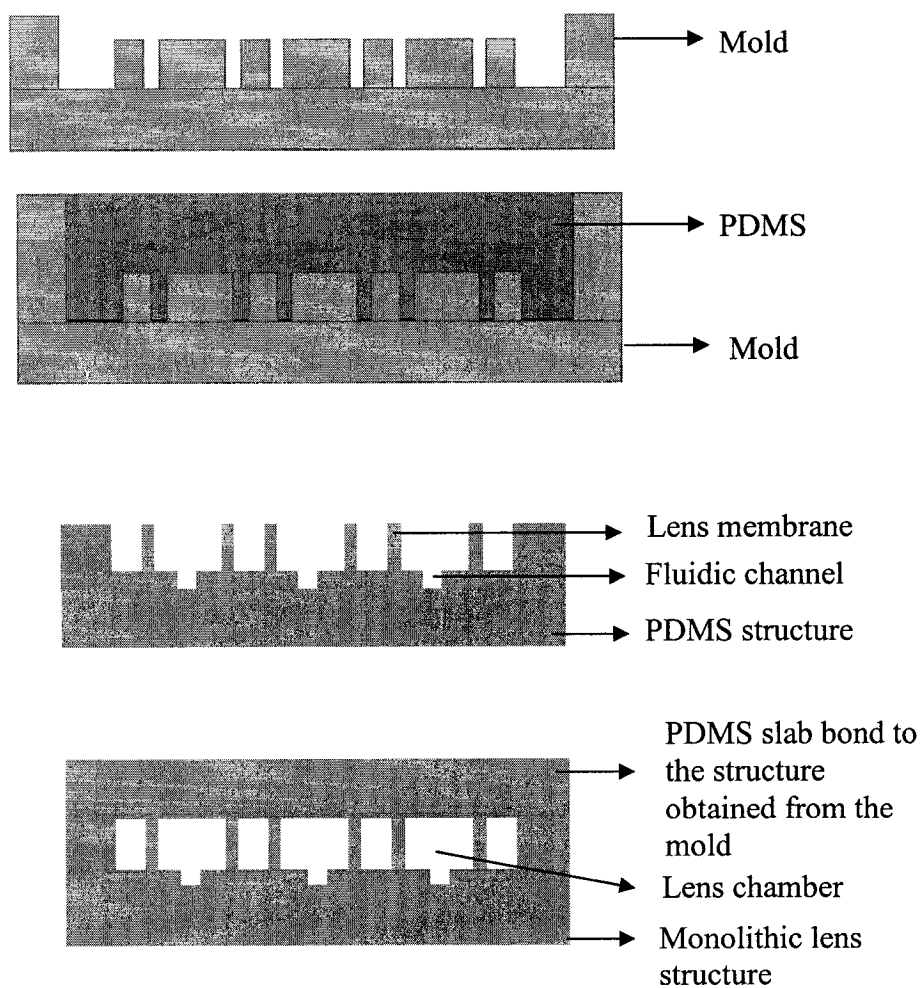


**Figure 6.4: Fabrication steps for monolithic wide-angle variable focal length lens system.**

## BIBLIOGRAPHY

- [1] L. S. Fan, Y. C. Tai, and R. S. Muller, "IC-Processed Electrostatic Micromotors," *Technical Digest, IEEE International Electron Devices Meeting* (San Francisco, CA, December 1988), pp. 666-669.
- [2] J. D. Zook, D.W. Burns and H. Guckel, "Characteristics of polysilicon resonant Micro beams," *Sensors and actuators Part A, Physical*, vol. 35, no. 1, 1992, pp.51-59.
- [3] S. C. Kim and K. D. Wise, "Temperature Sensitivity in Silicon Piezoresistive Pressure Transducers," *IEEE Trans. Electron Devices*, vol. 30, No. 7, July 1983, pp. 802-810.
- [4] K. D. Wise and K. Najafi, "Micro fabrication Techniques for Integrated Sensors and Microsystems," *Science*, vol. 254, Nov. 1991, pp. 1335-1341.
- [5] R. T. Howe, R. S. Muller, K.J. Gabriel and W. S. N. Trimmer, "Silicon Micromechanics: Sensors and Actuators on a Chip," *IEEE Spectrum*, July 1990, pp. 29-35.
- [6] Y. S. Lee and K. D. Wise, "A Batch-Fabricated Silicon Capacitive Pressure Transducer with Low Temperature Sensitivity," *IEEE Trans. Electron Devices*, vol. 29, no. 1, Jan.1982, pp. 42-48.
- [7] W. Riethmuller and W. Benecke, "Thermally Excited Silicon Microactuators," *IEEE Trans. Electron Devices*, vol. 35, no. 6, June 1988, pp. 758-763.
- [8] H. Fujita and A. Omodaka, "The Fabrication of an Electrostatic Linear Actuator by Silicon Micromachining," *IEEE Trans. Electron Devices*, vol. 35, no. 6, June 1988, pp. 731-734.
- [9] G. J. Maclay, W. J. Buttner, and J. R. Stetter, "Microfabricated Amperometric Gas Sensors," *IEEE Trans. Electron Devices*, vol. 35, no. 6, June 1988, pp. 793-799
- [10] B. Puers, L. Reynaert, W. Snoeys, and W. M. C. Sansen, "A New Uniaxial Accelerometer in Silicon Based on the Piezjunction Effect," *IEEE Transactions on Electron Devices*, vol. 35, no. 6, June 1988, pp. 764-770.



- [11] H. L. Chau and K. D. Wise, "An Ultraminiature Solid-State Pressure Sensor for a Cardiovascular Catheter," *IEEE Trans. on Electron Devices*, vol. 35, no. 12, Dec. 1988, pp. 2355-2361.
- [12] C. J. Kim, A. P. Pisano and R. S. Muller, "Silicon-Processed Overhanging Microgripper," *J. Microelectromech. Syst.*, vol. 1, no. 1, March 1992, pp. 31-36.
- [13] K. E. Petersen, "Silicon as a Mechanical Material," *Proc. IEEE*, vol. 70, no. 5, May 1982, pp. 420-457.
- [14] G. Stemme, "Micro Fluid Sensors and Actuators," *Proc. Sixth Int. Symp. Micro Machine and Human Sci.*, Nagoya, Japan, 1995, pp. 45-52.
- [15] J. Knutti, "Finding Markets for Microstructures," *Proc. Micromachining and Fabrication Process Technology IV, SPIE 3511*, 1998, pp. 17-23.
- [16] R. Wechsung, N. Unal, "Market Analysis for Microsystems: an Interim Report from the Nexus Task Force," *Proc. Micro Syst. Techn. 98*, Dec. 3, 1998, pp. 275.
- [17] "Market Analysis for Microsystems 1996-2002," *Nexus Report*, Oct. 1998.
- [18] S. A. Vittorio, "MicroElectroMechanical Systems (MEMS)," *Cambridge Scientific Abstracts, Released October 2001*.
- [19] L. S. Fan, Y. C. Tai, and R. S. Muller, "Integrated movable micromechanical structures for sensors and actuators," *IEEE Trans. Electron Devices* ED-35, June 1988, pp. 724-730.
- [20] D. Bishop, R. Giles, and C. Roxlo, "Micro-mirrors relieve communications bottlenecks," *Photonics Spectra*, vol. 34, no. 3, Mar. 2000, pp. 167-169.
- [21] J. D. Zahn, N. H. Talbot, D. Liepmann and A. P. Pisano, "Microfabricated Polysilicon Micro needles for Minimally Invasive Biomedical Devices," *Biomed. Microdevices*, vol. 2, no. 4, 2000, pp.295-303.
- [22] K. Takahashi, H. Sakai, K. Nagayama, A. Baba, K. Makihara and T. Asano, "Vaporization and Nucleation on Microheater in Microchannel with Nozzle," *Proc. 35<sup>th</sup> AIAA Thermophysics Conf.*, Anaheim, CA, June 11-14, AIAA Paper 2001-3075.
- [23] M. Mehregany and S. Roy, "Introduction to MEMS," *Microengineering Aerospace Systems*, Dr. H. Helvajian, Aerospace Press, AIAA Inc., 1999.

- [24] J. D. Lee, J. B. Yoon, J. K. Kim, H. J. Chung, C. S. Lee, H. D. Lee, H. J. Lee, C. K. Kim and C. H. Han, "A Thermal Inkjet Printhead with a Monolithically Fabricated Nozzle Plate and Self-Aligned Ink Feed Hole," *J. Microelectromechanical Syst.*, vol. 8, no. 3, Sept. 1999, pp. 229-236.
- [25] J. Stem, P. Ivey, S. Larcombe, N. Goodenough, N. Seed and A. Shelley, "An Ultra Compact, Low-cost, Complete Image-processing System," *Proc. ISSCC '95 – Int. Solid-State Circuits Conf.*, San Francisco, CA, IEEE, Feb. 1995, pp 230-231.
- [26] J. Davis and X. Chen, "Mixed Scale Motion Recovery Using Guidable Cameras," *Stanford Computer Science Technical Report CS- TR- 2000-08*.
- [27] J. S. Laudo, K. Wurm and C. Dodson, "Liquid Filled Underwater Camera Lens System," *Int. Optical Design Conf. 1998, Proc. SPIE 3482*, no. 32, pp. 698-702.
- [28] H. J. Tiziani, M. Wegner and D. Steudle, "Confocal Principle for Macro- and Microscopic Surface and Defect Analysis," *Opt. Eng.*, vol. 39, no. 1, Jan. 2000, pp. 32–39.
- [29] G. J. Woodgate and J. Harrold, "High Efficiency Reconfigurable 2D/3D Autostereoscopic Display," *SID 03 DIGEST*, May 2003, pp. 4.
- [30] E. C. Tam, "Smart Electro-optical Zoom Lens," *Opt. Lett.*, Optical Society of America, vol. 17, no. 5, Mar. 1992, pp. 369-372.
- [31] S. Larcombe, J. Stern, P. Ivey, and N. Seed, "An Ultra-miniature Camera and Processing System," *IEE Colloq. on Integrated Imaging Sensors and Processing*, Dec 1994, pp. 4/1-4/6.
- [32] S. E. Harris and A. V. Sokolov, "Broad Band Spectral Generation with Refractive Index Control," *Physical Review A*, vol. 55, no. 6, June 1997, pp. R4019-R4022.
- [33] M. Bolduc, M. D. Levine, "A Foveated Retina for the Robot Eye," *Vision Interface '94*, Banff, Alberta, May 18-20 1994, pp. 1-8.
- [34] E. I. Assia, "Accommodative Intraocular Lens: A Challenge for Future Development," *J. cataract and refractive surgery*, vol 23, no. 4, May 1997, pp. 458-460.
- [35] Y. Kuniyoshi, , N. Kita, S. Rougeaux and T. Suehiro, "Active Stereo Vision System with Foveated Wide Angle Lenses," *Asian Conf. on Computer Vision* Singapore, Dec. 5-8 1995, pp. 191-200.

- [36] T. Martinez, David V. Wick, and S. R. Restaino, "Foveated Wide Field-of-View Imaging System Using a Liquid Crystal Spatial Light Modulator," *Opt. Exp.*, vol. 6, no. 10, 2001, pp. 555 – 560.
- [37] R. Völkel, M. Eisner and K.J. Weible, "Miniaturized Imaging Systems," *Microelectron Eng.*, vol. 67-68, 2003, pp. 461-472.
- [38] D. Scribner, L. Buckley, R. Sands, and G. Zuccarello, "Inspiration From Nature," *SPIE Optoelectronic Magazine*, April 2003, pp. 21-22.
- [39] M. Land and D. Nilsson, "Animal Eyes," *Oxford University Press*, Oxford, 2002.
- [40] M. Land and F. Michael, "Animal Eyes-- Pure and Applied Optics," *J. of the Eur. Opt. Soc. Part A*, vol. 6, 1997, pp. 599-602.
- [41] R. W. Wood, "*Physical Optics*," The Macmillan Company, New York, 1911, pp. 66-68.
- [42] J. Kumler and M. Bauer, "Fisheye Lens Designs and Their Relative Performance," *Proc. SPIE - The Intl. Soc. Opt. Eng.*, vol. 4093, 2000, pp 360-369.
- [43] A. Basu and S. Licardie, "Alternative Models for Fish-Eye Lenses," *Pattern Recognition Letter*, vol. 16, April 1995, pp. 433-441.
- [44] J. P. Rolland, A. Rapaport and M. W. Krueger, "Design of an Anamorphic Fish-Eye lens," *Int. Opt. Design Conf. 1998, Proc. SPIE*, vol. 3482, no. 32, pp 274-277.
- [45] S. Shah and J. K. Aggarwal, "Depth Estimation Using Stereo Fish-Eye Lenses," *Proc. Int. Conf. on Image Processing*, Austin Texas, Nov. 1994, pp. 740 – 744.
- [46] J. N. Bright, M. J. Stevens, J. Hoh, T. B. Woolf, "Characterizing the Function of Unstructured Proteins: Simulations of charged polymers under Confinement," *J. Chem. Phys.*, vol. 115, no. 10, pp.4909-4918, Sep. 2001.
- [47] R. A. Duarte, S. Calixto, "Dynamical Optical Microelements on Dye-Sensitized Gels," *Applied Optics*, vol. 39, no. 22, p 3948-3954, August 2000.
- [48] D. J. Fischer, C. J. Harkrider and D. T. Moore, "Design and Manufacture of a Gradient-Index Axion," *Applied Optics-OT*, vol. 39, Issue16, June 2002, pp. 2687- 2694
- [49] R. Danzebrink and M. A. Aegerter, "Deposition of Optical Microlenses Arrays by Ink-jet Process," *Thin Solid Films*, vol. 392, 2001, pp. 223-225.

- [50] H. P. Hertzig, “*Micro-Optics: Elements, Systems and Applications*,” Taylor and Francis, London, 1997.
- [51] N. S. Ong, Y. H. Koh and Y. Q. Fu, “Microlens Array Produced Using Hot-embossing Process,” *Microelectron. Eng.*, vol. 60, 2002, pp. 365-379.
- [52] T. Okamoto, M. Mori, T. Karasawa, S. Hayakawa, I. Seo and H Sato, “Ultraviolet-cured Polymer Microlens Arrays,” *Applied Optics*, vol. 38, no. 14, 1999, pp 2991- 2996.
- [53] P. Nussbaum, I. Philipoussis, A. Husser and H. P. Herzig, “Simple Technique for Replication of Micro-Optical Elements,” *Opt. Eng.*, vol. 37, no. 6, June 1998. pp. 1804–1808.
- [54] B. Berge and J. Peseux, “Variable Focal Lens Controlled by an External Voltage: An Application of Electrowetting,” *Eur. Phys. J., E 3*, 2000, pp.159-163.
- [55] S. Kwon and L. P. Lee, “Focal Length Control by Microfabricated Planar Electrodes-based Liquid Lens ( $\mu$ PELL),” *Proc. 11th Int. Conf. Solid-State Sensors and Actuators*, Eurosensors XV, Transducers 2001, pp. 1348–1351.
- [56] M. Gunji, T. B. Jones and M. Washizu, “Dielectrophoretic Microfluidic Devices,” *14th IEEE International Conference on Micro Electro Mechanical Systems (MEMS 2001)*, Jan 21-25, p 385-388.
- [57] J. Lee and C. J. Kim, “Theory and Modeling of Continuous Electrowetting Microactuation,” *ASME Int. Mechanical Engineering Congress and Exposition, Proc. MEMS*, Nov. 1999, pp. 397-403.
- [58] L. G. Commander, S. E. Day, C. H. Chia and D. R. Selviah, “Microlenses Immersed in Nematic Liquid Crystal with Electrically Controllable Focal Length,” *EOS Topical Digest Meetings Microlens Arrays*, vol.5, 1995, pp. 72-76.
- [59] L. G. Commander, S.E. Day and D. R. Selviah, “Variable Focal Length Microlenses,” *Optics Communications*, vol. 177, 2000, pp. 157–170.
- [60] A. F. Naumov and G. D. Love, “Control Optimization of Spherical Liquid Crystal Lenses,” *Opt. Express*, vol. 4, 1999, pp. 344-352.
- [61] A. F. Naumov, M. Y. Loktev, I. R. Guralnik and G. Vdovin, “Liquid Crystal Adaptive Lenses with Modal Control,” *Optics Letter*, vol. 23, no. 13, July 1998, pp. 992-994.
- [62] T. Kaneko, T. Ohmi, N. Ohya and N. Kawahara, “A Compact and Quick-Response Dynamic Focusing Lens,” *Sensors and Actuators A*, vol. 70, 1998, pp. 92-97.

- [63] S. H. Ahn and Y. K. Kim, "Proposal of Human Eye's Crystalline Lens-like Variable Focusing Lens," *Sensors and Actuators*, vol. 78, 1999, pp. 48–53.
- [64] S. H. Ahn and Y. K. Kim, "Design and Fabrication of Variable Focusing Lens," *Microfluidic Devices and Systems, Proc. of SPIE*, vol. 3515, Santa Clara, CA, USA, 21-22 September, pp. 270-277, 1998.
- [65] D. Y. Zhang, V. Lien, Y. Berdichevsky, J. Choi and Y. H. Lo, "Fluidic Adaptive Lens with High Focal Length Tunability," *Applied Physics Letter*, vol. 82, no. 19, 2003, pp. 3171-3172.
- [66] C. Hardy and F. H. Perrin "The Principles of Optics," McGraw-Hill Book Company Inc., 1932.
- [67] A. Sommerfeld, "Optics," vol. 4, Academic Press, New York, 1954.
- [68] D. C. Giancoli, "Physics, Principles with Applications," 2<sup>nd</sup> Edition, Prentice Hall Inc., New Jersey, 1985.
- [69] [http://en.wikipedia.org/wiki/Lens\\_\(optics\)#Lens\\_construction](http://en.wikipedia.org/wiki/Lens_(optics)#Lens_construction), 04-02-2004.
- [70] E. Hecht, "Optics," 3<sup>rd</sup> ed., Addison-Wesley, 1999.
- [71] D. Gabor, "A New Microscopic Principle," *Nature* 161, 1948, pp. 777-778.
- [72] E. N. Leith and Y. N. Upatnick, "Reconstructed Wavefronts and Communication Theory," *J. Opt. Soc. Am.* 52, 1962, pp. 1123-1130.
- [73] L. B. Lesch, P. M. Hirsch and J. Jordan, "The Kinoform: A New Wavefront Reconstruction Device," *IBM J. Res. Dev.*, vol. 13, 1969, pp. 150-155.
- [74] <http://en.wikipedia.org/wiki/Light>, 04-02-2004.
- [75] <http://www.glenbrook.k12.il.us/gbssci/phys/Class/refrn/u1412b.html>, 04-02-2004.
- [76] <http://www.nrich.maths.org/discus/messages/board-topics.html>, 04-02-2004.
- [77] <http://hyperphysics.phy-astr.gsu.edu/hbase/geoopt/coma.html>, 04-02-2004.
- [78] [http://laxmi.nuc.ucla.edu:8248/M248\\_03/HHtun\\_01/sld042.htm](http://laxmi.nuc.ucla.edu:8248/M248_03/HHtun_01/sld042.htm), 04-02-2004.
- [79] D. C. Brown, "Decentering Distortion of Lenses," *Photogrammetric Eng.*, vol. 32, no. 3, May 1966, pp. 444– 462.
- [80] A. Ning "Plastic vs. Glass Optics: Factors to Consider," *part of SPIE "Precision Plastic Optics" short course note*. 1998.

- [81] I. K. Pasco, J. H. Everest, "Plastics Optics for Opto-Electronics," *Optics and Laser Technology*, vol. 10, 1978, pp. 71-76.
- [82] Y. Tanaka and H. Miyamae, "Analysis on Image Performance of a Moisture Absorbed Plastic Singlet for an Optical Disk", *SPIE Proceedings*, vol. 1354, 1990, pp. 395 – 401.
- [83] T. H. Jamieson, "Thermal effects in optical systems," *Optical Engineering*, vol. 20, 1981, pp.156-160.
- [84] John D. Lytle "Specifying Glass and Plastic Optics - What's the Difference?," *Proc. SPIE*, vol. 181, 1979, pp. 93 - 102.
- [85] [http://www.kri-inc.jp/trend/mcp/1999/04\\_TOC\\_99.html](http://www.kri-inc.jp/trend/mcp/1999/04_TOC_99.html), 04-02-2004.
- [86] J. D. Lytle, "Status and Future of Polymeric Materials in Imaging Systems," *Proc. SPIE*, vol. 1354, 1990, pp. 388-394.
- [87] O. Ermer, "3:1 Molecular Complex of Hydroquinone and C<sub>60</sub>," *Helv. Chim. Acta.*, vol. 74, no.6, 1991, pp.1339.
- [88] H. W. Kroto, J. R. Heath, S. C. O'Brien, R. F. Curl and R. E. Smalley, "C<sub>60</sub>: Buckminsterfullerene," *Nature*, vol 318, 1985, pp. 162.
- [89] W. Krätschmer, L. D. Lamb, K. Fostiropoulos and D. R. Huffman, "Solid C/sub 60/: A New Form of Carbon," *Nature*, vol. 347, Sept. 1990, pp.354-358.
- [90] F. Diederich and C. Thilgen, "Covalent Fullerene Chemistry," *Science*, vol. 271, 1996, pp.317.
- [91] F. Diederich and M. Gómez-López, "Supramolecular Fullerene Chemistry," *Chem. Soc. Rev.*, vol. 28, 1999, pp. 263-277.
- [92] J. Y. Ouyang, S. H. Goh and Y. Li, "Dynamic Mechanical Behavior of Supramolecular C60-Containing Polymeric Materials," *Chem. Phys. Letter*, vol. 347, 2001, pp. 344-348.
- [93] J. Y. Ouyang and S. H. Goh, "Crystallization, Morphology, and Dynamic Mechanical Behavior of Supramolecular Fullerene-Containing Poly (Ethylene-co-Acrylic Acid)," *Fullerenes, Natotubes, and Carbon Natonubes*, vol. 10, 2002, pp. 183-196.
- [94] J. Y. Ouyang, S. H. Goh, H. I. Elim, C. M. Gwee and W. Ji, "Dynamic Mechanical Behavior and Optical Limiting Property of Multifunctional Fullerenol/Polymer Composite," *Chem Phys Letts.*, vol. 366, 2002, pp. 224-230.

- [95] H. I. Elim, J. Y. Ouyang, J. He, S. H. Goh, S. H. Tang and W. Ji, "Nonlinear Optical Properties of Mono-Functional 1,2-Dihydro-1,2-Methanofullerene 60-61- Carboxylic Acid /Polymer Composites," *Chem Phys Letts.*, vol. 369, 2003, pp. 281-286.
- [96] [http://www.extreme-h2o.com/WWW/docs/scl\\_madeof](http://www.extreme-h2o.com/WWW/docs/scl_madeof), 04-02-2004.
- [97] <http://mednews.wustl.edu/medadmin/PANews.nsf/0/FC99AED5CF2DDE6C86256D9B006B9E0D>, 04-02-2004
- [98] K. Kim, S. Park, H. Manohara and J. B. Lee, "Polydimethylsiloxane (PDMS) for High Aspect Ratio Three Dimensional MEMS," *Proc. of the 2000 International Symposium on Mechatronics and Intelligent Mechanical Systems for the 21 Century*, Changwon, Korea, Oct. 4-7, 2000, pp. 55-59.
- [99] J. C. Lotters, W. Olthuis, P. H. Veltink and P. Bergveld, "The Mechanical Properties of the Rubber Elastic Polymer Polydimethylsiloxane for Sensor Applications," *J. Micromech. & Microeng.*, vol. 7, 1997, pp. 145-147.
- [100] D. Armani, C. Liu and N. Aluru, "Re-configurable fluid circuits by PDMS elastomer micromachining," *Proc. IEEE MEMS*, Orlando, FL, January 17-21 1999, pp 222-227.
- [101] M. Born and E. Wolf, "Total Reflection," *Principles of Optics*, 7th Edition, Cambridge University Press, Cambridge, United Kingdom, 1999, pp. 49-53.
- [102] M. Granstrom, M. Berggren and O. Inganasa, "Micrometer and Nanometer-Sized Polymeric Light Emitting Diodes," *Science*, vol. 267, 1996, pp. 1479-81.
- [103] J. C. Lotters, W. Olthuis, P. H. Veltink and P. Bergveld, "Polydimethylsiloxane as an Elastic Material Applied in a Capacitive Accelerometer," *J. Micromech. Microeng.*, vol. 6, March 1996, pp.52-54.
- [104] S.J. Clarson and J.A. Semlyen, *Siloxane polymers*, NJ: Prentice Hall, 1993, pp. 216-244.
- [105] ABCR 1994 *Research Chemicals and Metals Catalogue*, Karlsruhe, Germany.
- [106] R. G. Jones, W. Ando and J. Chojnowski, *Silicon-containing polymers*, Kluwer Academic Publishers, The Netherlands, 2000, pp.185-243.
- [107] D. W. Van Krevelen and P. J. Hoftyzer, *Properties of Polymers*, Elsevier, Amsterdam, 1976.

- [108] Y. Suematsu and T. Hayase, "An Advanced Division Sensor With Fovea," *IECON '90. 16th Annual Conference of IEEE Industrial Electronics Society*, vol. 1343, 1990, pp. 581-585.
- [109] N. Alvertos and E. L. Hall, "Omnidirectional Viewing for Robot Vision," *Proc. of the SPIE Symposium on Intelligent Robots*, Third International Conference on Robot Vision and Sensory Controls, Cambridge, MA, vol. 448, Nov. 6-10, 1983.
- [110] S. Shah and J. K. Aggarwal, "Intrinsic Parameter Calibration Procedure for a (high-distortion) Fish-Eye Lens Camera with Distortion Model and Accuracy Estimation," *Pattern Recognition*, vol. 29, no. 11, 1996, pp. 1775-1788.
- [111] S. Shimaizu, Y. Suematsu, and S. Yahata, "A Wide Angle Vision Sensor with High Distortion Lens-detection of Camera Location and Gaze Direction Based on Two-parallel-line Algorithm", *Proc. of the 1996 IEEE IECON. 22nd International Conference on Industrial Electronics, Control, and Instrumentation*, 1996, pp. 1600-1605.
- [112] [www.omnitech.com](http://www.omnitech.com), 04-02-2004.
- [113] A. Basu and S. Licardie, "Modeling Fish-Eye Lenses," *Proceedings of the 1993 IEEE/RSJ international conference on intelligent robots and systems*, Yokohama, Japan, 26-30, July 1993.
- [114] G. Carl, "Improving Focus Targeting in Interactive Fisheye Views," *Conf. on Human Factors in Computing Systems – Proc.*, vol. 4, no. 1, 2002, pp. 267-274.
- [115] M. T. Nathan, R. J. Michael, L. Xiaoqun and H. Ernest, "Techniques for Fisheye Lens Calibration Using a Minimal Number of Measurements," *Proc. of SPIE - The Int. Soc. for Opt. Eng.*, vol. 4197, 2000, pp. 181-190.
- [116] D. Daly, R. F. Stevens, M. C. Hutlcy, and N. Davies "The Manufacturing of Microlenses by Melting Photoresist," *Meas. Sci. and Tech.*, vol. 1, 1990, pp. 759-766.
- [117] A. Schilling, R. Merz, C. Ossmann and H. P. Herzig, "Surface Profiles of Reflow Microlenses Under the Influence of Surface Tension and Gravity," *Opt. Eng.*, vol. 39, no. 8, 2000, pp. 2171-2176.
- [118] P. Ruther, B. Gerlach, J. Gottert, M. Ilie, J. Mohr, A. Muller and C. Oßmann, "Fabrication and Characterization of Microlenses Realized by a Modified LIGA Process," *Pure Appl. Opt.*, vol. 6, 1997, pp. 643-653.



- [119] L. C. Ping, Y. Hsiharn and C. C. Kong, "A New Microlens Array Fabrication Method Using UV Proximity Printing," *J. Micromech. Microeng.*, vol. 13, 2003, pp. 748-757.
- [120] M. T. Gale, L. D. Baraldi, and R. E. Kunz, "Replicated Microstructures For Integrated Optics," *Proc. SPIE*, vol. 2213, 1994, pp.2-10.
- [121] P. Nussbaum, R. Volkel, H. P. Herzig, M. Eisner and S. Haselbeck, "Design, Fabrication and Testing of Microlens Arrays for Sensors and Microsystems," *Pure Appl. Opt.*, vol. 6, 1997, pp. 617-636.
- [122] M. T. Gale, J. Pedersen and H. Povel, "Active Alignment of Replicated Microlens Arrays on a Charge-Coupled Device Imager," *Opt. Eng.*, vol. 36, no. 5, May 1997, pp. 1510-1517.
- [123] Y. Fu, N. Kok and A. Bryan, "Novel one-step Method of Microlens Mold Array Fabrication," *Opt. Eng.*, vol. 40, no.7, July 2001, pp. 1433-1434.
- [124] H. J. Trost, S. Ayers, T. Chen, W.R. Cox, M. Grove and R. Hoenigman, "Using Drop-on-Demand Technology for Manufacturing GRIN Lenses," *Proc. 2001 Annual Meeting ASPE*, 10-15, Nov 2001 Arlington, VA.
- [125] R. Danzebrink, M. A. Aegerter, "Deposition of Micropatterned Coating Using an Ink-jet Technique," *Thin Solid Films*, vol. 351, 1999, pp. 115-118.
- [126] S. Moon and S. Kang, "Fabrication of Polymeric Microlens of Hemispherical Shape Using Micromolding," *Opt. Eng.*, vol. 41, no. 9, 2002, pp. 2267-2270.
- [127] J. Yao, F. Gao and Y. Guo, "Fabrication of Refractive Microlens Array by Etching Dichromate Gelatin With Enzyme Solution" *Opt. Eng.*, vol. 40, no. 9, 2001, pp. 2022-2025.
- [128] Z. Jaroszewicz, A. Kolodziejczyk and M. Sypek, "Microlens Arrays Produced With the Help of the Sampling Filter," *Opt. Eng.*, vol. 37, no. 11, 1998, pp. 3002-3006.
- [129] S. H. Park, H. Jeon, Y. J. Sung and G. Y. Yeom, "Refractive Sapphire Microlenses Fabricated by Chlorine-Based Inductively Coupled Plasma Etching," *Appl. Optics*, vol. 40, Issue 22, August 2001, pp. 3698-3702.
- [130] M. Wakaki, Y. Komachi, G. Kani, H. Fukumoto and S. Kawabata, " Fabrication of Microlenses and Microlens Array Using Local Melting of Glass Plate by CO<sub>2</sub> Laser" *Proc. of SPIE* , vol. 4426, 2002, pp. 120-123.
- [131] X. Zhang, Q. Tang, X. Yi and X. Pei, "Cylindrical Microlens Array Fabricated by Argon Ion-Beam Etching" *Opt. Eng.*, vol. 39, Nov 2000, pp. 3001-3007.

- [132] R. Matz, H. Weber and G. Weimann, "Laser-Induced Dry Etching of Integrated InP Microlenses," *Appl. Phys. A*, vol. 65, 1997, pp. 349-353.
- [133] H. Jiang, X. Yuan, Z. Yun, Y. C. Chan and Y. L. Lam, "Fabrication of Microlens in Photosensitive Hybrid Sol-Gel Films Using a Gray Scale Mask," *Mater. Sci. and Eng. C*, vol. 16, 2001, pp. 99-102.
- [134] J. Yao, J. Su, J. Du, Y. Zhang, F. Gao, Y. Gao and Z. Cui, "Coding Gray-Tone Mask for Refractive Microlens Fabrication," *Microelectr. Eng.*, vol. 53, 2000, pp. 531-534.
- [135] C. C. Barghorn, O. Soppera and D. J. Lougnot, "Fabrication of Microlenses by Direct Photo-Induced Crosslinking Polymerization," *Appl. Surf. Sci.*, vol. 168, 2000, pp. 89-91.
- [136] R. Iijima, M. Fujimoto and Y. Maruo, "Document Scanner Using Polymer Waveguides with a Microlens Array," *Opt. Eng.*, vol. 41, no. 11, Nov. 2002, pp. 2743-2748.
- [137] D. M. Rector, D. M. Ranken and J. S. George, "High-Performance Confocal System for Microscopic or Endoscopic Applications," *Methods*, vol. 30, 2003, pp. 16-27.
- [138] H. J. Tiziani, R. Achi, R. N. Krämer, T. Hessler, M. T. Gale, M. Rossi and R. E. Kunz, "Microlens Arrays for Confocal Microscopy," *Optics & Laser Technology*, vol. 29, no. 2, 1997, pp. 85-91.
- [139] R. Völkel, H. P. Herzig, P. Nussbaum, P. Blattner, R. Dändliker, E. Cullmann and W. B. Hügler, "Microlens Lithography and Smart Masks," *Microelectr. Eng.*, vol. 35, 1997, pp. 513-516.
- [140] R. H. Douglas, J. C. Partridge and N. J. Marshall, "The Eyes of Deep-Sea Fish I: Lens Pigmentation, Tapeta and Visual Pigments," *Progress in Retinal and Eye Research*, vol 17, no 4, 1998, pp 597-636.
- [141] G. Oliver and P. Gruss, "Current Views on Eye Development," *TINS*, vol. 20, no. 9, 1997, pp. 415-421.
- [142] W. S. Jagger and P. J. Sands, "A Wide-Angle Gradient Index Optical Model of the Crystalline Lens and Eye of the Rainbow Trout," *Vision Res.*, vol. 36, no. 17, 1996, pp. 2623-2639.
- [143] K. P. Pflibsen, O. Pomerantzeff and R. N. Ross, "Retinal Illuminance Using a Wide-angle Model of the Eye," *J. Opt. Soc. Am. A*, vol. 5, no. 1, Jan. 1988, pp. 146-150.

- [144] I. Escudero-Sanz and R. Navarro, "Off-axis Aberrations of a Wide-angle Schematic Eye Model," *J. Opt. Soc. Am. A*, vol. 16, no. 8, Aug. 1999, pp.1881-1891.
- [145] <http://www.glenbrook.k12.il.us/gbssci/phys/Class/refrn/u14l6c.html>, 04-02-2004.
- [146] D. Berreman, "Variable Focus Liquid Crystal Lens System," *US Patent No. 4,190,330*, 1980, filed 1977.
- [147] S. Sato, "Liquid-Crystal Lens-Cell with Variable Focal Length," *Jap. J. Appl. Phys.*, vol. 18, no. 9, Sept. 1978, pp.1679-1684.
- [148] S. Masuda, S. Fujioka, M. Honma, T. Nose and S. Sato, "Dependence of Optical Properties on the Device and Material Parameters in Liquid Crystal Microlenses," *Jap. J. Appl. Phys.*, vol. 35, no. 9A, Sept. 1996, pp. 4668-4672.
- [149] Y. Choi, J. H. Park, J. H. Kim and S. D. Lee, "Fabrication of a Focal Length Variable Microlens Array Based on a Nematic Liquid Crystal," *Opt. Mater.*, vol. 21, 2002, pp. 643-646.
- [150] M. Washizu, "Electrostatic Actuation of Liquid Droplets for Micro-Reactor Applications," *IEEE Ind. App. Soc.*, New Orleans, Louisiana, Oct. 1997, pp. 1867-1873.
- [151] A. Torkkeli, J. Saarilahti, and A. Häärä, "Electrostatic Transportation of Water Droplets on Superhydrophobic Surfaces," *Proc. IEEE MEMS Conference*, Interlaken, Switzerland, Jan., 2001, pp.475-478.
- [152] M. G. Pollack and R. B. Fair, "Electrowetting-based Actuation of Liquid Droplets for Microfluidic Application," *Appl. Phys. Letter*, vol. 77, no. 11, Sept. 2000, pp.1725-1726.
- [153] C. Quilliet and B. Berg, "Electrowetting: A Recent Outbreak," *Current Opinion in Colloid & Interface Science* 6, 2001, pp. 34-39.
- [154] <http://www.research.philips.com/InformationCenter/Global/FHomepage.asp?lNodeId=13&lArticleId>, 04-02-2004.
- [155] T. Shibaguchi and H. Funato, "Lead-Lanthanum Zirconate-Titanate (PLZT) Electrooptic Variable Focal-Length Lens with Strip Electrode," *Jap. J. of Appl. Phys.*, vol. 31, no. 9B, Sept. 1992, pp. 3196-3200.
- [156] N. Chronis, G. L. Liu, K. H. Jeong and L. P. Lee, "Tunable Liquid-Filed Microlens Array Integrated with Microfluidic Network," *Optics Express*, vol. 11, no. 19, Sept. 2003, pp.2370-2378.

- [157] S. T. Kowel, D. S. Cleverly and P. G. Kronreich, "Focusing by Electrical Modulation of Refraction in a Liquid Crystal Cell," *Appl. Opt.*, vol. 23, no. 2, 1984, pp. 278-289.
- [158] N. A. Riza and M. C. DeJule, "Three-Terminal Adaptive Liquid-Crystal Lens Device," *Opt. Lett.*, vol. 19, no. 14, 1994, pp.1013-1015.
- [159] P. W. McOwan, M. S. Gordon and W. J. Hossack, "A Switchable Liquid Crystal Binary Gabor Lens," *Opt. Commun.*, vol. 03, 1993, pp.189-193.
- [160] G. Williams, N. Powell, A. Purvis and M. G. Clark, "Electrically Controllable Liquid Crystal Fresnel Lens," *SPIE* 1168, 1989, pp. 352-357.
- [161] J. S. Patel and K. Rastani, "Electrically Controlled Polarization-Independent Liquid-Crystal Fresnel Lens Arrays," *Opt. Lett.*, vol. 16, no. 7, 1991, pp. 532-534.
- [162] M. Chang, "Total Internal Reflection Lens," *Appl. Opt.*, vol. 24, no. 9, 1985, pp. 1256-1259.
- [163] J. Eschler, S. Dickmann, D. A. Mlynski and H. Molsen, "Fast Adaptive Lens Based on Deformed Helix Ferroelectric Liquid Crystal," *Ferroelectrics*, vol. 181, 1996, pp. 21-28.
- [164] N. Suguira and S. Morita, "Variable Focus Liquid-Filled Optical Lens," *Appl. Opt.*, vol. 32, no. 22, 1993, pp. 4181-4186.
- [165] I. C. Khoo and S. T. Wu, *Optics and Nonlinear Optics of Liquid Crystals*, 1st edn., World Scientific Publishing, Singapore, 1993, p. 160 and pp. 193.
- [166] W. Hass, J. Adams and J. B. Flannery, "New Electro-Optic Effect in a Room Temperature Nematic LC," *Physical review letter*, vol. 25, no. 19, 1970, pp. 1326-1327.
- [167] <http://www.cargille.com/index.html>, 04-02-2004.
- [168] M. J. Webber, *Handbook of Optical Materials*, CRC press, New York, 2003.
- [169] D. N. Nikogosyan, *Properties of Optical and Laser-Related Materials: A Handbook*, John Wiley & Sons Inc., December 1997.
- [170] G. Wyszecki and W. S. Stiles, *Color science: Concepts and Methods, Quantitative Data and Formulae*, 2d ed., John Wiley & Sons, New York, 1982, pp. 99.
- [171] D. A. Atchison and G. Smith, "Continuous Gradient Index and Shell Models of the Human Lens," *Vision Res.*, vol. 35, 1995, pp. 2529-2538.

- [172] D. Meschede, *Optics, Light and Lasers: The Practical Approach to Modern Aspects of Photonics and Laser Physics*, John Wiley & Sons Inc., January 2004.
- [173] <http://www.ims.fhg.de/>, 04-02-2004.
- [173] <http://mathforum.org/dr.math/faq/formulas/faq.sphere.html>, 04-02-2004.
- [174] Z. Drozdowicz, *The Book of Photons Tools*, Oriel Instruments, pp. 15-2